X-RAY ABSORPTION SPECTROSCOPY AND STRUCTURAL SIMULATION OF MANGANESE LITHIUM BORATE-BASED GLASS SYSTEM

PATTARAPONG NIJAPAI

A Thesis Submitted in Partial Fulfillment of the Requirements for the
Degree of Doctor of Philosophy in Physics
Suranaree University of Technology
Academic Year 2021

การใช้เทคนิคการดูดกลืนรังสีเอกซเรย์และการจำลองโครงสร้างของระบบแก้ว แมงกานีส ลิเทียม โบเรท

นายภัทรพงศ์ นิจอภัย

มหาวิทยาลัยเทคโนโลยีสุรนารี

วิทยานิพนธ์นี้เป็นส่วนหนึ่งของการศึกษาตามหลักสูตรปริญญาวิทยาศาสตรดุษฎีบัณฑิต

สาขาวิชาฟิสิกส์

มหาวิทยาลัยเทคโนโลยีสุรนารี

ปีการศึกษา 2564

X-RAY ABSORPTION SPECTROSCOPY AND STRUCTURAL SIMULATION OF MANGANESE LITHIUM BORATE-BASED GLASS SYSTEM

Suranaree University of technology has approved this thesis submitted in partial fulfillment of the requirement for the Degree of Doctor of Philosophy.

Thesis Examining Committee

(Assoc. Prof. Dr. Puangratana Pairor)
Chairperson

(Assoc. Prof. Dr. Prapan Manyam)
Member (Thesis Advisor)

(Prof. Dr. Rattikorn Yimnirun)
Member

(Dr. Pinit Kidkhunthod)
Member

(Assoc. Prof. Dr. Jakrapong Kaewkhao)
Member

(Assoc. prof. Dr. Yupaporn Ruksakulpiwat)
Vice Rector for Academic Affairs
and Quality Assurance

(Prof. Dr. Santi Maensiri)
Dean of Institute of Science

มหาวิทยาลัยเทคโนโลยีสุรนารี

ภัทรพงศ์ นิจอภัย : การใช้เทคนิคการดูดกลืนรังสีเอกซเรย์และการจำลองโครงสร้างของระบบแก้ว แมงกานีส ลิเทียม โบเรท (X-RAY ABSORPTION SPECTROSCOPY AND STRUCTURAL SIMULATION OF MANGANESE LITHIUM BORATE-BASED GLASS SYSTEM), อาจารย์ที่ปรึกษา: รองศาสตรจารย์ ดร.ประพันธ์ แม่นยำ, 107 หน้า

คำสำคัญ: เทคนิคการดูดกลืนรังสีเอกซเรย์, การจำลองโครงสร้าง, แก้ว

ในช่วงไม่นานมานี้แก้วที่มีโครงสร้างรากฐานจากโบเรทกำลังได้รับความนิยมในการศึกษาเพื่อที่จะนำมาใช้เป็นอุปกรณ์จัดเก็บพลังงาน เช่น เป็นส่วนประกอบของตัวเก็บประจุแบบยิ่งยวด, เป็นขั้วแคโทดของแบตเตอรี่ เป็นต้น วิทยานิพนธ์ฉบับนี้ได้ศึกษาแก้วที่มีรากฐานจากโบเรท-แมงกานีส-ลีเทียม $xMnO_2$-(1-x)(LiO_2-$2B_2O_3$) เมื่อ x =0.2, 0.25 และ 0.3 ด้วยเทคนิคทางการดูดกลืนรังสีเอกซเรย์ (XAS), การจำลองพลวัตของโมเลกุล (MD) และเทคนิคการปรับแต่งด้วยวิธีการย้อนกลับของมอนติ-คาร์โล (RMC) ซึ่งแบบจำลองโครงสร้างของแก้วที่ได้จากวิธีการจำลองทางคอมพิวเตอร์ MD และ MD-RMC-XAS สอดคล้องกับผลที่วัดได้จากการทดลอง โดยที่แมงกานีสและออกซิเจนมีเลขโคออดิเนชันอยู่ที่ 4.34, 4.42 และ 4.50 ตามลำดับ ส่วนการศึกษาเลขออกซิเดชันของแมงกานีสในแก้วตัวอย่างพบว่า มีการผสมกันระหว่างเลขออกซิเดชัน Mn^{2+} และ Mn^{3+} ในอัตราส่วนประมาณ 60:40

มหาวิทยาลัยเทคโนโลยีสุรนารี

สาขาวิชาฟิสิกส์ ลายมือชื่อนักศึกษา_____

ปีการศึกษา 2564 ลายมือชื่ออาจารย์ที่ปรึกษา_____

PATTARAPONG NIJAPAI : X-RAY ABSORPTION SPECTROSCOPY AND STRUCTURAL SIMULATION OF MANGANESE LITHIUM BORATE-BASED GLASS SYSTEM, THESIS ADVISOR : ASSOC. PROF. PRAPAN MANYAM, Ph.D. 107 PP.

Keyword: XAS, Computer Simulation, Glass

Recently, glasses based on borate have aroused interest in energy storage device technology. For example, they can serve as a supercapacitor component or be used as the cathode in batteries. In this thesis, the structure of manganese lithium borate-based glass, denoted as xMnO2-(1-x)(Li_2O-$2B_2O_3$) where x is 0.2, 0.25, and 0.3, was studied using X-ray absorption spectroscopy (XAS), molecular dynamics (MD) simulation, and reverse Monte Carlo (RMC) refinement methods. A good agreement between the structural models from MD simulation, MD-RMC-XAS method, and the obtained experimental data was achieved. The mean Mn-O coordination numbers were found to be 4.37, 4.42, and 4.50, respectively. The oxidation state of Mn in MLB glasses was determined to be a mixture of Mn^{2+} and Mn^{3+} with a ratio of 60:40.

มหาวิทยาลัยเทคโนโลยีสุรนารี

School of Physics Student's signature Pattarapong Nijapai

Academic Year 2021 Advisor's signature P. Manyam

ACKNOWLEDGEMENTS

The following are individuals to whom I would like to express my sincere gratitude for their support and contribution to this thesis.

Firstly, I extend my heartfelt thanks to my supervisor, Prof. Dr. Rattikorn Yimnirun, for his helpful supervision, inspiration, and encouragement throughout my Ph.D.

Secondly, I would also like to express my appreciation to my advisor, Assoc. Prof. Dr. Prapan Manyam, for the valuable advice and kindness provided.

Next, I extend my gratitude to Dr. Pinit Kidkhunthod for his excellent guidance during the XAS experiments and computer simulation, and to Prof. Dr. Alastair N. Cormack for the invaluable suggestions that helped me refine the simulation process. I would also like to thank Prof. Dr. Cormack for taking good care of me during my stay in Alfred, New York, USA.

In addition, the Novel Glass group collaborated exceptionally well, with significant contributions from Dr. Jessada Khajonrit and Mr. Amornthep Montreeuppathum.

Finally, I express my deepest thanks to my parents, friends, and, most importantly, "my cat" for their inspiration and unwavering support.

Pattarapong Nijapai

CONTENTS

Page

ABSTRACT IN THAI I

ABSTRACT IN ENGLISH II

AICKNOWLEDGEMENTS III

CONTENTS IV

LIST OF TABLES VI

LIST OF FIGURES VII

LIST OF ABBREVIATION XI

CHEPTER

I INTRODUCTION 1

1.1 Background 1

1.2 Lithium borate glasses electrode materials 2

1.3 Structural property of composition of Mn, Li, B and O 5

1.4 Characterization technique 9

1.5 Thesis outline 11

II GLASS FABRICATION BY MELT-QUENCHING TECHNIQUE 12

2.1 Melt-quenching 12

2.2 Density measurement 13

III X-RAY ABSORPTION SPECTROSCOPY 15

3.1 Introduction 15

3.2 XANES 19

3.3 EXAFS 21

IV COMPUTER SIMULATION TO CHARACTERIZATION GLASS STRUCTURE 27

4.1 Introduction 27

4.2 Molecular Dynamic simulation 28

4.3 Reverse Monte Carlo refinement 29

มหาวิทยาลัยเทคโนโลยีสุรนารี

CONTENTS (Continued)

Page

4.4 FEFF calculation 31

V LOCAL STRUCTURE INVESTIGATION OF MN IN MANGANESE LITHIUM BORATE-BASED GLASS BY COMPUTER SIMULATION AND X-RAY ABSORPTION SPECTROSCOPY 34

5.1 Introduction 34

5.2 Experimental method 36

5.2.1 Sample preparation 36

5.2.2 XAS experiment 38

5.2.3 Computer simulation 38

5.3 Result 44

5.3.1 XAS result 44

5.3.2 Computer simulation result 47

5.4 Discussion 58

VI SUMMARY AND CONCLUSION 63

REFERENCES 67

APPENDICES

APPENDIX A THE COORDINATION NUMBER CALCULATOR PROGRAM IN FORTRAN95 COMPILER 73

APPENDIX B THE BOND ANGLE DISTRIBUTION CALCULATOR IN FORTRAN95 COMPILER 77

APPENDIX C THE FEFF8.2 INPUT CONVERTER IN FORTRAN95 COMPILER 82

CURRICULUM VITAE 96

LIST OF TABLES

Table **Page**

1.1 Computed properties of the $LiMnBO_3$ polymorphs. 6

5.1 Short-range Buckingham potential parameters for MLB. 39

5.2 EXAFS fitting parameters including interatomic distances (R), coordination numbers and Debye Waller factors (σ^2) of MLB glass samples. 46

5.3 Average coordination number and first shell distance of MLB glass from calculation 62

มหาวิทยาลัยเทคโนโลยีสุรนารี

LIST OF FIGURES

Figure **Page**

1.1 Room temperature magnetization hysteresis loop of $0.5V_2O_5$-$0.5(Li_2O$-$xB_2O_3)$ glass samples: (a) x=1, (b) x=2, (c) x=3. 3

1.2 The first ten charge/discharge curves of the V_2O_5-$LiBO_2$ glass within a potential window of 1.5 - 4.0 V at 50 mA/g rate (Afyon et al., 2014). 4

1.3 The rate capability of the V_2O_5-$LiBO_2$ glass within 1.5 - 4.0 V at 50, 100, 200 and 400 mA/g rates at room temperature (Afyon et al., 2014). 4

1.4 Electrochemical measurements for $LiMnBO_3$ (II) cathode material. (a) Charge-discharge studies (b) Cycle life. Insert figure AC impedance spectra of $LiMnBO_3$ (II). 5

1.5 Schematic diagrams of the (a) hexagonal and (b) monoclinic $LiMnBO_3$ structure. 5

1.6 Crystal structures of $LiMnBO_3$: (a) skew [001] view of the hexagonal phase, (b) skew [100] view of the monoclinic phase. 7

1.7 View of the crystal structure of $Li_7Mn(BO_3)_3$ along [001] corresponding to the direction of columns of linked MnO_4 tetrahedra pairs (pink) interconnected by BO_3^{3+} ions (B green, O red, Li black). 8

1.8 Columns of pairs of MnO_4 tetrahedra (pink) interconnected by BO_3^{3+} ions extending along the crystallographic c-axis showing one translational unit (B green, O red) (Afyon et al., 2013). 8

1.9 Evolution of the number of papers reporting on the structural characterization of glassy materials by XAS spectroscopy. Source: ISI Web of Science. 9

2.1 The schematic of measurement of sample density using Archimedes principle. 14

3.1 Theoretical and algorithm for XANES and EXAFS spectra (BL-5.2 SLRI). 16

3.2 Schematic of incident, transmitted and fluorescence X-ray beam. 17

LIST OF FIGURES (Continued)

Figure		Page
3.3	XANES and EXAFS phenomena.	18
3.4	Layout of BL5.2 at the Synchrotron Light research Institute (SLRI) in Thailand.	18
3.5	Samples from the manganese K-edge XANES spectrum.	20
3.6	Illustration of photoelectron backscattered from the surrounding atom, red circle and blue circles are an absorbing atom and scattering atoms respectively.	22
3.7	Examples of scattering paths consisting of 2, 3 and 4 legs where the arrows note for the legs and the blue and red spheres represent the absorbing atoms and surrounding atoms, respectively.	23
4.1	Simplified schematic of the Molecular Dynamic algorithm.	29
4.2	Reverse Monte Carlo algorithm.	31
4.3	Flow diagram for FEFF modules.	33
5.1	XPS profiles of glass samples: (a) 0.2MnO_2-0.8(Li_2O-2B_2O_3), (b) 0.25MnO_2-0.75(Li_2O-2B_2O_3), and (c) 0.30MnO_2-0.70(Li_2O-2B_2O_3) (J.Khajornrit et al., 2018).	35
5.2	XPS spectra of $LiMnBO_3$ (III) materials (a) Li 1s, (b) O 1s, (c) B 1s, and (d) Mn 2p (Andersson et al., 2002).	36
5.3	The prepared lithium borate glass by melt-quench technique.	37
5.4	The prepared manganese lithium borate glass by melt-quench technique.	37
5.5	Procedure for molecular dynamics simulation.	40
5.6	Flow chart of this work.	43
5.7	XANES spectra of Mn K-edge of 0.2MnO_2-0.8(Li_2O-2B_2O_3), 0.25MnO_2-0.75 (Li_2O-2B_2O_3) and 0.3MnO_2-0.7(Li_2O-2B_2O_3) glass samples and standard samples	45
5.8	The $k^3\chi(k)$ function extracted from the absorption spectrum for MLB glasses at Mn K-edge	45

LIST OF FIGURES (Continued)

Figure **Page**

5.9 The corresponding $\chi(R)$ function for MLB glasses at Mn K-edge. 46

5.10 View of the structure of 0.2M-0.8LB glasses which show Mn^{2+} (pink), Mn^{3+} (purple), B (dark blue), Li (light blue) and O (red). 47

5.11 View of the structure of 0.25M-0.75LB glasses which show Mn^{2+} (pink), Mn^{3+} (purple), B (dark blue), Li (light blue) and O (red). 48

5.12 View of the structure of 0.3M-0.7LB glasses which show Mn^{2+} (pink), Mn^{3+} (purple), B (dark blue), Li (light blue) and O (red). 48

5.13 15 pairs radiant distribution function of 0.2M-0.8LB glasses. 49

5.14 15 pairs radiant distribution function of 0.25M-0.75LB glasses. 50

5.15 15 pairs radiant distribution function of 0.3M-0.7LB glasses. 51

5.16 The distributions of Mn^{2+}-O (pink) and Mn^{3+}-O (purple) coordination numbers obtained from the calculations for 0.2M-0.8LB glasses. 52

5.17 The distributions of Mn^{2+}-O (pink) and Mn^{3+}-O (purple) coordination numbers obtained from the calculations for 0.25M-0.75LB glasses. 53

5.18 The distributions of Mn^{2+}-O (pink) and Mn^{3+}-O (purple) coordination numbers obtained from the calculations for 0.3M-0.7LB glasses. 53

5.19 The angle distributions of O-Mn^{2+}-O (black) and O-Mn^{3+}-O (red) from the calculations for 0.2M-0.8LB glasses. 54

5.20 The angle distributions of O-Mn^{2+}-O (black) and O-Mn^{3+}-O (red) from the calculations for 0.25M-0.75LB glasses. 55

5.21 The angle distributions of O-Mn^{2+}-O (black) and O-Mn^{3+}-O (red) from the calculations for 0.3M-0.7LB glasses. 55

5.22 XANES calculation spectra of Mn K-edge of 0.2M-0.8LB, 0.25M-0.75LB and 0.3M-0.7LB glass samples and experiment result. 56

5.23 The comparison of $k^3\chi(k)$ function (left) and corresponding $\chi(R)$ function (right) between final calculation (black line) and experiment (red circle) of 0.2M-0.8LB glass. 57

LIST OF FIGURES (Continued)

Figure **Page**

5.24 The comparison of $k^3\chi(k)$ function (left) and corresponding $\chi(R)$ function (right) between final calculation (black line) and experiment (red circle) of 0.25M-0.75LB glass..... 57

5.25 The comparison of $k^3\chi(k)$ function (left) and corresponding $\chi(R)$ function (right) between final calculation (black line) and experiment (red circle) of 0.3M-0.7LB glass..... 58

5.26 The comparison of the EXAFS data between MD-RMC-EXAFS refinement with the first shell model fitting of EXAFS result for 0.2M-0.8LB glass. 59

5.27 Linear combination fitting (red) of 0.2M-0.8LB glass with pure Mn^{2+}(pink) and pure Mn^{3+}(green) system..... 59

5.28 Pair radiant distribution function of Mn-O in 0.2M-0.8LB glass for each Mn oxidation state (left) and merged RDF (right)..... 60

5.29 Pair radiant distribution function of Mn-O in 0.25M-0.75LB glass for each Mn oxidation state (left) and merged RDF (right)..... 61

5.30 Pair radiant distribution function of Mn-O in 0.3M-0.7LB glass for each Mn oxidation state (left) and merged RDF (right)..... 61

5.31 The example of Mn cluster with 6 Å cutoff range of Mn^{2+}(left) and Mn^{3+} (right)..... 62

มหาวิทยาลัยเทคโนโลยีสุรนารี

LIST OF ABBREVIATION

MLB	Manganese Lithium Borate
XAS	X-ray Absorption Spectroscopy
XANES	X-ray Absorption Near Edge Structure
EXAFS	Extended X-ray Absorption Fine Structure
MD	Molecular Dynamic
RMC	Reverse Monte Carlo
RDF	Radial Distribution Function
CN	Coordination Number
BAD	Bond Angle Distribution

มหาวิทยาลัยเทคโนโลยีสุรนารี

CHEPTER I
INTRODUCTION

1.1 Background

Glasses and glass ceramics are examples of advanced functional materials. These have been elucidated in terms of their characteristics and methodology (Karmakar, 2017). Due to their applications in solid-state batteries, optical detectors, optical fibers, and other fields, glasses are gaining popularity. In comparison to crystal products, glasses offer various advantages, including the flexibility to be manufactured in any size or shape. Lithium borate glasses, among the most researched of all glasses, are notable for their potential applications (Ramteke and Gedam, 2014, Berkemeier et al., 2007, Pye et al., 2012, Rao et al., 1996).

A significant focus lies in the advancement of electrode materials for supercapacitors. The precise capacitance of each supercapacitor material is influenced by various factors, including electrode materials, electrolyte, and others. Concerning electrode potential materials, carbon-based materials exhibit higher capacitance than metal oxide-based pseudo-capacitor materials (Lokhande et al., 2011, Zhao et al., 2013). Manganese oxide compound materials, such as Mn_2O_4, MnO_2, and MnO, were selected as supercapacitor electrode materials due to their environmental friendliness, cost-effectiveness, a range of oxidation states, and high specific capacitance, reaching 1400 F/g and 1370 $F.g^{-1}$ (Qi et al., 2016, Toupin et al., 2004). The Li and Mn elements have garnered interest as potential cathode materials for rechargeable Li-ion batteries, boasting a high energy density of 1000 $Wh.kg^{-1}$ and a lower cost compared to $LiCoO_2$ (Ozoemena and Chen, 2016, Yu and Zhou, 2013). Composite materials of lithium-borate glasses have recently gained attention in the field of energy storage (Afyon et al., 2014).

While crystalline high-capacity metal oxide electrode materials are available, they come with disadvantages such as ion penetration through the crystalline lattice and electrode swelling. Researchers are therefore exploring the use of amorphous glass as an alternative to crystalline electrode materials. Changes in the angle linking network-forming polyhedral bonding, such as the Si-O-Si bond angle (ranging from 125° to 165°) and the P-O-P bond angle (ranging from 123° to 180°) in phosphate glass, are linked to the flexibility of the glass structure. The bond angle in the boroxol ring in the borate structure drastically alters in the case of borate glass. Both of these materials exhibit exceptional ability to shape glass (Stoch, 2001). The vanadium lithium borate-based glasses (V_2O_5-$LiBO_2$) have a high specific capacity of roughly 400 mAh.g^{-1}, as per prior studies, and maintain a capacity of 300 mAh.g^{-1} for 100 cycles. V_2O_5-$LiBO_2$ glasses are being considered as potential cathode materials for Li-ion rechargeable batteries.

The study of glass structure can be highly advantageous in this context. Computer simulations, which enable the examination of a glass in all its microscopic details, are theoretically a valuable tool for investigating the production history dependence of glass properties. Despite this potential, only a limited number of simulations have been conducted to comprehensively address this question.

1.2 Lithium borate glasses electrode materials

Borate-based glasses were produced and characterized using the VSM method, as outlined by Laorodphan et al. The M-H loops of the glass samples at room temperature are presented in Figure 1.1. The magnetization of the $0.5V_2O_5$-$0.5(Li_2O$-$xB_2O_3)$ samples with x=1.0 and 2.0 exhibited a linear relationship with the applied field, indicating their paramagnetic nature. An increase in B_2O_3 concentration led to a decrease in magnetization (Laorodphan et al., 2016).

S. Afyon has conducted research on vanadium lithium borate glasses as cathode materials in rechargeable lithium-ion batteries. In the context of rechargeable LIBs, a glassy material produced through the Li_2O-B_2O_3-V_2O_5 method, referred to as V_2O_5-$LiBO_2$

glass in this document, has been documented. The synthesis involves melting a combination of 80% V_2O_5 and 20% $LiBO_2$ at 900°C, followed by quenching to room temperature to create the glass content. The resulting cell undergoes discharge with a capacity of 327 mAh/g, followed by a recharge with a capacity of 308 mAh/g in the subsequent step. In a standard V_2O_5-$LiBO_2$ glass electrode fabrication, the active material comprises 70 wt% V_2O_5 and 20 wt% $LiBO_2$. Galvanostatic cells made from such electrodes were measured by discharging to 1.5 V and then charging to 4.0 V at a rate of 50 mA/g. Figure 1.2 illustrates the first ten galvanostatic charge/discharge curves of the V_2O_5-$LiBO_2$ glass.

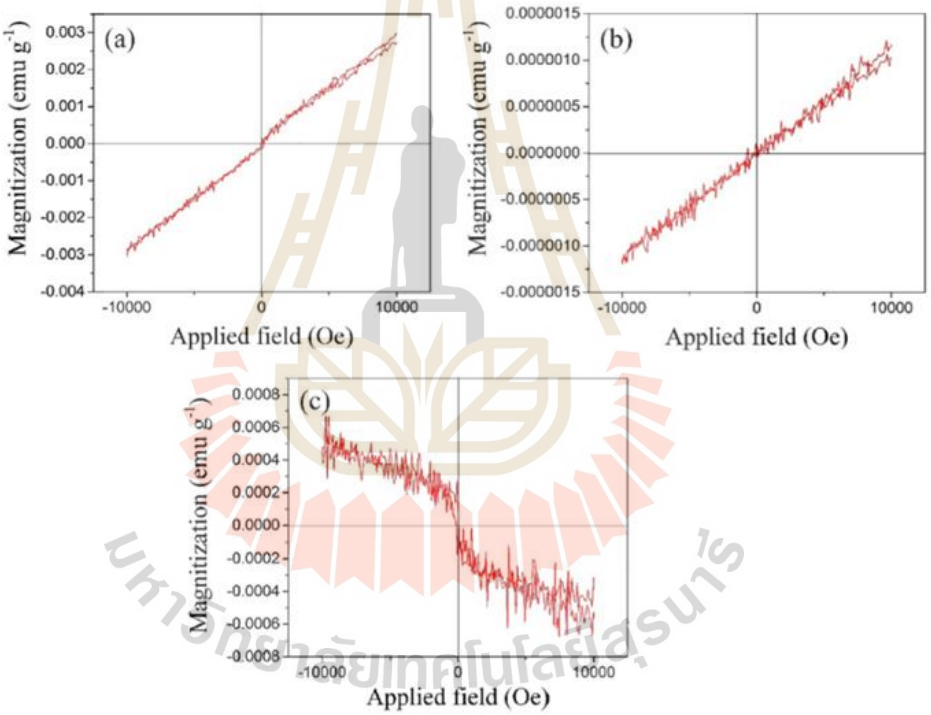

Figure 1.1 Room temperature magnetization hysteresis loop of $0.5V_2O_5$-$0.5(Li_2O$-$xB_2O_3)$ glass samples: (a) x=1, (b) x=2, (c) x=3.

The rate capability of V_2O_5-$LiBO_2$ glass is depicted in Figure 1.3 between 1.5 and 4.0 V. Capacities of 293, 236, and 180 mAh/g are achieved at rates of 50, 100, and 200 mA/g, respectively. Upon increasing the rate to 400 mA/g on the 35th cycle, the discharge capacity decreases to 125 mAh/g. However, it recovers to 260 mAh/g on the 45th cycle when the rate is reduced back to 50 mA/g. Charging and discharging

experiments for synthesized $LiMnBO_3$ (II) within a voltage range of 1.5 - 4.5 V are presented in Figure 1.4. The initial discharge capacity is determined to be 310 $mAh.g^{-1}$, suggesting the possible intercalation and de-intercalation of more than one Li atom per formula unit (f.u) of $LiMnBO_3$ (II) (Veena et al., 2019).

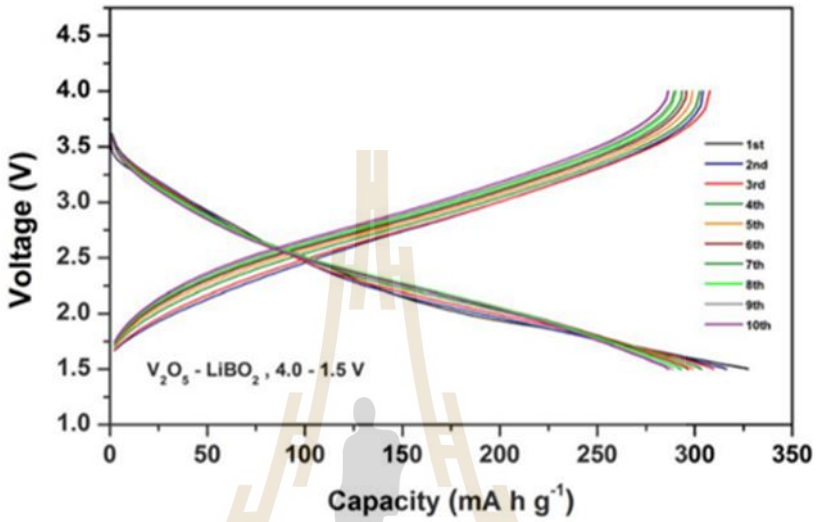

Figure 1.2 The first ten charge/discharge curves of the V_2O_5-$LiBO_2$ glass within a potential window of 1.5 - 4.0 V at 50 mA/g rate (Afyon et al., 2014).

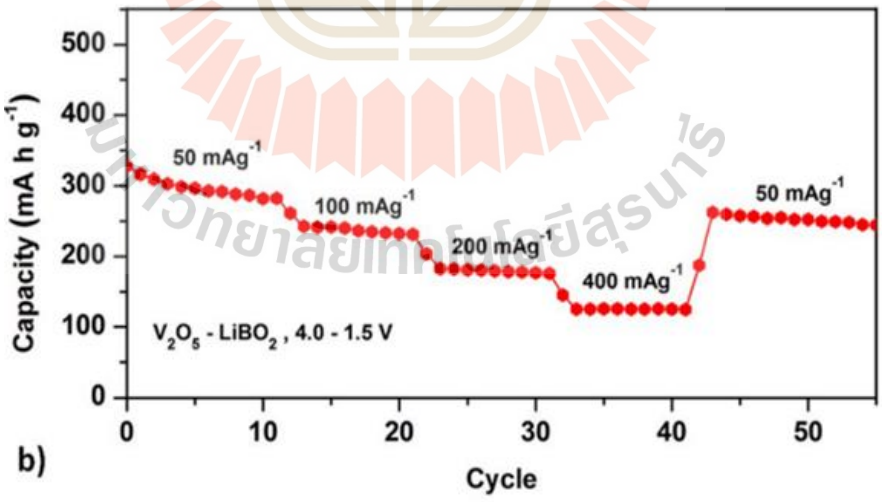

Figure 1.3 The rate capability of the V_2O_5-$LiBO_2$ glass within 1.5 - 4.0 V at 50, 100, 200 and 400 mA/g rates at room temperature (Afyon et al., 2014).

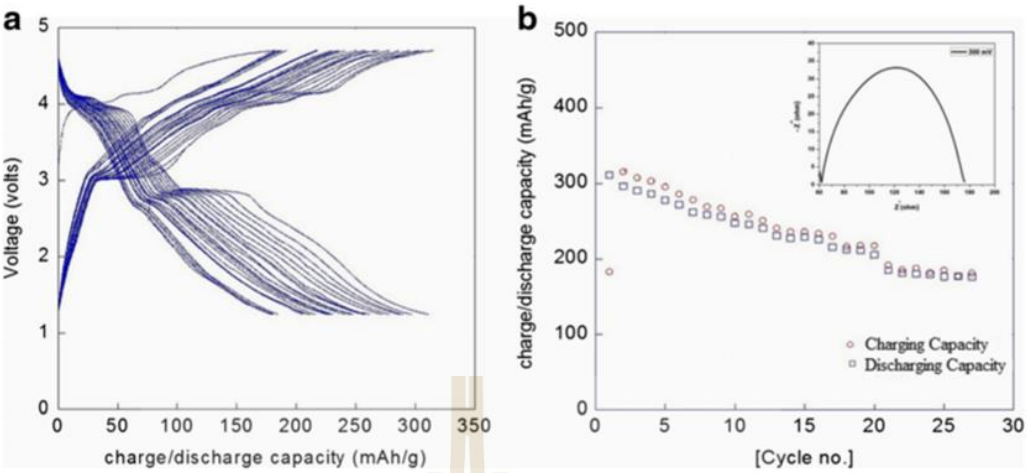

Figure 1.4 Electrochemical measurements for $LiMnBO_3$ (II) cathode material. (a) Charge-discharge studies (b) Cycle life. Insert figure AC impedance spectra of $LiMnBO_3$ (II).

1.3 Structural property of composition of Mn, Li, B and O

The atomic and molecular structures of the LiMnBO2 polymorphs in crystals are illustrated in Figure 1.5, depicting Mn triangle constructs with planar hexagons on the edges (Legagneur et al., 2001). The monoclinic trimeric structure, characterized by a single chiral center and trigonal di-pyramidal arrangement, reveals that each Li and Mn site has an upper and lower position relative to the other (Bondareva et al., 1978).

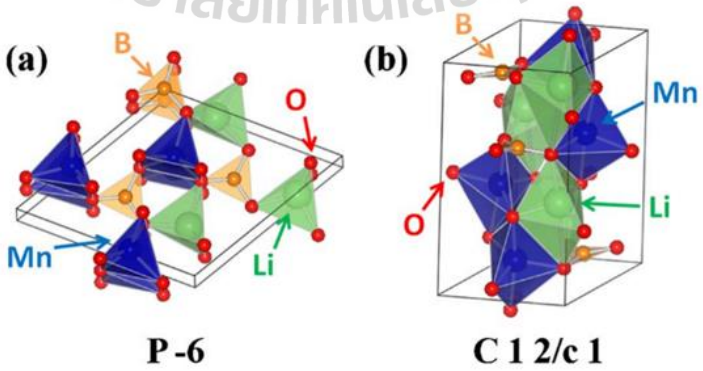

Figure 1.5 Schematic diagrams of the (a) hexagonal and (b) monoclinic $LiMnBO_3$ structure.

After performing ab initio computations and assessing the voltage and energy density of monoclinic and monoclinic $LiBO_3$ in terms of both charge state transition and thermodynamic charge-discharge processes, we have gained insights into their stability. The variations in length are presented in Table 1.1, providing a comparative understanding of the charge and discharge stability.

While the hexagonal phase is the computationally expected ground state for $LiMnBO_3$, the energy gap between it and the monoclinic phase is 5 meV per atom, which is close to the numerical precision limit for this process. It is small enough to be readily resolved by entropic results (Kim et al., 2011).

Table 1.1 Computed properties of the $LiMnBO_3$ polymorphs**.**

Phase	Average voltage (V)	Theoretical Grav. Energy Density (Wh/L)	Theoretical Vol. Energy Density (Wh/L)	Theoretical Capacity (mAh/g)
Hexagonal	4.11	912	2922	222
Monoclinic	3.70	822	2635	222

The crystal structures of the two LiMnBO3 modifications are depicted in Figure 1.6. In the hexagonal phase, MnO_5 square pyramids are arranged by sharing their equatorial edges. MnO_5 polyhedral chains extend along the c-axis, interconnected by planar BO_3 groups. Li atoms exhibit tetrahedral coordination, forming LiO_4 tetrahedra chains along the c-axis, parallel to those of the square pyramids. In the monoclinic process, MnO_5 adopts a trigonal bipyramidal geometry, forming polyhedral chains through edge-sharing along the direction. Previous theoretical work indicates that the preferred diffusion direction of Li ions in both phases has a one-dimensional character parallel to the c-axis.

Afyon et al. discovered a lithium-rich compound, $Li_7Mn(BO_3)_3$, exhibiting a first discharge capacity of 280 $mAhg^{-1}$ with an exchange rate of 3 Li per unit. The synthesis

involved thermalizing Li_2O, MnO, and B_2O_3 in precise stoichiometric quantities, resulting in the formation of this novel Li-rich compound. The crystal structure of $Li_7Mn(BO_3)_3$, as depicted in Figure 1.7, comprises six separate BO_3^{3+} ions, with only one entirely connected to Li^+ ions, the crystallographically distinct ions having a (B-O) range of 1.31 - 1.43 Å. All additional borate units are linked to two Mn^{2+} ions ((Mn-O) = 2.01 - 2.08 Å) and ten Li^+ ions ((Li-O) = 1.87 - 2.21 Å) in a tetrahedral manner (Afyon et al., 2014).

The MnO4-tetrahedra are arranged in columns that extend down the crystallographic c-axis, as illustrated in Figure 1.8. The sole Li atoms are located in the first coordination spheres of these tetrahedra. Pairs of tetrahedra are joined together by several BO_3^{3+} units, and another unit connects the tetrahedra pairs within the columns. The BO_3^{3+} groups at the ends of the MnO_4-tetrahedra provide the fourth oxygen atoms required for formation.

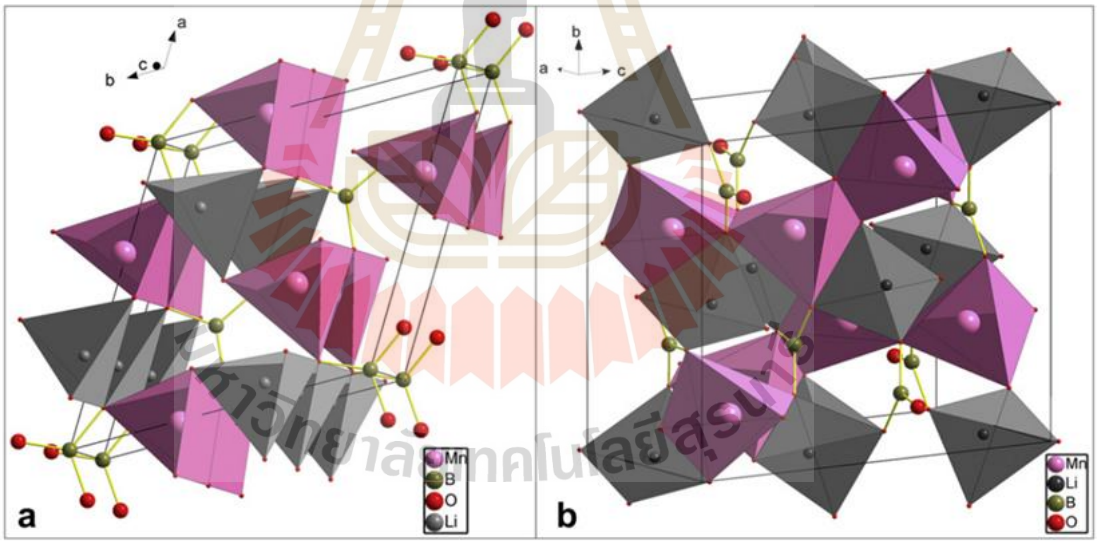

Figure 1.6 Crystal structures of $LiMnBO_3$: (a) skew [001] view of the hexagonal phase, (b) skew [100] view of the monoclinic phase.

Compared to other Mn^{2+} oxide compounds, manganese's tetrahedral coordination at such a low oxidation state is unique to our knowledge. Typically, MO6 octahedra or MO_5 polyhedra (where M = Fe, Mn, and Co in $LiMBO_3$) with trigonal bipyramidal or square-pyramidal geometry have been most frequently observed. This

tetrahedral coordination may contribute to the stabilization of the borate manganate framework when it reaches higher oxidation states (Mn^{n+} with n > 4) (Afyon et al., 2013).

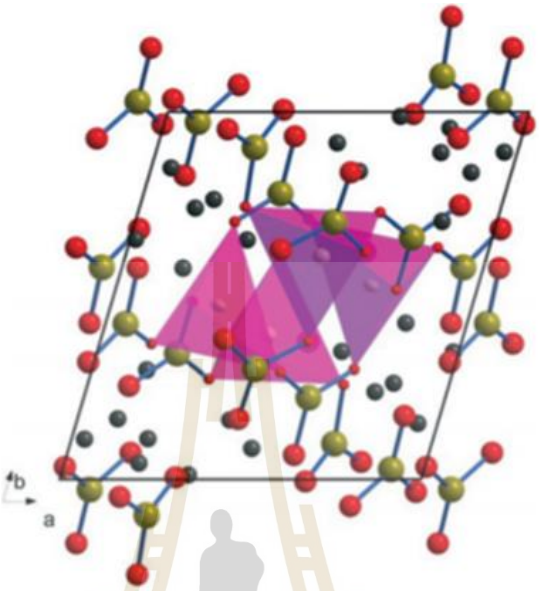

Figure 1.7 View of the crystal structure of $Li_7Mn(BO_3)_3$ along [001] corresponding to the direction of columns of linked MnO_4 tetrahedra pairs (pink) interconnected by BO_3^{3+} ions (B green, O red, Li black).

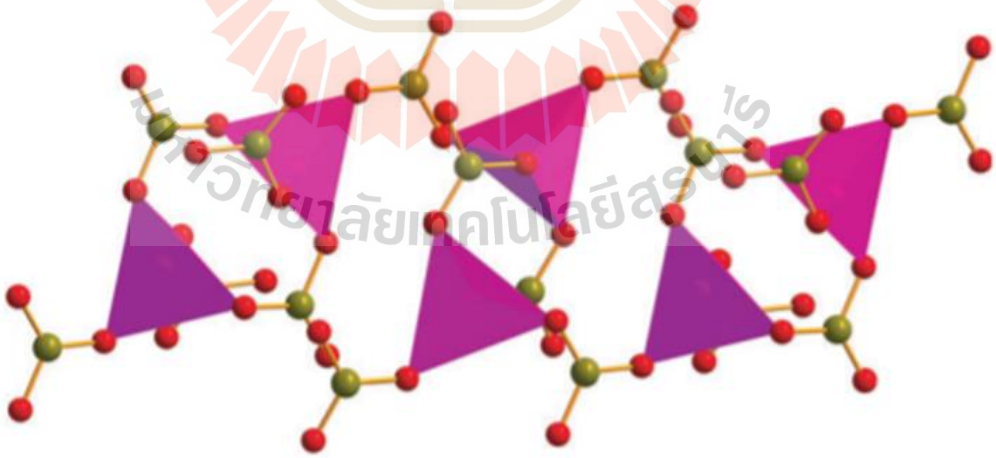

Figure 1.8 Columns of pairs of MnO_4 tetrahedra (pink) interconnected by BO_3^{3+} ions extending along the crystallographic c-axis showing one translational unit (B green, O red) (Afyon et al., 2013).

1.4 Characterization technique

In the past, X-ray Absorption Spectroscopy (XAS) has been widely employed to characterize the short-range order and electronic structures of various classes of glassy materials, and in some cases, the medium-range order. Figure 1.9 illustrates the number of papers presenting experimental findings on the structural characterization of glassy materials published between 1975 and 2016. Acronyms such as XAS (X-ray Absorption Spectroscopy), EXAFS (Extended X-ray Absorption Fine Structure), and XANES (X-ray Absorption Near Edge Structure), along with the keywords 'glass' or 'glasses,' were used as search keys in this bibliographic analysis using the ISI Web of Science. The figure indicates that, following a significant initial surge, the number of structural studies on glassy materials peaked at approximately 40 - 50 articles per year around 20 years ago.

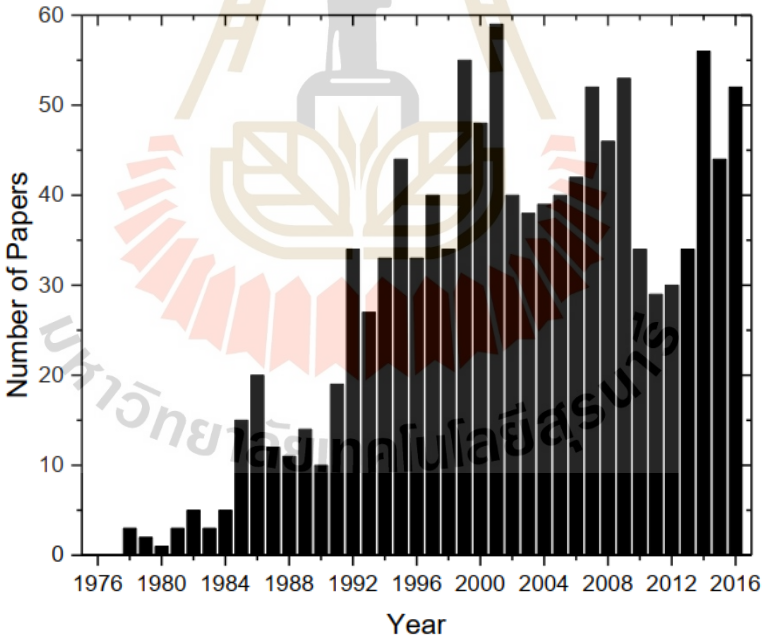

Figure 1.9 Evolution of the number of papers reporting on the structural characterization of glassy materials by XAS spectroscopy. Source: ISI Web of Science.

The X-ray Absorption Spectroscopy (XAS) technique has found application in the characterization of various types of glasses, encompassing oxides, metallic, fluoride,

chalcogenide, and halide glasses. Beyond the analysis of artificial or natural glasses, the XAS approach has been employed in studying glassy materials under standard conditions, exploring their structure in both solid and liquid states. This technique has also been utilized for investigating natural magma glasses (Mastelaro and Zanotto, 2018).

The computer simulation of glass materials has been under development for a long time. In the 1980s and 1990s, Monte Carlo methods played crucial roles in investigating structural changes below and above the glass transition. A notable addition during this period was the development of the Reverse Monte Carlo (RMC) modeling technique. In RMC modeling, atoms in an initial configuration are moved to minimize deviation from experimental structural data, such as X-ray and/or neutron diffraction data, using a standard Monte Carlo (MC) algorithm. A distinctive feature of this method is its reliance not on interatomic potentials, but on experimental Radial Distribution Function (RDF) data. RMC modeling has been successfully applied to structural modeling of liquids and glasses.

On the other hand, the Molecular Dynamics (MD) simulation method is entirely deterministic and provides information about the time dependence of the system's configuration. Similar to the MC method, careful consideration is required when choosing suitable interatomic potentials for calculating force and energy. The methodology of MD simulation has been extensively described (Frenkel et al., 1996), and several monographs summarize MD simulations of glasses. A critical aspect of this method lies in constructing reliable interatomic potentials capable of reasonably reproducing structures and properties. Numerous potentials have been developed, and various potential models are explained in detail in the book by Leach. (Takada and Cormack, 2008).

1.5 Thesis outline

This thesis focuses on the fabrication of manganese lithium borate-based glasses using a melt-quenching technique, as outlined in Chapter II. The structural analysis of these glasses has been conducted through Molecular Dynamics (MD) simulation, Reverse Monte Carlo (RMC) modeling, and X-ray Absorption Spectroscopy (XAS), including X-ray Absorption Near Edge Structure (XANES) and Extended X-ray Absorption Fine Structure (EXAFS) techniques. Detailed explanations of these techniques are provided in Chapters III and IV. Chapter V presents the results of the structural study of manganese lithium borate glasses, employing a combination of neutron diffraction, MD simulation, RMC refinement, and the EXAFS technique.

มหาวิทยาลัยเทคโนโลยีสุรนารี

CHEPTER II

GLASS FABRICATION BY MELT-QUENCHING TECHNIQUE

2.1 Melt-quenching

In the production of glasses for this study, the melt-quenching method was employed. This widely used technique initiates with the meticulous mixing of raw materials, including oxides or carbonates, to achieve the desired glass composition. Subsequently, the mixed ingredients undergo heating in a furnace, typically exceeding 1300 °C. This elevated temperature results in the formation of a homogeneous glass melt. The next crucial step is quenching, where the molten glass is rapidly cooled, preventing the development of a crystalline structure and resulting in the formation of an amorphous solid-referred to as glass frit.

The obtained glass frit, consisting of small particles, is versatile and can undergo further processing steps based on the intended application. Whether applied directly or subjected to additional processes such as molding, pressing, or sintering, the melt-quenching method provides flexibility in shaping the final glass product.

Key advantages of the melt-quenching method include the creation of homogenous glasses with consistent properties, control over glass composition through the adjustment of raw material mixtures, and suitability for mass production, making it a cost-effective approach for large-scale glass manufacturing.

However, it's important to note that the rapid cooling inherent in melt quenching may introduce imperfections in the glass, such as surface irregularities or internal stresses. Additionally, the technique may not be universally applicable to all glass compositions, particularly those requiring highly controlled crystallinity.

The preparation of the manganese lithium borate (MLB) glass samples used in this investigation, detailed in Section 5.2, was conducted by A. Montreeuppathum and J. Khajonrit (Montreeuppathum et al., 2020, Khajonrit et al., 2018).

2.2 Density measurement

In this study, the determination of sample density is conducted through the application of Archimedes' principle. The measurement involves leveraging the buoyancy force when a sample is submerged in a fluid. To establish the density of the submersion liquid, standard steel balls with known and uniform radii are initially employed. These steel balls serve as reference objects, and their densities are used to calibrate the system before measuring the glass samples.

For accurate weight measurements, a micro-balance with a precision of 10 μg is utilized. The density measurement process is illustrated in Figure 2.1 showcasing a hanging basket arrangement to immerse the sample in the liquid. This arrangement ensures the sample is effectively positioned within the liquid medium for precise measurements.

Toluene is chosen as the reference submersion liquid due to its advantageous properties, including low surface tension and low vapor pressure. These properties minimize the likelihood of liquid evaporation during the measurement process, ensuring accuracy.

The relationship between masses and densities measured through these methods is expressed by Equation (2.1), where the density of the sample is determined by comparing its buoyant force in the liquid to the known buoyant forces of reference steel balls. This comprehensive approach provides a robust methodology for obtaining accurate and reliable density measurements for the glass samples studied in this research.

$$\rho_{obj} = \frac{\rho_l m_{obj}}{m_{obj} - m_{obj,l}} \tag{2.1}$$

Where ρ_{obj} is the density of object.

ρ_l is the density of the submersion liquid.

m_{obj} is the mass of the object in air.

$m_{obj,l}$ is the effective mass measured in the submersed liquid.

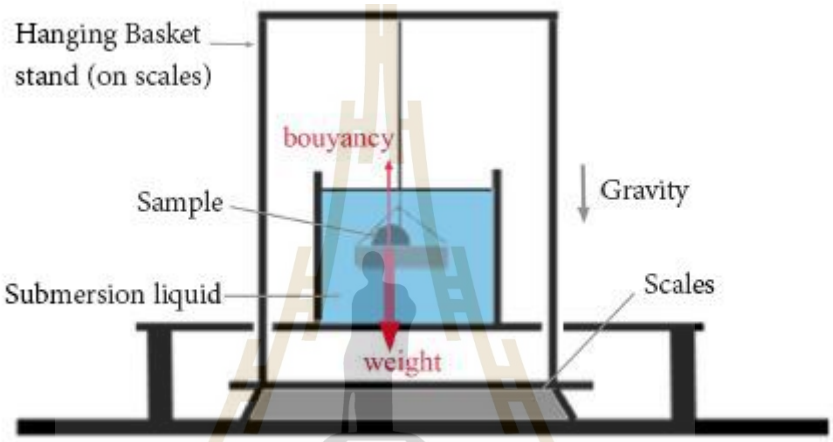

Figure 2.1 The schematic of measurement of sample density using Archimedes principle.

มหาวิทยาลัยเทคโนโลยีสุรนารี

CHEPTER III
X-RAY ABSORPTION SPECTROSCOPY

3.1 Introduction

X-ray absorption spectroscopy, or XAS, is a widely used method for studying the atomic local structure and electronic states. The terms "X-ray absorption near edge structure" (XANES) and "Extended X-ray Absorption Fine Structure" (EXAFS) are used to describe this, as seen in Figure 3.1. In general, an X-ray excites a core electron in an atom, which can either be promoted to an unoccupied level or ejected from the atom. Both of these methods result in a core hole. According to XAS principles, an electron is ejected by an X-ray source with enough energy for excitation.

A typical XAS system is mainly divided into two parts: the input system and the output system. The input involves the detection of an electron gas ionized signal in the incident chamber (I_0). The output captures the electron ionized signal in the transmitted chamber (I). The electron X-ray absorptions can be explained by using Beer's law, as shown in Equation 3.1.

$$\mu(E)x = ln\frac{I_0}{I} \tag{3.1}$$

Where $\mu(E)$ is transmission coefficient.

x is thickness of sample.

I_0 is incident light intensity.

I is transmitted light intensity.

มหาวิทยาลัยเทคโนโลยีสุรนารี

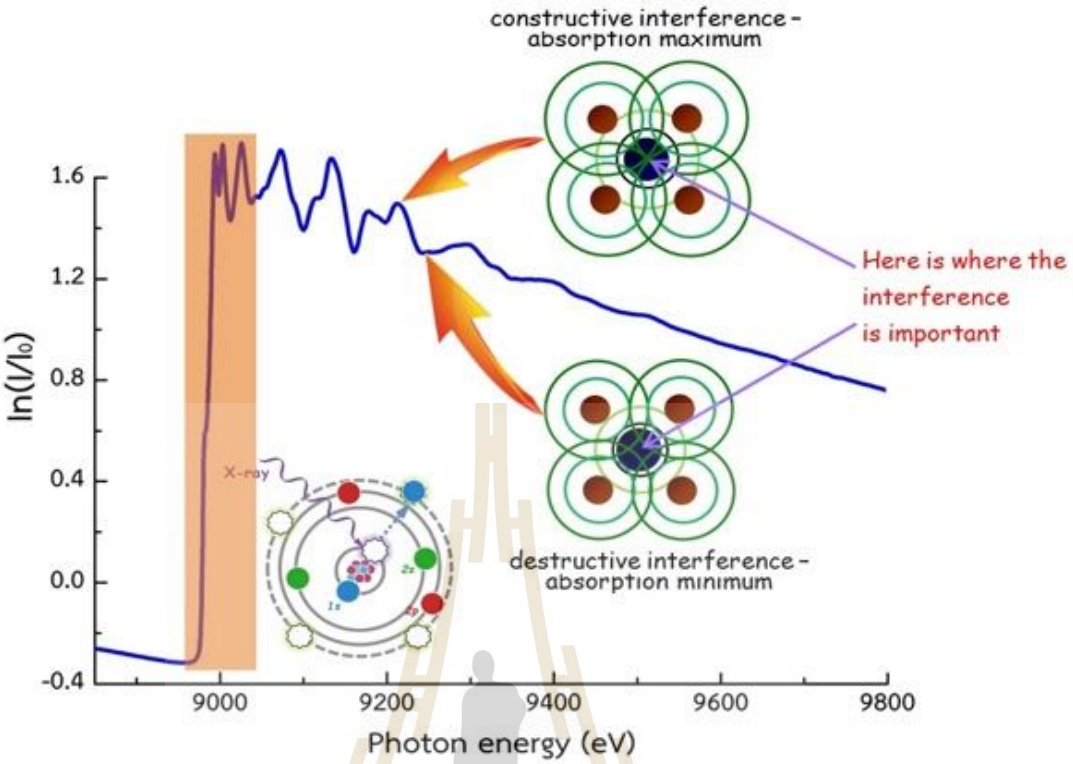

Figure 3.1 Theoretical and algorithm for XANES and EXAFS spectra (BL-5.2 SLRI).

Following an x-ray absorption event, two primary mechanisms govern the decay of the excited atomic state. The first mechanism, illustrated in Figure 3.2, is x-ray fluorescence, where a higher-energy core-level electron fills the deeper core hole, ejecting an x-ray of well-defined energy. These atom-specific fluorescence energies can be effectively harnessed for identifying atoms in a solution and measuring their concentrations due to their characteristic nature.

The second de-excitation process for the core hole is the Auger Effect. In this phenomenon, an electron descends from a higher electron level, and a second electron is emitted into the continuum, potentially exiting the sample. In the hard x-ray regime (> 2 keV), x-ray fluorescence is more likely to occur than Auger emission. However, for lower-energy x-ray absorption, Auger processes become more prevalent. Both fluorescence and Auger emission methods can be employed to determine the absorption coefficient, although fluorescence is slightly more common, as depicted by the following equation:

$$\mu(E) \propto \frac{I_f}{I_0} \tag{3.2}$$

Where I_f is the monitored intensity of a fluorescence line (or, again, electron emission) associated with the absorption process.

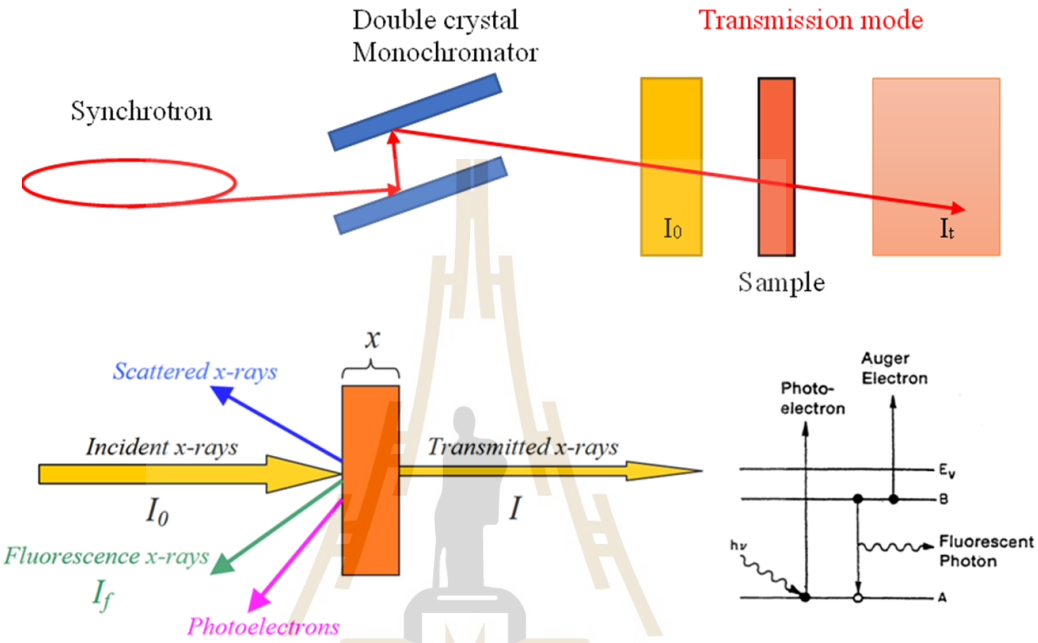

Figure 3.2 Schematic of incident, transmitted and fluorescence X-ray beam.

Figure 3.3 presents a visual representation of the photoelectron scattering processes in both the single-scattering regime, specifically Extended X-ray Absorption Fine Structure (EXAFS), and the multiple scattering regime, known as X-ray Absorption Near Edge Structure (XANES). It is important to note that the single scattering approximation is assumed in EXAFS, although multiple scattering can be considered within the EXAFS framework. On the other hand, in XANES, all scattering pathways, categorized based on the number of scattering events (e.g., (3), (4), (5), etc.), contribute to the absorption cross section. In the EXAFS scenario, the photoelectron undergoes scattering interactions with only a single neighboring atom, whereas in XANES, contributions from various scattering events collectively influence the absorption cross section.

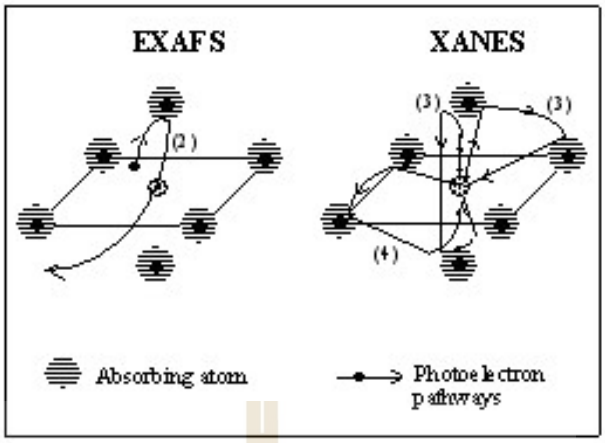

Figure 3.3 XANES and EXAFS phenomena.

In this thesis, X-ray Absorption Spectroscopy (XAS) experiments were conducted at Beam Line 5.2 of the Synchrotron Light Research Institute (as depicted in (Figure 3.4, BL5.2 SLRI, Nakhon Ratchasima, Thailand). The spectra were acquired in the fluorescence mode, utilizing a Ge (220) double crystal setup optimized for K-edge XAS measurements of transition metal elements. The XAS monochromator provided an energy resolution ($\Delta E/E$) of 2×10^{-4} eV.

For data processing, the ATHENA and ATEMIS programs (Ravel and Newville, 2005) were employed. These programs were instrumental in normalizing, correcting, and evaluating each measured X-ray Absorption Near Edge Structure (XANES) and Extended X-ray Absorption Fine Structure (EXAFS) spectrum. The meticulous use of these tools ensures the accuracy and reliability of the XAS data analysis throughout the study.

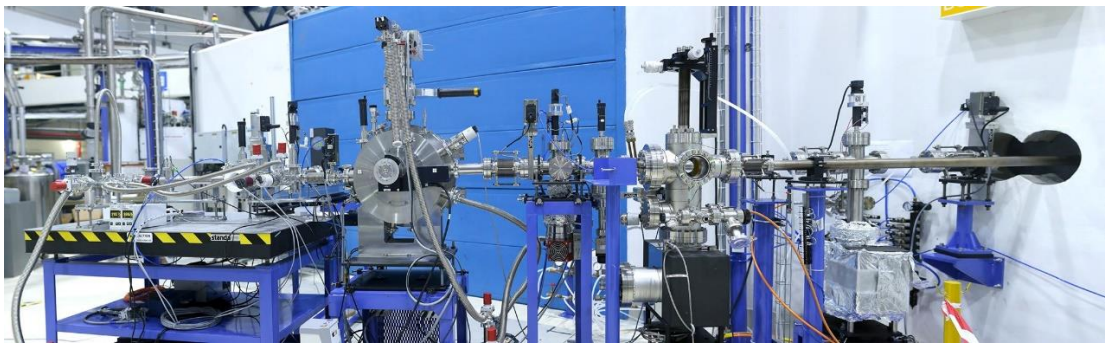

Figure 3.4 Layout of BL5.2 at the Synchrotron Light research Institute (SLRI) in Thailand.

3.2 XANES

A commonly employed term to encompass the examination of spectra obtained through X-ray absorption spectroscopy operations is "X-ray absorption near-edge structure" (XANES). This spectroscopic approach facilitates an element-specific and locally bonding-sensitive study, allowing for the calculation of the partial density of empty states within a molecule. The XANES spectra result from fundamental mechanisms, including the photo absorption of an X-ray into a core level, followed by photoelectron emission and filling of the core hole by an electron in another level. Additionally, fluorescence contributes to the spectra by filling the core hole with an electron in another level, followed by the emission of an Auger electron (Henderson et al., 2014).

Furthermore, X-ray Absorption Near-Edge Structure (XANES) spectra serve as a valuable tool for measuring the oxidation state, phase, and structure of a given sample. This capability is rooted in four distinctive characteristics of XANES spectra, collectively known as the fingerprint technique. The first component is the absorption edge, which is influenced by the sample atom's oxidation state. Typically, as the oxidation state changes, the absorption edge increases by approximately ~3 eV. Consequently, XANES becomes a powerful method for determining the oxidation state of each oxide. The second element is the pre-edge, a small peak appearing just before the absorption edge. The peak height is significantly influenced by the symmetry of the atomic structure. For instance, in less symmetrical structures like tetrahedral sites, the peak height is high, whereas in highly symmetrical structures, the peak height is low. Two other distinct features in the XANES spectrum are the spectral spire, also known as the white line, and the area after the spire, induced by multiple scattering. As illustrated in Figure 3.5, XANES proves effective in distinguishing between various oxide phases due to these distinctive features.

Due to the restricted kinetic energy range (5-150 eV) within the XANES region, beginning approximately 5 eV beyond the absorption threshold, the amplitude of photoelectron backscattering by neighboring atoms becomes quite substantial. This

phenomenon results in the predominance of numerous scattering events in XANES spectra. In contemporary scientific applications, the most prevalent use of XANES has been to investigate the oxidation state and coordination environment of transition metals such as Manganese (Mn), Vanadium (V), and Iron (Fe) in various materials, including minerals and amorphous substances like glasses and melts.

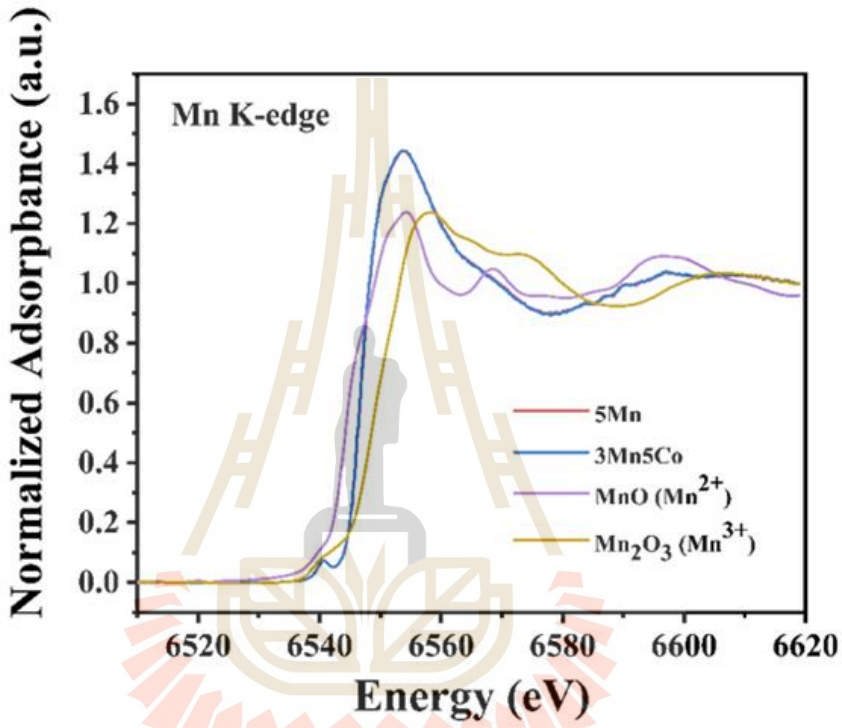

Figure 3.5 Samples from the manganese K-edge XANES spectrum.

In this study, normalized XANES spectra of all samples at the Mn K-edges were compared with those of standard materials exhibiting different Mn oxidation states, including MnO (Mn^{2+}), MnO_2 (Mn^{4+}), and Mn_2O_3 (Mn^{2+}/Mn^{3+}). The determination of the Mn oxidation state ratio was achieved by fitting the linear combination of two distinct oxidation states, derived from the calculation results, to the experimental XANES spectra using ATHENA.

3.3 EXAFS

Extended X-ray Absorption Fine Structure (EXAFS) is a phenomenon characterized by the distinctive oscillations observed in x-ray absorption above an x-ray absorption edge. This phenomenon occurs when an incident x-ray photon possesses enough energy to eject an electron from the inner shells of its atom. The ejected electrons form an outgoing photoelectron wave that can be backscattered from nearby atoms. Notably, the characteristic oscillations originate not only from the outgoing photoelectron but also from the backscattered photoelectron. In the high kinetic energy range (150-2000 eV), the final state of the excited photoelectron is predominantly determined by single backscattering events due to the low amplitude of photoelectron scattering. The interaction of the outgoing photoelectron with neighboring atoms is illustrated in Figure 3.6.

The interference between the outgoing and backscattered photoelectron waves is contingent on variations in the electron density of the absorbing atom, which, in turn, is influenced by the energy of the ejected photoelectron. Constructive interference enhances both the electron density and the probability of photon absorption. As a result, the oscillations observed above the edge stem from changes in interference, transitioning from destructive to constructive patterns and vice versa. Additionally, the nature of these oscillations is highly sensitive to the short-range order in materials. Therefore, Extended X-ray Absorption Fine Structure (EXAFS) proves to be a valuable tool, particularly applicable to amorphous systems such as glasses and liquids (Filipponi, 2001, Greaves, 1985). The photoelectron travels as a spherical wave with a wavelength $\lambda = 2k\pi$ with:

$$k = \sqrt{\frac{2m_e}{\hbar}(E - E_0)} \approx \sqrt{0.2625(E - E_0)} \tag{3.3}$$

Where E_0 is the edge energy.

E is the incident x-ray photon energy.

k is a photoelectron wave number.

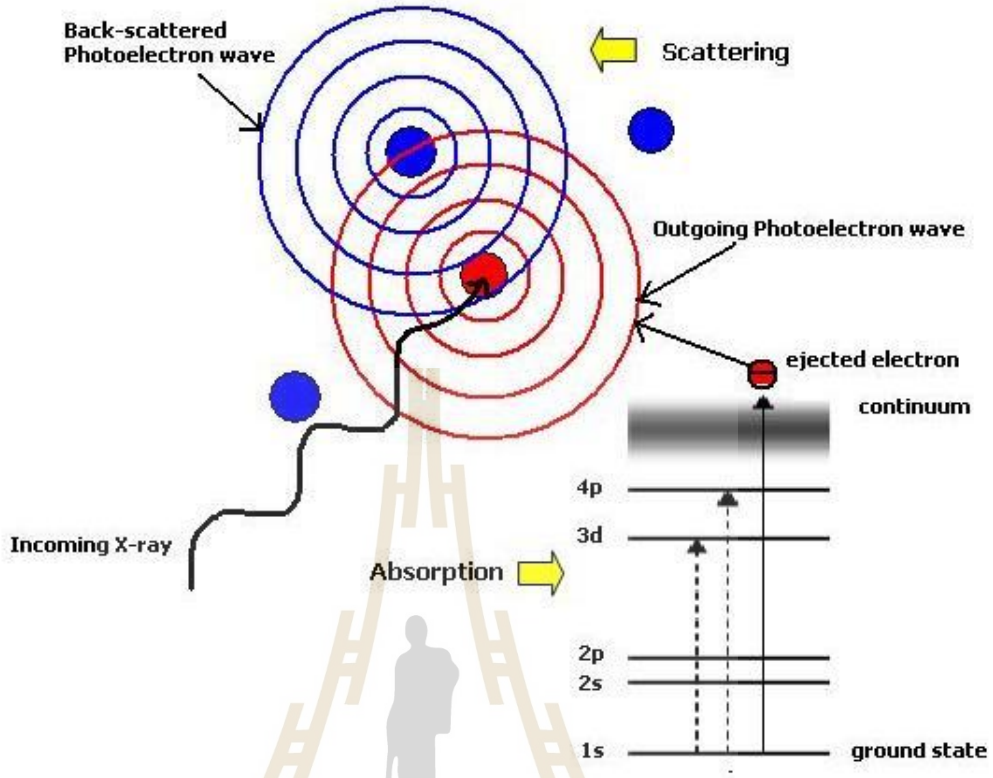

Figure 3.6 Illustration of photoelectron backscattered from the surrounding atom, red circle and blue circles are an absorbing atom and scattering atoms respectively.

In the absence of interference effects, corresponding to isolated atoms, the absorption coefficient is denoted as $\mu_0(k)$. The Extended X-ray Absorption Fine Structure (EXAFS) signal is then regarded as the deviation in absorption from this baseline and is conventionally expressed as:

$$\chi(k) = \frac{\mu(k)-\mu_0(k)}{\mu_0(k)} \tag{3.4}$$

Where $\mu_0(k)$ is the flat absorption of the selected atom.

$\mu(k)$ is the oscillating contribution to the backscattered photoelectron.

The EXAFS oscillation, $\chi_i(k)$ is the sum of modified sine waves with different frequency and phase from each backscattering coordination shell j, around the centered atom i which can be generally written as:

$$\chi_i(k) = \sum_j A_j(k) sin\, \psi_{ij}(k) \quad (3.5)$$

Where A_j is the total backscattering amplitude of the jth shell of backscattering atoms.

$\psi_{ij}(k)$ is the corresponding total phase function.

Multiple Scattering (MS) involves an event where the photoelectron is scattered by more than one surrounding atom before returning coherently to the absorbing atom. A scattering path is defined by the number of legs, accounting for 2, 3, or 4 legs, through which the photoelectron travels (with the possibility of more paths). For each scattering path, the amplitude and the phase shift are calculated separately (O'day et al., 1994), and the effect of multiple scattering is already included in the EXAFS equation (3.6). MS effects can significantly influence the EXAFS signal, with approximately 90% of the total EXAFS signal contributed by single scattering effects. In certain cases, especially in amorphous materials, only single scattering events may be sufficient to produce an EXAFS spectrum that accurately reflects the local structure of such materials.

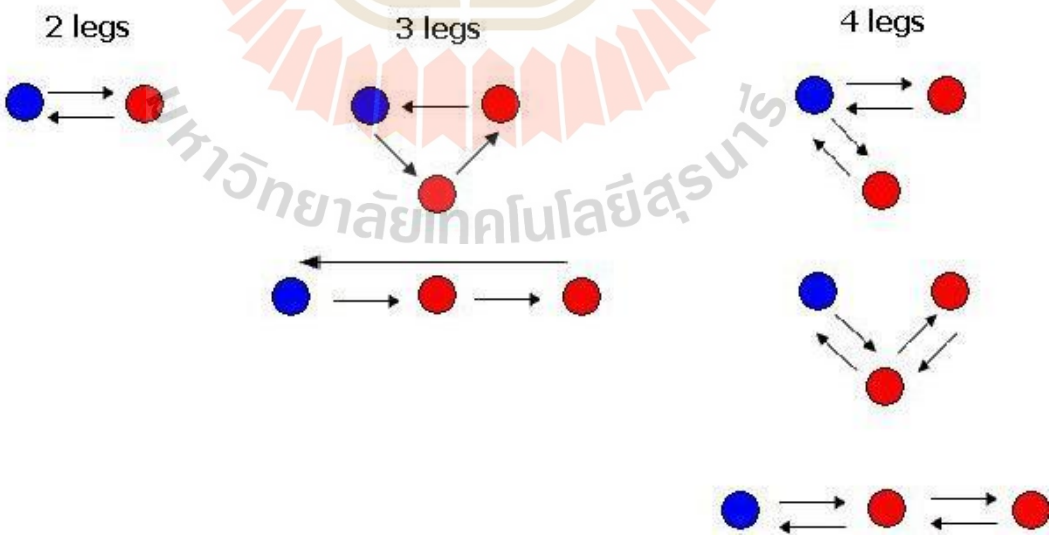

Figure 3.7 Examples of scattering paths consisting of 2, 3 and 4 legs where the arrows note for the legs and the blue and red spheres represent the absorbing atoms and surrounding atoms, respectively.

From the development of scattering theory including the contributions of multiple scattering equation (equation 3.5) can be written to be the standard EXAFS equation as:

$$\chi_i(k) = S_0^2 \sum_j \frac{N_j |f_j(k)|}{k|R_j^2|} exp(-2k^2\sigma_j^2)\, exp\left(\frac{-2R_j}{\lambda_j(k)}\right) sin[2kR_j + \phi_{ij}(k)] \quad (3.6)$$

Where N_j is number of backscattering atoms in the jth shell.

R_j is distance between the central atom i and the backscattering atoms in the jth shell in term of single scattering.

S_0^2 is amplitude reduction factor.

$f_j(k)$ is effective amplitude function for each scattering path.

$exp(-2_k^2\sigma_j^2)$ is Debye-Waller factor in the harmonic approximation with a Gaussian distribution in probability density.

σ_j is Debye-Waller parameter accounting for thermal and disorder in structure.

$\lambda_j(k)$ is photoelectron mean free path.

$exp\,(\frac{-2R_j}{\lambda_j(k)})$ is mean free path factor.

$2kR_j + \phi_{ij}(k)$ is total phase equal to $\psi_{ij}(k)$.

$\phi_{ij}(k)$ is phase shift due to the coulomb potential of the central atom i and the back backscattering atom j.

In this case the EXAFS signal of disorder materials can be calculated from the partial distribution functions, $g_{\alpha\beta}(r)$ where the effect of a non-Gaussian distribution of a probability density of atom j surrounding atom $i, P(r)$, can be modelled by employing a cumulant expansion method. The effect of non-Gaussian disorder affects

not only result to the Debye-Waller factor, it will affect the phase shifts as well. Equation 3.5 can be written in an another form :

$$\chi_i(k) = \sum_j \frac{F_j(k)}{kr_j^2} sin(2k\, r_j + \phi_{ij}(k)) \tag{3.7}$$

Or in the more general form (Koningsberger and Prins, 1987) :

$$\chi_i(k) = Im \sum_j \frac{S_0^2 F_j(k)}{k} \int \frac{P(r_j,\Lambda)}{r_j^2} \exp\left(i\left(2kr_j + \phi_{ij}(k)\right)\right) dr_j \tag{3.8}$$

Where

$$P(r_j, \Lambda) = P(r_j) exp\ (\tfrac{-2r_j}{\Lambda}) \tag{3.9}$$

Consider the integral of equation 3.9 $\int P(r_j) exp\ (\frac{-2r_j}{\Lambda}) dr$ we will get

$$\int P(r_j) exp\ (\tfrac{-2r_j}{\Lambda}) dr = \frac{1}{R_0^2} exp\ (i2kR_0) exp\ (-W + i\phi) \tag{3.10}$$

Where $R_0 = \langle r \rangle$ is the average value of r, W and ϕ are defined as the terms of n^{th} order cumulants C_n that

$$-W + i\phi = \sum_{n=1} \frac{(2ik)^n}{n!} C_n \tag{3.11}$$

when $$W = \sigma^2 \frac{(2k)^2}{2!} - C_4 \frac{(2k)^4}{4!} + \cdots \tag{3.12}$$

and $$\phi = 2k\Delta R - C_3 \frac{(2k)^3}{3!} + \cdots \tag{3.13}$$

In general cases of disorder systems, four cumulants are usually sufficient and from the approximation, equation 3.8 can be written for the disorder EXAFS system as:

$$\chi_i(k) = Im \sum_j \frac{S_0^2 N_j F_j^{eff}(k)}{k(R_{0,j}+\Delta R_j)^2} exp\left[-2k^2\sigma_j^2 + \frac{2}{3}k^4 C_{4,j}\right] exp\left[i\left(2k\left(R_{0,j} + \Delta R_j\right) - \frac{4}{3}k^3 C_{3,j} + \phi_j^{eff}(k)\right)\right] \tag{3.14}$$

From equation 3.14, in this study of amorphous system, the EXAFS spectra will be generated using a MD-RMC EXAFS methodology that the cumulant terms will be compensated by the average of hundreds of cluster models (various r-distances and coordination numbers).

มหาวิทยาลัยเทคโนโลยีสุรนารี

EXAFS signals in this study were also calculated from the MD and MD-RMC configurations by extracting the individual clusters within the restricted distance of the first peak of the partial distribution function, $g(r)$, of the absorbing atom and neighboring atoms such as Mn and O atoms. The FEFF code was used to calculate all spectra. After calculating the EXAFS signal for each cluster from the simulation, all the generated EXAFS signals were averaged properly and finally compared with the corrected EXAFS spectra after normalization. Chapters V will show the results of the MD-RMC EXAFS calculation based on this methodology.

มหาวิทยาลัยเทคโนโลยีสุรนารี

CHEPTER IV
COMPUTER SIMULATION TO CHARACTERIZATION GLASS STRUCTURE

4.1 Introduction

In recent years, various techniques have been developed to analyze and generate more detailed structural models of glasses from diffraction data. Theoretical models can be obtained through Molecular Dynamics (MD) simulation and Monte Carlo methods. However, in recent times, data fitting or refinement procedures based on these methods have also been developed, including the Reverse Monte Carlo (RMC) method. In addition to these direct structural probes, spectroscopy techniques, particularly Extended X-ray Absorption Fine Structure (EXAFS), are increasingly applied to structural studies of amorphous systems, especially liquids and glasses. A.Filipponi demonstrated that when carefully applied, EXAFS proves to be a fruitful technique for obtaining information about the local environment of a specifically targeted atom type in a disordered material, in terms of partial pair distribution functions, $g(r)$ (Filipponi et al., 2000).

In this thesis, I have opted to integrate multiple techniques, namely EXAFS, Molecular Dynamics (MD), and Reverse Monte Carlo (RMC), to achieve a more precise structural model for the manganese lithium borate-base glasses discussed earlier. Enhanced structural models for these glasses are particularly valuable in the context of borate-base glasses, primarily due to their electrical properties and potential applications as cathode materials (Yamada et al., 2010). Hence, in this chapter, a fundamental improved structural model for these glasses will be established by showcasing the amalgamation of several techniques.

4.2 Molecular Dynamic simulation

Molecular Dynamics (MD) simulation is a theoretical tool used for modeling the detailed microscopic behavior of various systems, encompassing glasses, liquids, solids, polymers, surfaces, and clusters. In an MD simulation, the classical equations of motion governing the microscopic time evolution of a system with many bodies are numerically solved, considering the appropriate boundary conditions for the system's geometry or symmetry (Bush et al., 1994, Woodley et al., 1999). This method allows the monitoring of microscopic mechanisms of energy and mass transfer in chemical processes, enabling the calculation of dynamical properties such as absorption spectra, rate constants, and transport properties. Additionally, MD simulation can be employed to sample from a statistical mechanical ensemble and determine equilibrium properties (see Figure 4.1). These properties include average thermodynamic quantities (pressure, volume, temperature, etc.), structure, and free energies along reaction paths (Alder and Wainwright, 1959).

In this thesis, a pair potential known as Buckingham Potentials was employed using the MD simulation package DL_POLY version 4.09 (Todorov et al., 2006). Equation 4.1 illustrates the potentials utilized in this simulation.

$$\varphi_{ij}(r) = A_{ij} exp\left(\frac{-r_{ij}}{\rho_{ij}}\right) - \frac{C_{ij}}{r_{ij}^6} + \frac{q_i q_j}{4\pi\varepsilon_0 r_{ij}} \tag{4.1}$$

Where ρ_{ij}, A_{ij} and C_{ij} are the parameters derived from an empirical calculation. In this, the first two terms are the Buckingham potentials, and the last term denotes the Coulomb potentials.

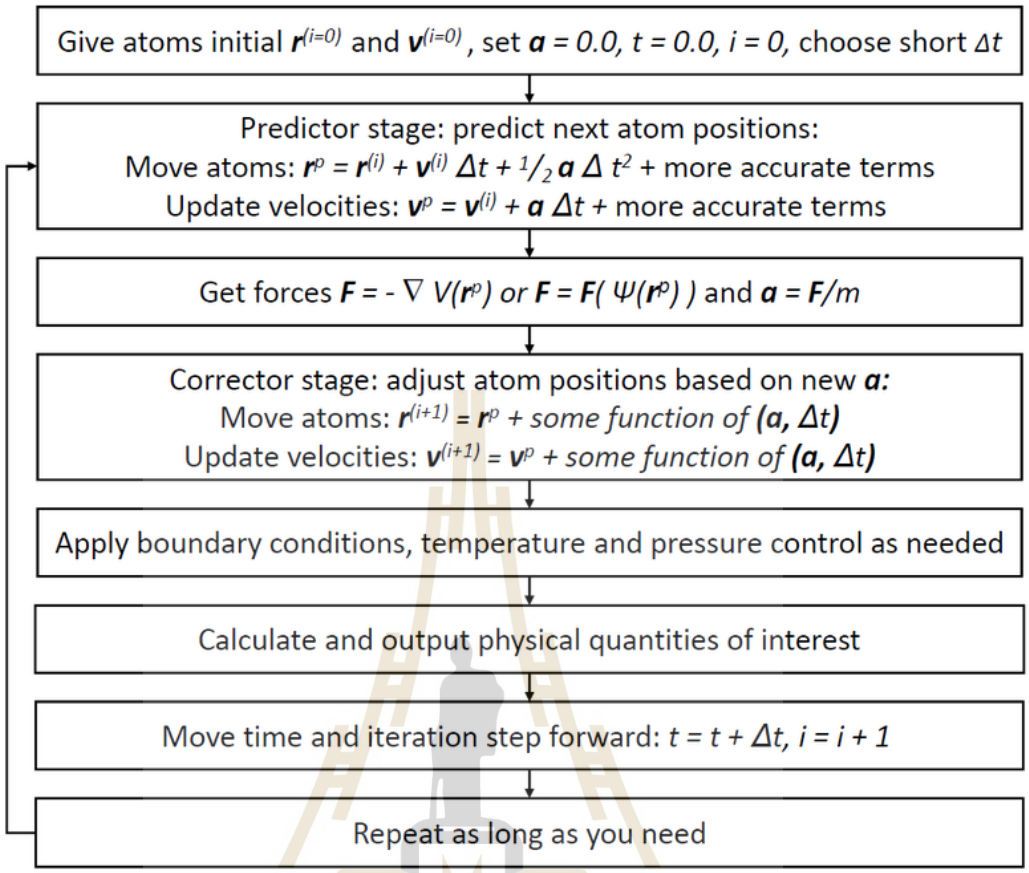

Figure 4.1 Simplified schematic of the Molecular Dynamic algorithm.

4.3 Reverse Monte Carlo refinement

The basic concept of the RMC technique is straightforward. It operates with a box of atoms at a plausible sample density. Once a satisfactory fit is achieved, all atoms are randomly moved while the structure factors are generated and compared to the data. Typically, the input data consists of neutron diffraction, X-ray diffraction, Extended X-ray Absorption Fine Structure (EXAFS), and Nuclear Magnetic Resonance (NMR). If the fit is unsatisfactory, the atoms are randomly repositioned, recalculating the structure factors with each move until a minimum is attained.

The modeling involves a configuration of atoms in a box with periodic boundary conditions. The pair distribution function $g^C(r)$ and total structure factor $A^C(Q)$ of the

configuration are calculated and compared to the experimentally determined functions $g^E(r)$ or $A^E(Q)$. Following each random move of the atoms in the box, $A^C(Q)$ is compared to $A^E(Q)$ (or $g^C(r)$ is compared to $g^E(r)$), and a decision is made to accept or reject the move, as illustrated in Figure 4.2 below.

During the RMC modeling of the configuration, several constraints can be applied. One commonly used constraint is related to the closest distance of approach between two atoms. Chemical information about bond lengths may prohibit atoms from coming too close. For each pair of atom types, a closest approach distance can be specified. The modeled configuration provides information such as partial pair distribution functions, angular distributions, and insights into the likely locations of atoms (Gereben et al., 2007a).

The RMC technique is predominantly employed for modeling diffraction and EXAFS results. In principle, any experimental technique can be simulated if the measured signal can be expressed as a function of atomic coordinates. When initiating the RMC technique, the initial RMC configuration is constructed from the output configuration of the MD simulation. This is done because obtaining a structure that closely resembles reality is remarkably straightforward when considering only extremely minor atom movements. This process, known as RMC-refinement, is highly effective and is principally employed in this thesis.

มหาวิทยาลัยเทคโนโลยีสุรนารี

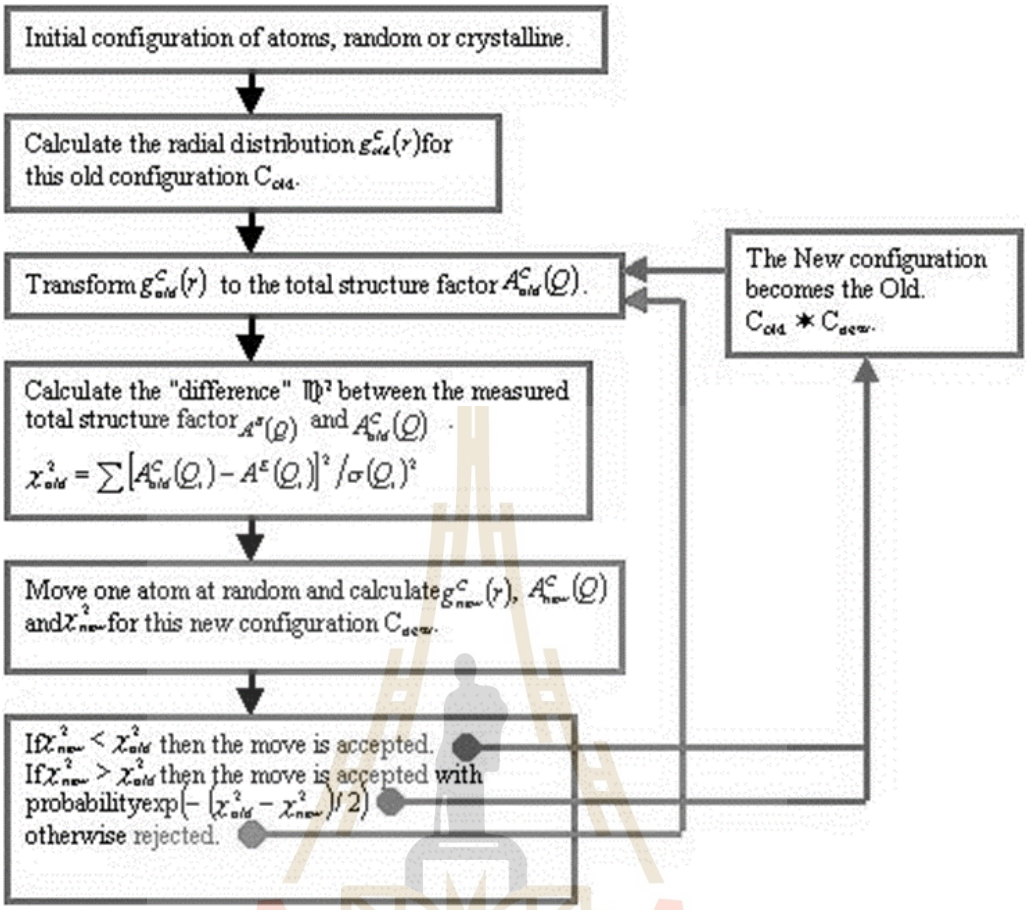

Figure 4.2 Reverse Monte Carlo algorithm.

4.4 FEFF calculation

A comprehensive approach to XAS, encompassing XANES and EXAFS, along with various other x-ray spectroscopies, has become feasible through calculations rooted in standard quasiparticle theory and the RSGF formalism. Typically, simplified models are utilized in these calculations to incorporate many-body effects. Recent theoretical advancements enable the efficient calculation of crucial many-body damping factors in these core-level x-ray spectroscopies using ab initio techniques (Rehr and Albers, 2000, Rehr et al., 2009, Rehr et al., 2010).

The outcomes of the FEFF calculations reveal substantial enhancements in amplitude and phase when employing new methods to calculate inelastic losses, self-

energies, and Debye–Waller factors compared to semi-empirical approaches. This improvement is observed for both near-edge spectra (XANES) and EXAFS (Figure 4.3). The approach considers solid-state effects, such as edge shifts, fine structure, and temperature-dependent Debye–Waller factors, and is applicable to general aperiodic materials.

While the system under investigation is amorphous and lacks a conventional unit cell, the FEFF computation methodology remains applicable. In a typical system, a single unit cell is utilized to compute and represent the entire system. However, in an amorphous system, where no distinct unit cell exists, all relevant atoms are treated as though they are at the center of individual unit cells during each calculation to achieve the final outcome of the system.

มหาวิทยาลัยเทคโนโลยีสุรนารี

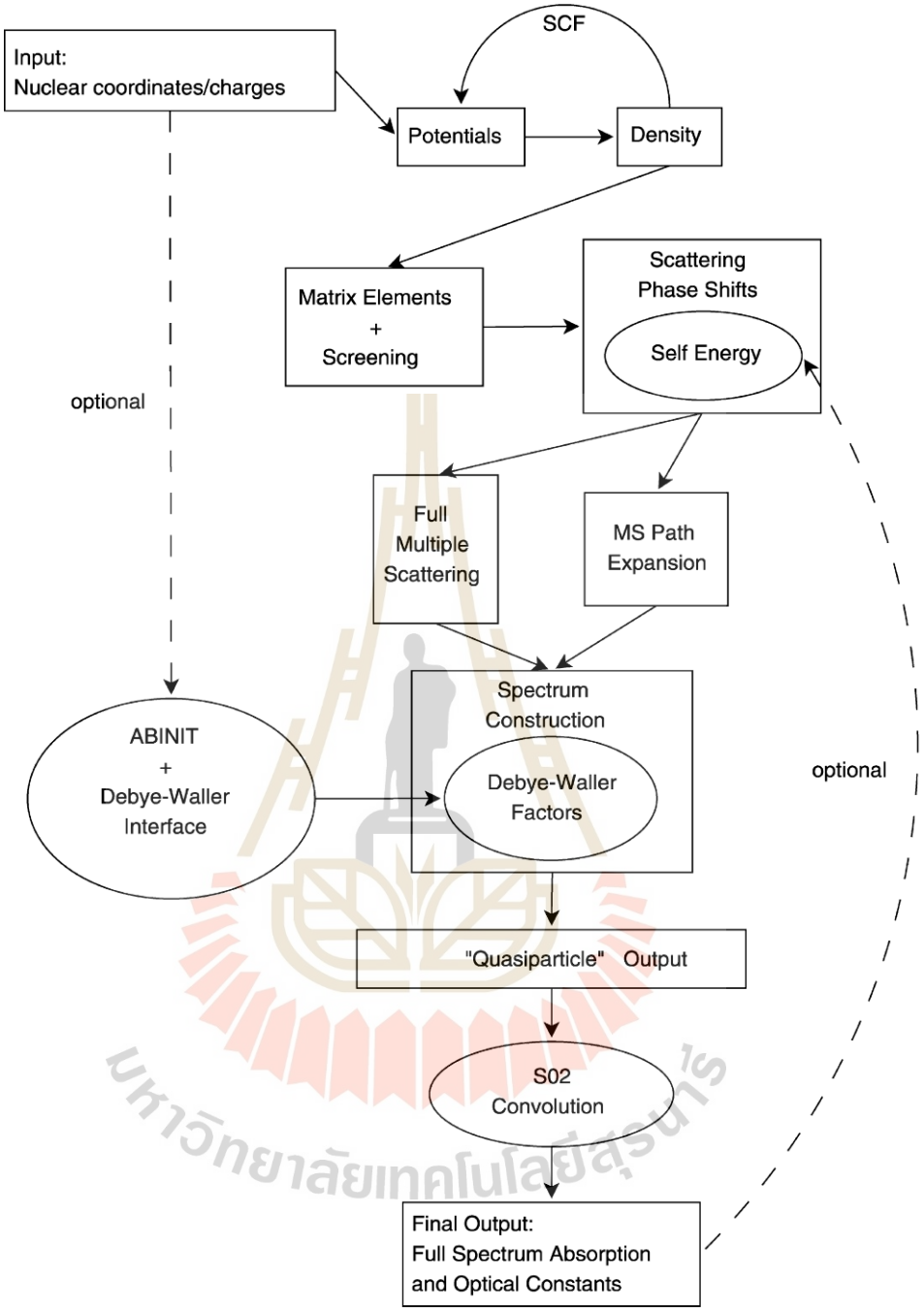

Figure 4.3 Flow diagram for FEFF modules.

CHEPTER V

LOCAL STRUCTURE INVESTIGATION OF MN IN MANGANESE LITHIUM BORATE-BASED GLASS BY COMPUTER SIMULATION AND X-RAY ABSORPTION SPECTROSCOPY

5.1 Introduction

The exploration of novel glass materials has recently garnered significant attention in the field of energy storage resources. While metal oxides in crystalline form, when used as electrode materials, can exhibit high capacities, they also present limitations. In crystalline electrodes, as lithium ions permeate the lattice, structural issues such as lattice expansion and electrode swelling may occur, leading to instabilities during charge/discharge cycles. To address these challenges, manganese lithium borate glasses have been investigated for potential applications as cathode materials. Figure 5.1 illustrates XPS results confirming the mixing of oxidation states of Mn^{2+} and Mn^{3+} in all glass samples. The binding energy values for Mn^{2+} and Mn^{3+} in the Mn $2p_{3/2}$ peak are approximately ~641 and ~643 eV, respectively, while in the Mn $2p_{1/2}$ peak, they are ~653 eV and ~655 eV. The calculated Mn $2p_{3/2}$ ratios of Mn^{2+} (~641 eV)/Mn^{3+} (~643 eV) for the 0.2M-0.8(LB), 0.25M-0.75(LB), and 0.3M-0.7(LB) samples are 42.14/24.87%, 54.27/12.23%, and 56.4/8.34%, respectively (Khajonrit et al., 2018).

Dr. Ragupathi's research specifically focused on $LiMnBO_3$ (Andersson et al., 2002). When analyzing the $LiMnBO_3$ (II) spectrum, it appears as a combination of Li, Mn, and O spectra in Figure 5.2. Figure 5.2(a) indicates a peak at 55.14 eV of binding energy, consistent with similar studies. The binding energies of carbonyl oxygen and M bonding O pairs in Figure 5.2(b) result in peaks in the oxygen range at 532.02 and 529.88 eV, respectively. The B^{1+} oxidation state of boron is represented by the B1s peak in Figure

Figure 5.2(c) at 191.24 eV. Figure 5.2(d) displays Mn (2p) spectra, with binding energies of 642.47 and 653.97 eV corresponding to Mn ($2p_{3/2}$) and Mn ($2p_{1/2}$) energy levels, respectively.

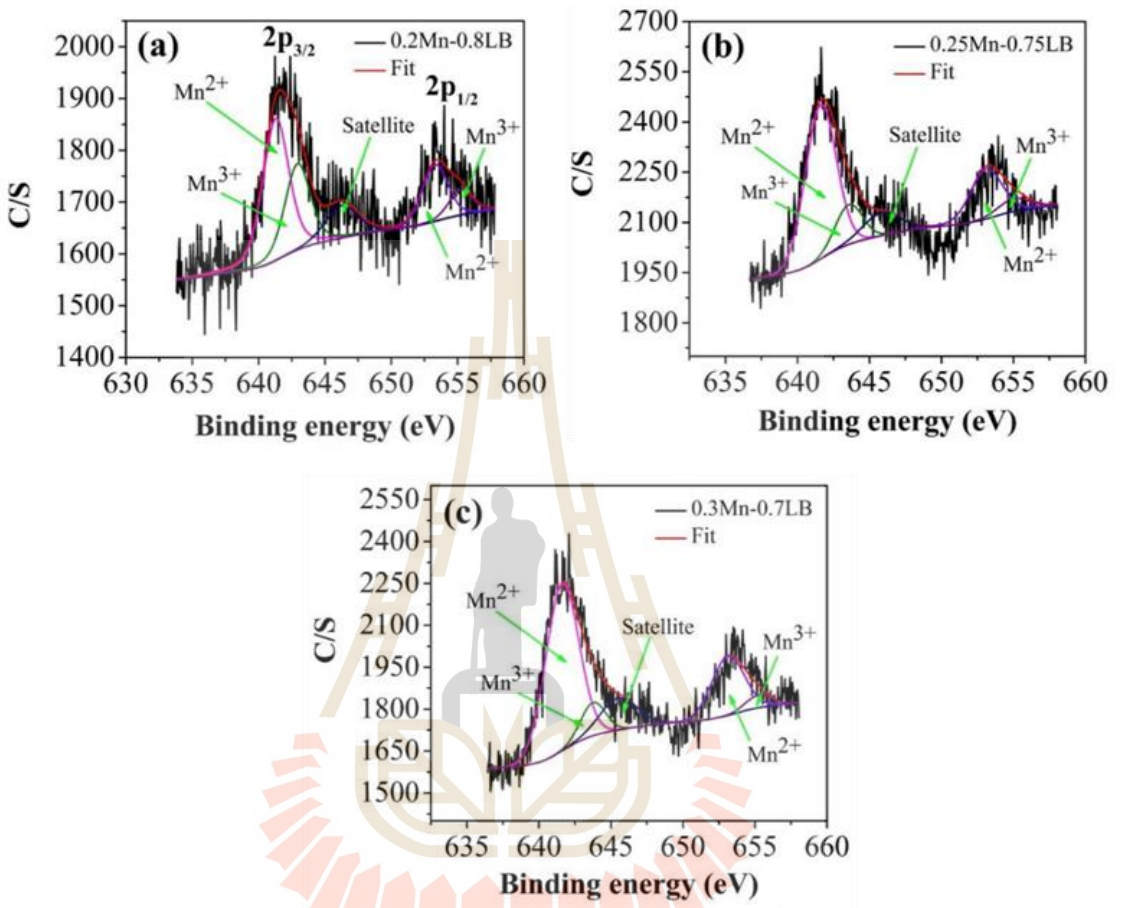

Figure 5.1 XPS profiles of glass samples: (a) $0.2MnO_2$-$0.8(Li_2O$-$2B_2O_3)$, (b) $0.25MnO_2$-$0.75(Li_2O$-$2B_2O_3)$, and (c) $0.30MnO_2$-$0.70(Li_2O$-$2B_2O_3)$ (J.Khajornrit et al., 2018).

To gain deeper insights into the nature of inclusions in these glasses, glass samples were fabricated with compositions $xMnO_2$-$(1$-$x)(Li_2O$-$2B_2O_3)$, where x is 0.2, 0.25, and 0.3, using melt-quenching techniques. X-ray Absorption Spectroscopy (XAS) measurements were employed to investigate the inclusions within the glasses. Additionally, Molecular Dynamics (MD) simulation and Reverse Monte Carlo (RMC) refinement, utilizing Extended X-ray Absorption Fine Structure (EXAFS) data, were employed to reveal detailed information about the local structure concerning manganese in the glasses.

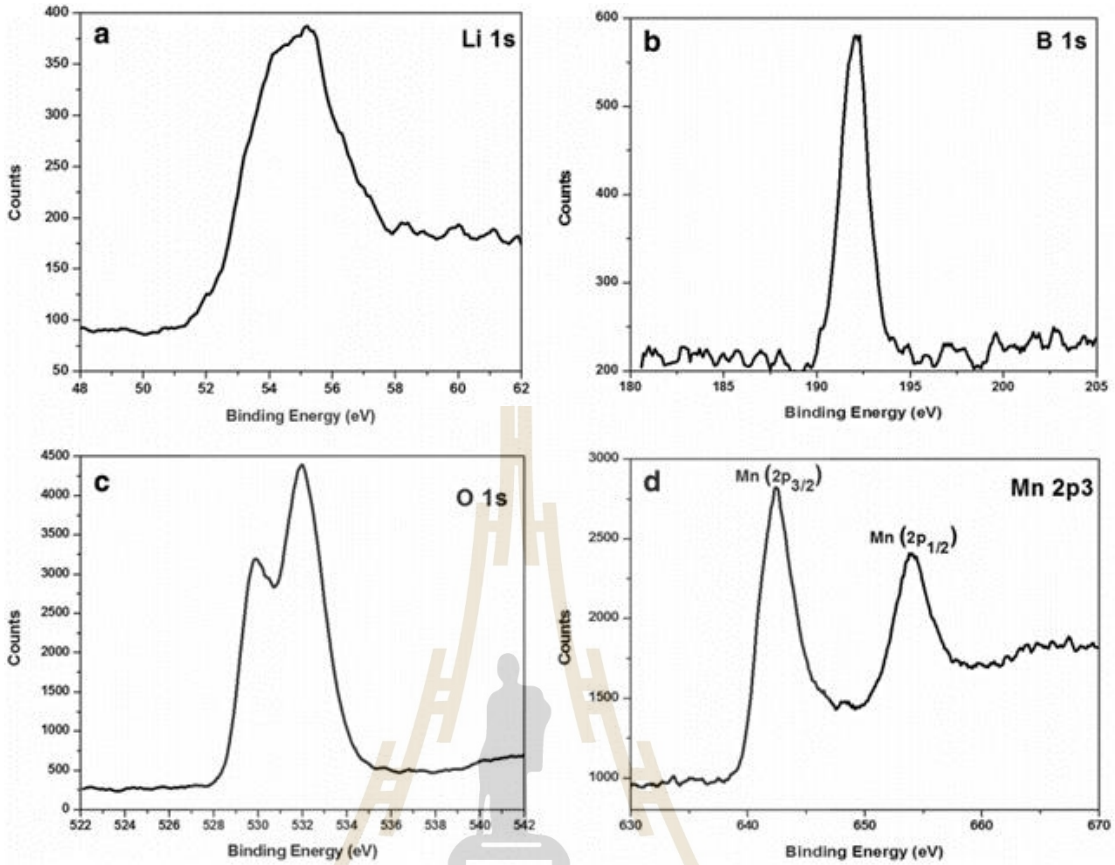

Figure 5.2 XPS spectra of $LiMnBO_3$ (III) materials (a) Li 1s, (b) O 1s, (c) B 1s, and (d) Mn 2p (Andersson et al., 2002).

5.2 Experimental method

5.2.1 Sample preparation

The manganese-lithium-borate glasses were prepared using the melt-quench technique, involving two processes: lithium borate and manganese-lithium borate glass preparation. In the lithium borate preparation, lithium carbonate (Li_2CO_3, 99%) and boric acid (H_3BO_3, 99.8%) were mixed and heated in an electric furnace at 1100 °C for 1 hour. The resulting melts were poured onto a stainless plate, quickly pressed, and then cooled to room temperature (Figure 5.3). For the manganese-lithium borate glass preparation, the obtained lithium borate glass sample and manganese dioxide (MnO_2, 99%) were thoroughly ground and mixed to obtain a fine powder and

a homogeneous mixture. Finally, the homogenized powder was heated at 1,150 ℃ for 1 hour, and the resulting melts were quickly pressed with the stainless plate. The glasses were successfully prepared and exhibited a brown color (Figure 5.4).

Figure 5.3 The prepared lithium borate glass by melt-quench technique.

Figure 5.4 The prepared manganese lithium borate glass by melt-quench technique.

5.2.2 XAS experiment

To investigate the local environment and behavior of Mn in the manganese-lithium-borate (MLB) glass, X-ray Absorption Spectroscopy (XAS) experiments were conducted at BL-5.2, SLRI. The experiment was set up for Mn K-edge in FL-mode with an edge energy of 6539 eV. The manganese oxidation state was examined through the X-ray Absorption Near Edge Structure (XANES) regions, while the neighboring atoms of manganese were studied qualitatively using Extended X-ray Absorption Fine Structure (EXAFS) spectra.

The XANES data were normalized and compared with standard data using the ATHENA program to analyze XAS results. For a detailed understanding of the local environment around Mn atoms in the glass samples, the EXAFS data of the glass structure were assessed and fitted using the first shell model in the ARTEMIS program.

5.2.3 Computer simulation

A molecular dynamic simulation of $Li7Mn(BO3)_3$ was conducted by J. Roos (Roos et al., 2015) using well-established atomistic and Density Functional Theory (DFT) methods. In this study, a MD simulation was performed for $xMnO_2$-(1-x)(Li_2O-$2(B_2O_3)$) (MLB) where x= 0.2, 0.25, and 0.3, respectively. The DL_POLY 4.09 molecular dynamics simulation package was employed, and Buckingham potentials with parameters provided by J.Roos et al. were used, starting with a number density of 2.329 g/cm^3, 2.446 g/cm^3, and 2.622 g/cm^3, respectively. The stoichiometry equation was utilized to represent the atomic number for each element, as shown in the following equation.

$$\frac{g}{MW} = \frac{N}{6.02\times10^{23}} \tag{5.1}$$

Where g is number of density in g/cm^3.

MW is molecular weight of each element.

N is number of atoms.

The parameters used in the potential are presented in Table 5.1. Based on XPS evidence suggesting a mixing of oxidation states for Mn, the ion charges of Mn were determined to be 3+ and 2+. With the exception of the O-O interaction, all like-like interactions were assumed to be purely ionic in nature. The simulation commenced from a random configuration in which the interatomic distances were set according to minimum distance chemical constraints.

Table 5.1 Short-range Buckingham potential parameters for MLB.

Interaction	A (eV)	ρ (Å)	C (eV Å^6)
Li^+ - O^{2-}	638.712146	0.290560	0.00
Mn^{2+} - O^{2-}	2601.394	0.278	0.00
Mn^{3+} - O^{2-}	2580.723796	0.277521	0.00
B^{3+} - O^{2-}	539.797394	0.340031	0.00
O^{2-} - O^{2-}	22764.3	0.149	46.94

Figure 5.5 illustrates that the initial simulation was conducted using an NPT Berendsen thermostat at 2000K with 0.001 ps time steps. The system equilibrated after 10,000 steps and was run for an additional ten million steps (10 ns). After this equilibration, the simulation temperature was rapidly decreased by -100K using the NPT Berendsen thermostat for each calculation step until 300K, with one million steps (1 ns) each, and the box size was optimized by allowing the system to re-equilibrate into a disordered (glassy) form for 100,000 steps in NVT.

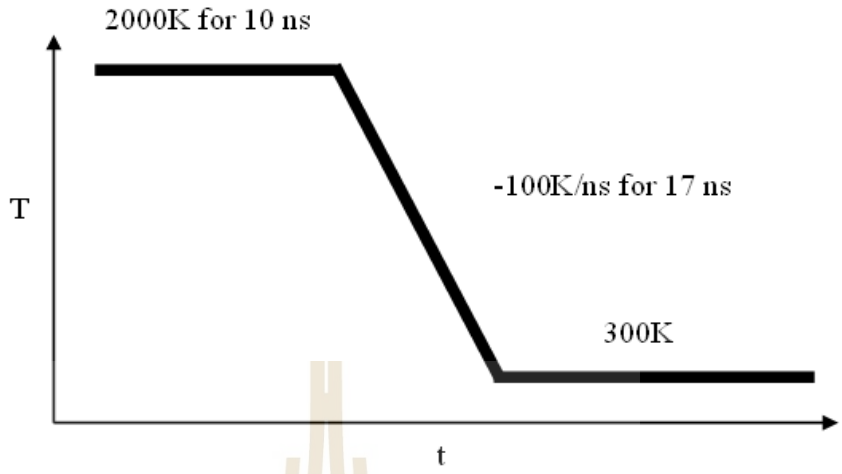

Figure 5.5 Procedure for molecular dynamics simulation.

To determine the precise ratio between Mn^{2+} and Mn^{3+}, the process initiates with a pure Mn^{2+} system and then gradually introduces a subsequent 10% Mn^{2+} to Mn^{3+} in each step until it reaches pure Mn^{3+}. Subsequently, the accurate ratio of Mn^{2+} to Mn^{3+} is established using the ATHENA program's linear combination fitting of XANES spectra of Mn K-edge. These spectra are generated by performing FEFF calculations on all Mn clusters using the FEFF8.2 software. In this process, some O atoms are appropriately removed to neutralize the total charge, as we consider the remaining oxygen in terms of the carbon dioxide generated during the sample melting. The final atomic configuration of the MD simulation serves as the starting point for a Reverse Monte Carlo (RMC) refinement to the experimental data. The structural model generated by the MD simulation is constrained by the use of effective pair potentials. In practice, it is anticipated that three-body interactions will significantly impact the glass's structure. The absence of these interactions is expected to result in significant disparities between the glass structure predicted by the simulation and the experimental findings.

The MD-RMC EXAFS technique requires the RMC coefficient file to generate backscattering factors (amplitudes + phases) using the FEFF algorithm. In this process, the chi.dat file output from FEFF is crucial, where its second column contains

$\chi(k)$, representing the elementary 'response' due to a single neighbor (Jóvári et al., 2007). Given the limited data from our experiments, we specifically focused on the Mn K-edge. To ensure accurate backscattering factors, the self-consistent field (SCF) card should be activated in the FEFF input file. It's important to note that iterative calculations may not always converge, so adjusting SCF parameters (e.g., n_scf and ca) might be necessary to achieve convergence.

Given the scarcity of experimental data, potential parameters were chosen randomly until an optimal set was found before initiating the RMC refinement process. The MD method served as a reliable starting configuration for the Reverse Monte Carlo (RMC) refinement of atom positions within the MD configuration. This aimed to achieve a better fit to the experimental diffraction data.

The MD-RMC refinement procedure was applied to simultaneously refine EXAFS data obtained from both rapidly and slowly quenched MLB glasses. To ensure the correctness of the employed potentials and prevent atoms from diffusing too far from their initial positions, a maximum atom move of 0.05 Å per step was set in the RMC procedure. At the end of the refinement, the deviation of atoms from their initial positions was checked to ensure they had not moved significantly, relative to their ionic sizes. Within a 10 Å cutoff distance, the positions of nearby atoms around Mn were identified, and the FEFF8.2 program calculated the XANES and EXAFS spectra of Mn. The average spectra were then compared with the experimental spectra using an automatic background adjustment in the ATHENA software.

The radial distribution function (RDF, $g(r)$) quantifies the probability of finding a particle at a distance r from another specified particle. It varies significantly for different states of matter such as solids, gases, and liquids, reflecting the distinctive characteristics of each material. The bulk density, denoted as ρ, represents the average density across a liquid and remains constant for a given liquid. On the other hand, the local density, denoted as $\rho(r)$, signifies the density of the liquid at a specific distance r from another molecule, relying on the structural arrangement of the liquid. The RDF

was computed in the DL_POLY software, based on the local density of the system, as expressed in the following equation:

$$g(r) = \frac{dn_r}{4\pi r^2 dr * \rho} \tag{5.2}$$

Where dn_r is a function that computes the number of particles within a shell of thickness dr.

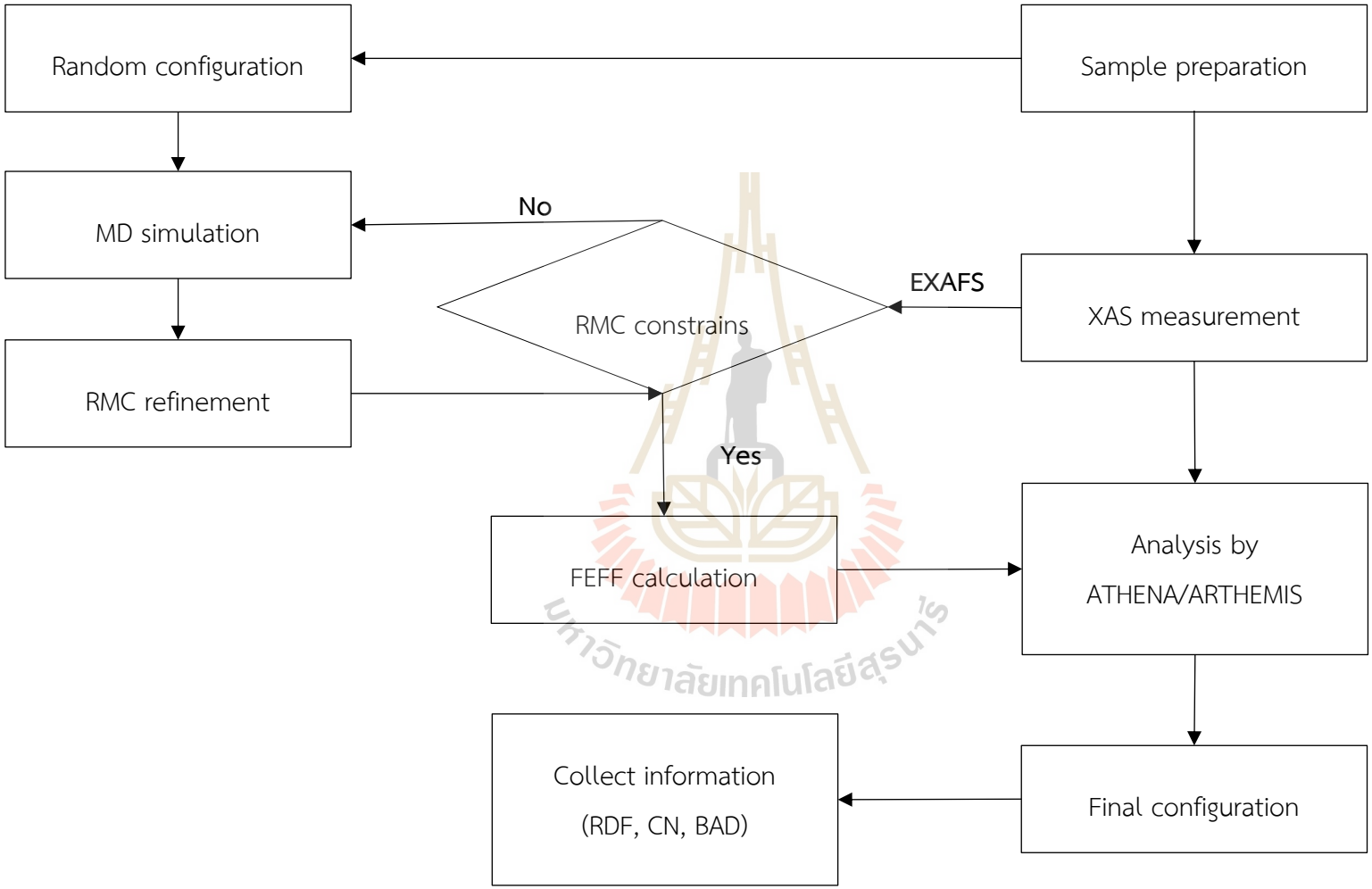

Figure 5.6 Flow chart of this work.

5.3 Result

5.3.1 XAS result

To investigate the electronic excitations of Mn in the MLB glass structure, X-ray absorption spectroscopy (XAS) was employed. Fluorescence mode experiments were conducted with the sample holder fixed at a 45-degree angle to the incident synchrotron light source. Calibration of the Mn K-edge spectra was accomplished using a standard Mn-foil from BL-5.2, resulting in an edge energy of 6539 eV. XANES spectra were explored in the range of 6510–6600 eV.

The Mn spectra features were further analyzed by comparing them with standard Mn compounds, such as MnO (edge energy 6544 eV), Mn_2O_3 (edge energy 6548 eV), and $MnSO_4.H_2O$ (edge energy 6547 eV). Figure 5.7 the normalized Mn K-edge XANES spectra was performed. Edge energy of all spectra represent to manganese oxidation state which is between MnO and Mn_2O_3. While the oscillation feature of all samples is similar to the feature of $MnSO_4.H_2O$, they indicate the mixing oxidation state of the samples. In order of Mn local structure, we are still at a place where we can't go much further with the explanation.

The manganese environment was elucidated through the analysis of the EXAFS spectrum, as depicted in Figure 5.8. The k-space spectrum was transformed into R-space using Fourier transformations within the wavenumber range of 3-9 $Å^{-1}$. Owing to the amorphous nature of the material, the R-space spectrum exhibited a predominant intensity region, specifically the first shell intensity within the range of 1-2 Å, corresponding to oxygen, as illustrated in Figure 5.9.

The parameters derived from the EXAFS fitting, including interatomic distances (R), model coordination numbers, and Debye-Waller factors (σ^2), are presented in Table 5.2. The variation in the interatomic distance of Mn-O with higher Mn content is attributed to the smaller atomic radius of Mn^{2+} (83 pm) compared to Mn^{3+} (64 pm).

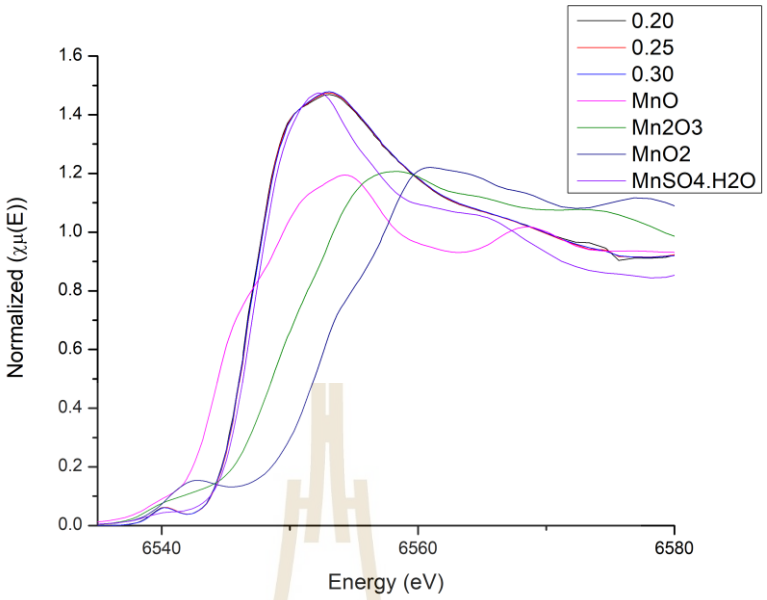

Figure 5.7 XANES spectra of Mn K-edge of $0.2MnO_2$-$0.8(Li_2O$-$2B_2O_3)$, $0.25MnO_2$-$0.75(Li_2O$-$2B_2O_3)$ and $0.3MnO_2$-$0.7(Li_2O$-$2B_2O_3)$ glass samples and standard samples.

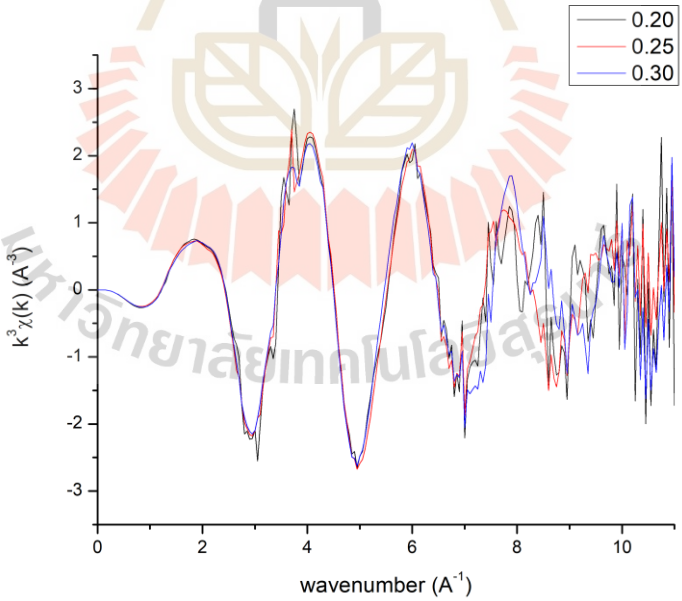

Figure 5.8 The $\boldsymbol{k^3\chi(k)}$ function extracted from the absorption spectrum for MLB glasses at Mn K-edge.

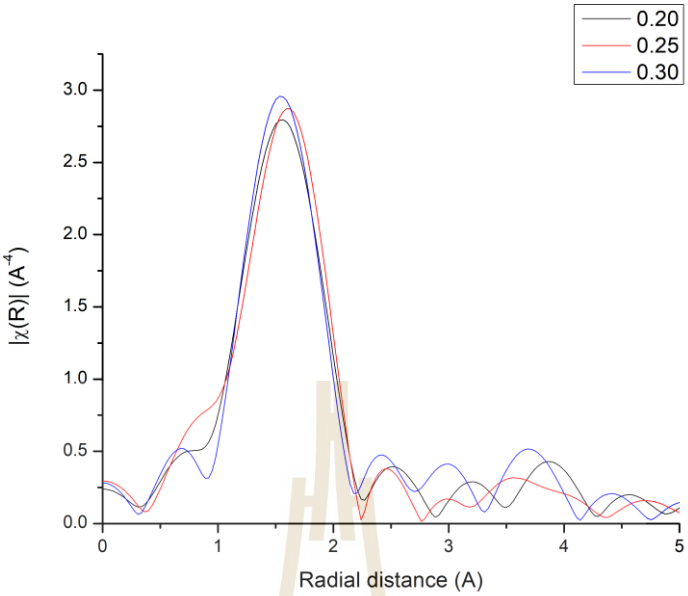

Figure 5.9 The corresponding $|\chi(R)|$ function for MLB glasses at Mn K-edge.

Table 5.2 EXAFS fitting parameters including interatomic distances (R), coordination numbers and Debye Waller factors (σ^2) of MLB glass samples.

Sample	Paths	Coordination number	σ^2	R (Å)
0.20Mn	Mn-O	3.019	0.01169	2.08524
0.25Mn	Mn-O	2.989	0.01169	2.08623
0.30Mn	Mn-O	2.911	0.01169	2.08845

5.3.2 Computer simulation result

5.3.2.1 MD and RMC structure model

The final configurations of 0.2M-0.8LB, 0.25M-0.75LB, and 0.3M-0.7LB are depicted in Figure 5.10-5.12, illustrating Mn^{2+} (pink), Mn^{3+} (purple), B (dark blue), Li (light blue), and O (red). The final densities of these systems are 2.5614 g/cm^3, 2.6043 g/cm^3, and 2.6650 g/cm^3, respectively, influenced by the applied NPT Berendsen thermostat in the cool-down process. The models exhibit fully random atomic positions inside the box, confirming an amorphous system. The radial distribution functions of the 15 pairs for the three models are shown in Figure 5.13-5.15. Despite the absence of crystalline peaks in the results, it is confirmed that the system remains amorphous.

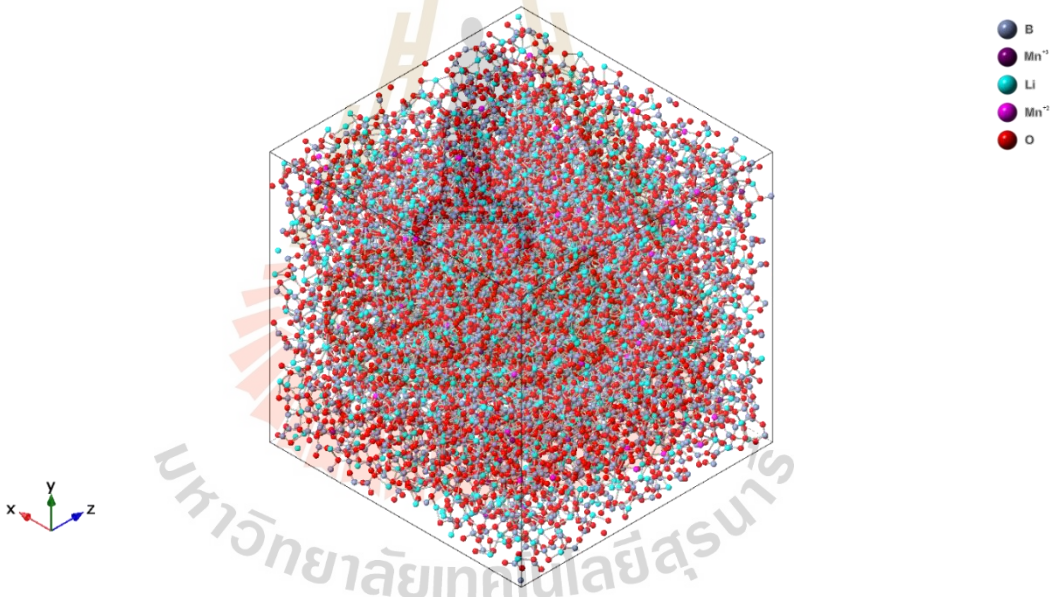

มหาวิทยาลัยเทคโนโลยีสุรนารี

Figure 5.10 View of the structure of 0.2M-0.8LB glasses which show Mn^{2+} (pink), Mn^{3+} (purple), B (dark blue), Li (light blue) and O (red).

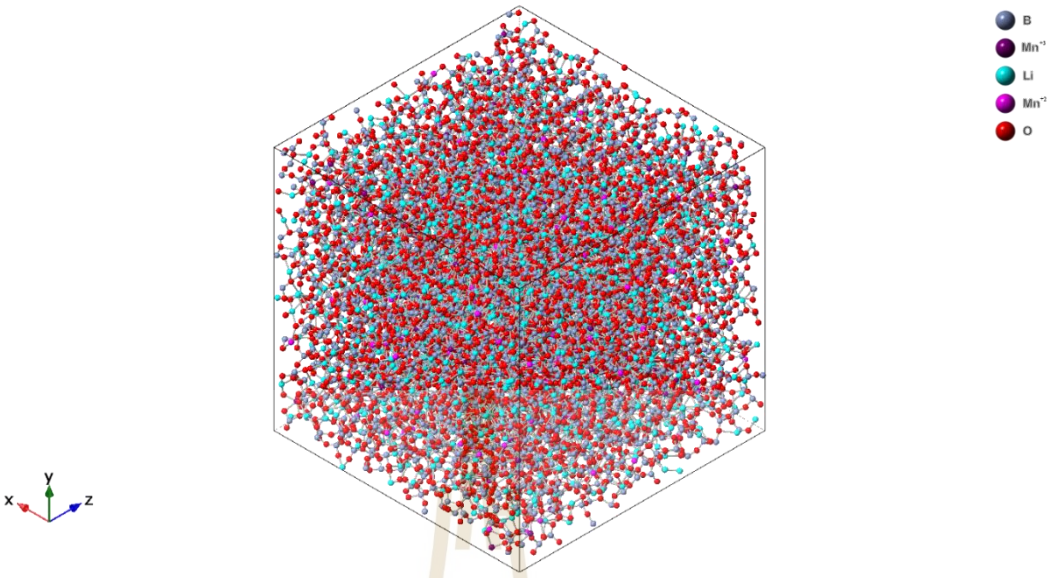

Figure 5.11 View of the structure of 0.25M-0.75LB glasses which show Mn^{2+} (pink), Mn^{3+} (purple), B (dark blue), Li (light blue) and O (red).

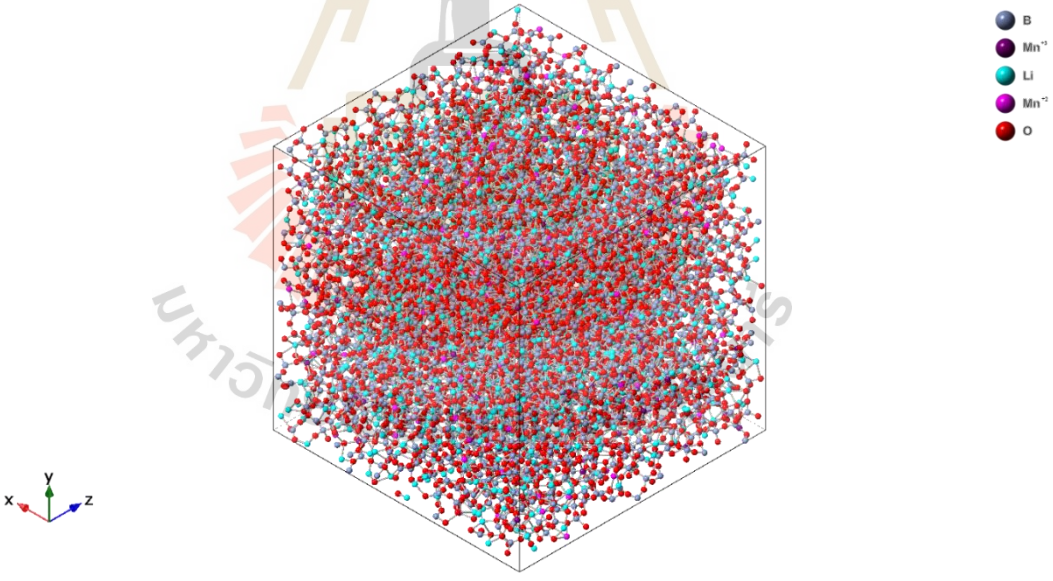

Figure 5.12 View of the structure of 0.3M-0.7LB glasses which show Mn^{2+} (pink), Mn^{3+} (purple), B (dark blue), Li (light blue) and O (red).

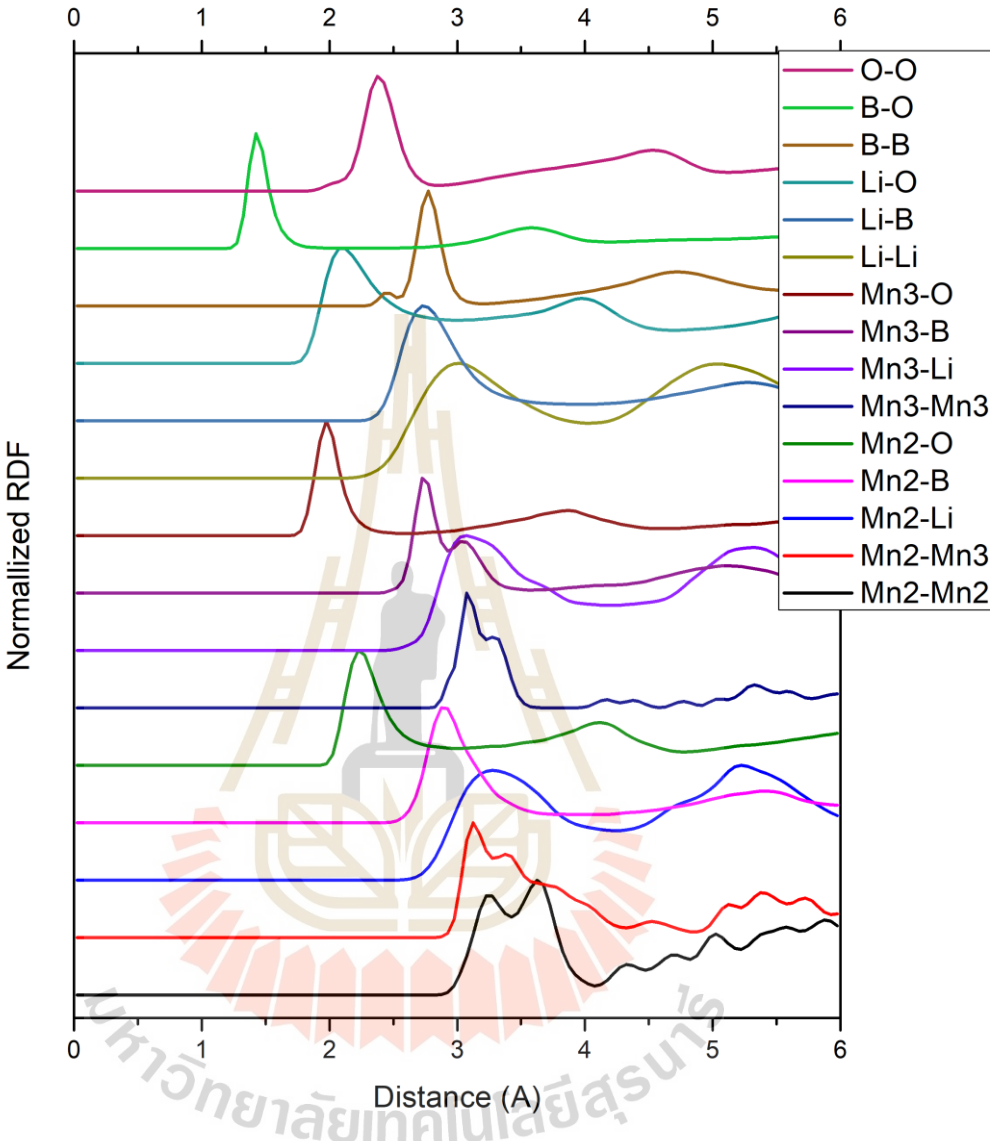

Figure 5.13 15 pairs radiant distribution function of 0.2M-0.8LB glasses.

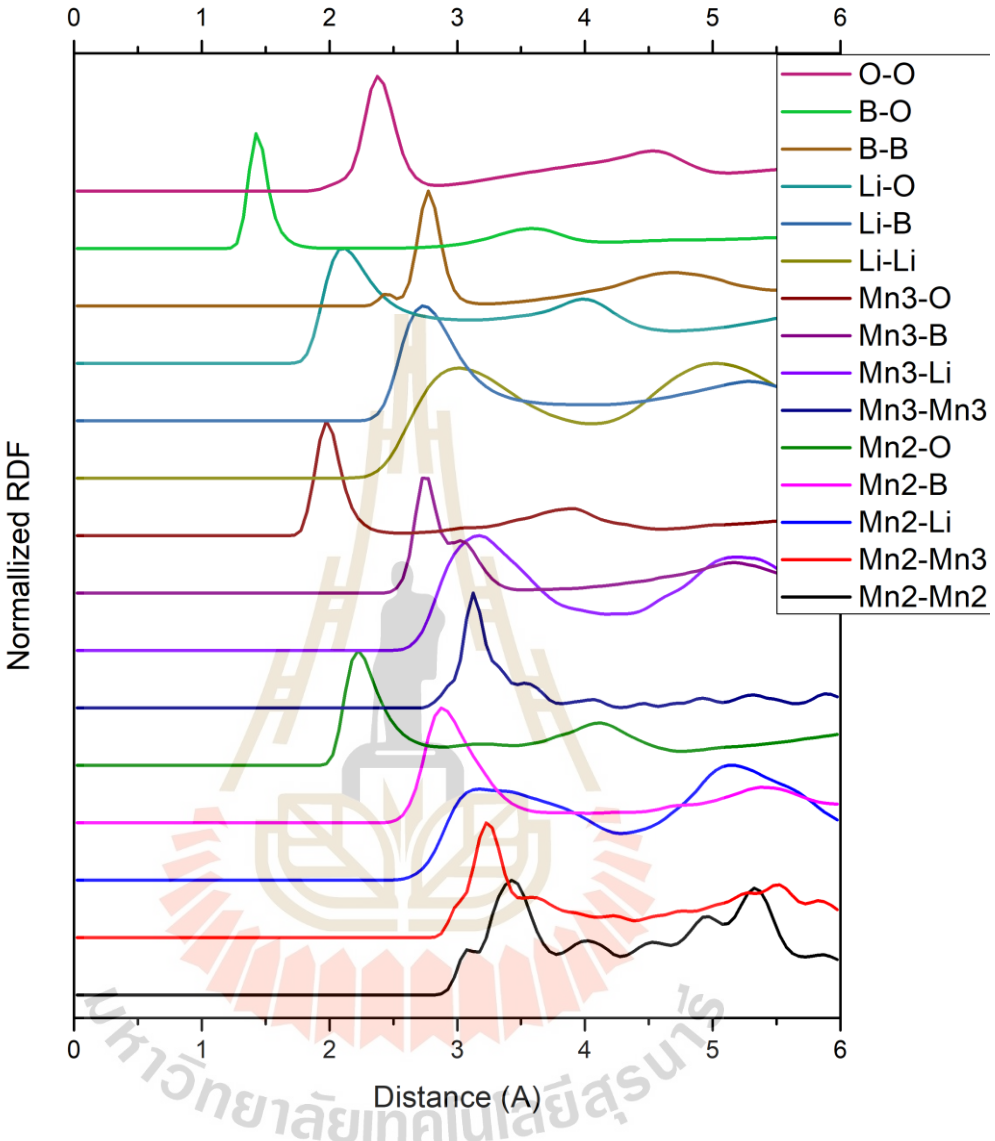

Figure 5.14 15 pairs radiant distribution function of 0.25M-0.75LB glasses.

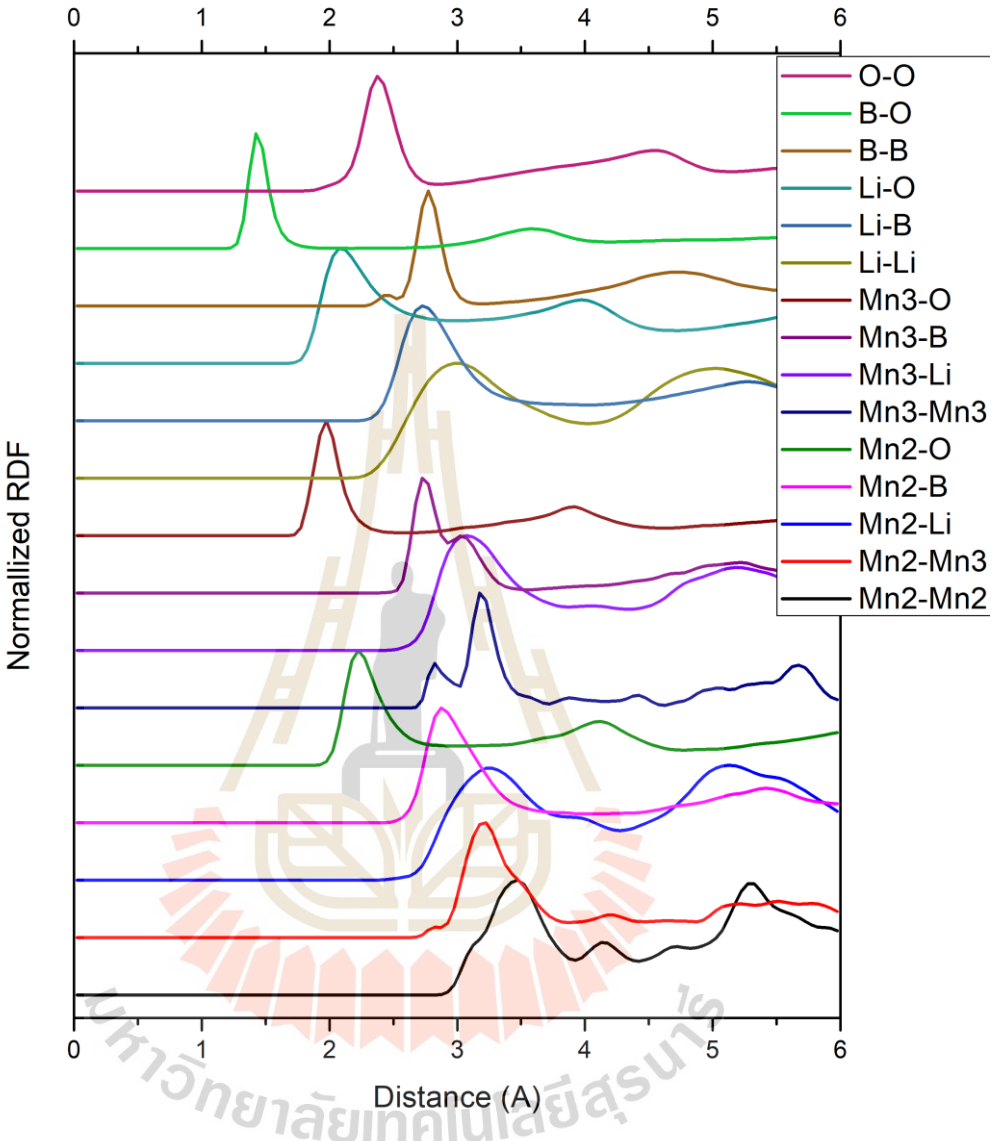

Figure 5.15 15 pairs radiant distribution function of 0.3M-0.7LB glasses.

Figure 5.16-5.18 illustrate the distributions of Mn-O coordination numbers calculated from the final configuration models generated by the isolation program (see APPENDIX A). From this distribution, a similarity is observed between Mn^{2+} and Mn^{3+}, where approximately 30% of Mn^{2+} ions have coordination numbers of 3, around 37% have coordination numbers of 4, approximately 16% have coordination numbers of 5, and about 37% have coordination numbers of 2. For Mn^{3+}, around 36% have coordination numbers of 5, approximately 46% have coordination numbers of 6, and about 13% have coordination numbers of 7. Increasing the Mn concentration has a direct impact on the coordination number, with Mn^{2+} and Mn^{3+} both experiencing considerable increases in 3-fold, 4-fold for Mn^{2+}, and 5-fold, 6-fold for Mn^{3+} increments, respectively.

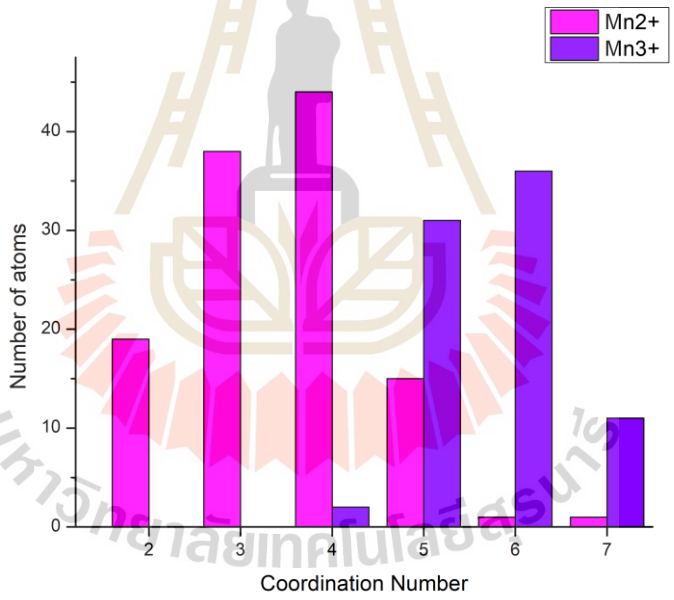

Figure 5.16 The distributions of Mn^{2+}-O (pink) and Mn^{3+}-O (purple) coordination numbers obtained from the calculations for 0.2M-0.8LB glasses.

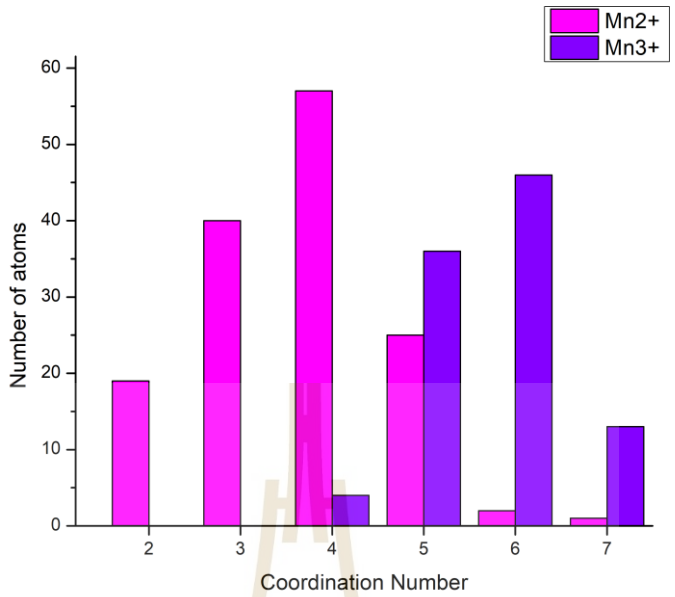

Figure 5.17 The distributions of Mn^{2+}-O (pink) and Mn^{3+}-O (purple) coordination numbers obtained from the calculations for 0.25M-0.75LB glasses.

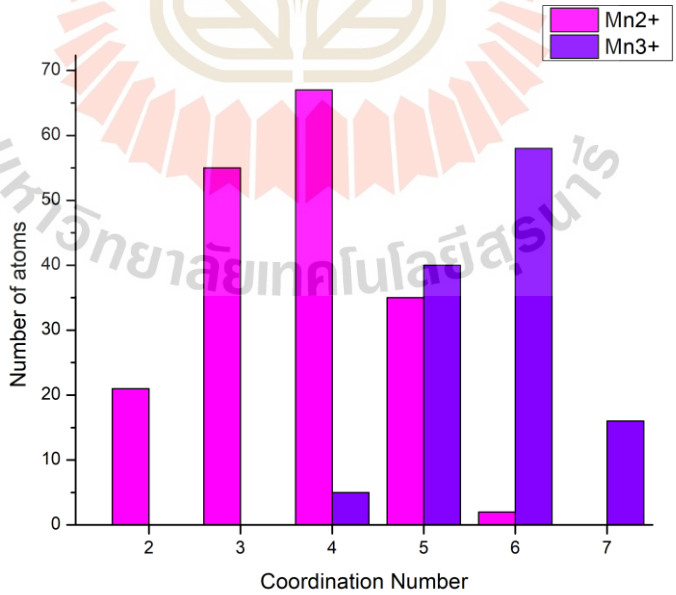

Figure 5.18 The distributions of Mn^{2+}-O (pink) and Mn^{3+}-O (purple) coordination numbers obtained from the calculations for 0.3M-0.7LB glasses.

O-Mn^{2+}-O and O-Mn^{3+}-O bond angle distribution (BAD) values have been calculated and compared with those obtained from the reference configuration (Figure 5.19-5.21) using the program in APPENDIX B. The upper limit of the "bond" has been set to the minimum of the corresponding partial pair correlation functions. A noticeable feature in each case is the peak close to 60°, corresponding to the close packing of three equal hard spheres. Additionally, the BAD shows a broad peak at about 110°. The differences in peak positions of the O-Mn^{2+}-O and O-Mn^{3+}-O BADs can be qualitatively explained by considering the ratio of atomic radii. Mn^{3+} is the smallest among the three atomic species. Therefore, the bond angles centered on Mn^{3+} should shift to higher values compared to the O-Mn^{2+}-O distribution, as the O atom can move closer to the line joining Mn^{2+} atoms.

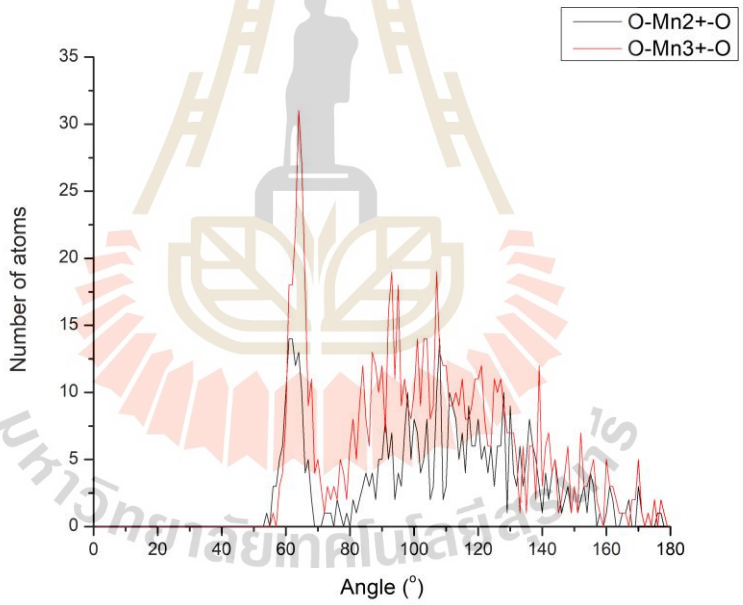

Figure 5.19 The angle distributions of O-Mn^{2+}-O (black) and O-Mn^{3+}-O (red) from the calculations for 0.2M-0.8LB glasses.

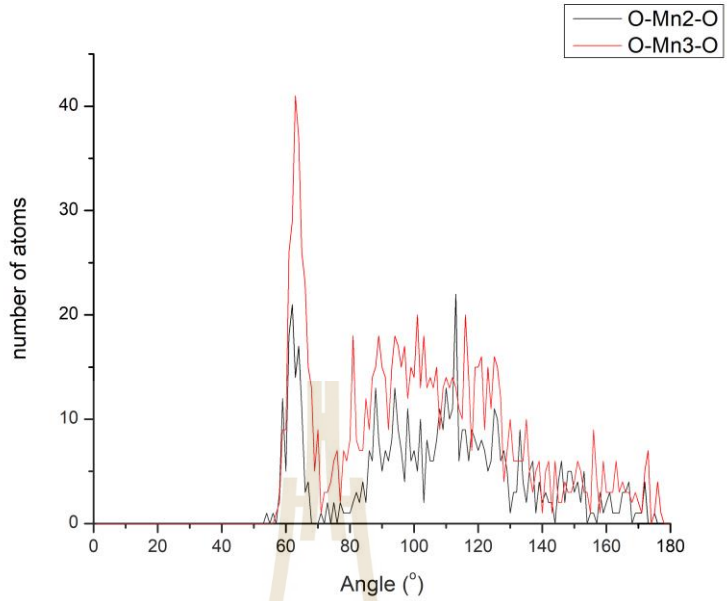

Figure 5.20 The angle distributions of O-Mn^{2+}-O (black) and O-Mn^{3+}-O (red) from the calculations for 0.25M-0.75LB glasses.

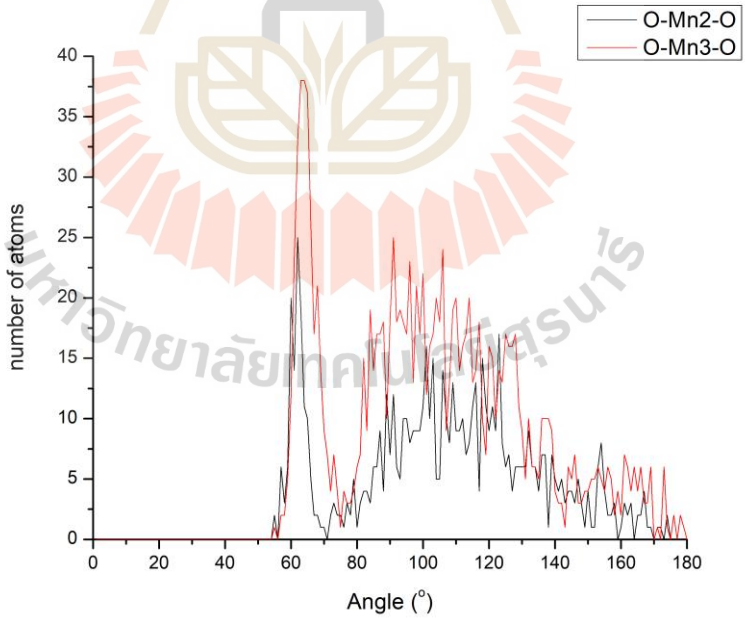

Figure 5.21 The angle distributions of O-Mn^{2+}-O (black) and O-Mn^{3+}-O (red) from the calculations for 0.3M-0.7LB glasses.

5.3.2.2 FEFF calculation

All atomic positions in each Mn cluster were collected by the FEFF convertor program in APPENDIX C. The XANES spectra of MLB glasses from FEFF calculations are shown in Figure 5.22. The absorption edges of all samples are at 6546 eV, consistent with XPS and XANES linear combination fitting, indicating that Mn is in a mixed oxidation state with a Mn^{2+} to Mn^{3+} ratio of approximately 6:4. The features of the calculation and the experiment align fairly well. Some of the white line intensity in the computation was slightly higher than that of the experiment due to the absence of O, which was eliminated during the charge neutralization process.

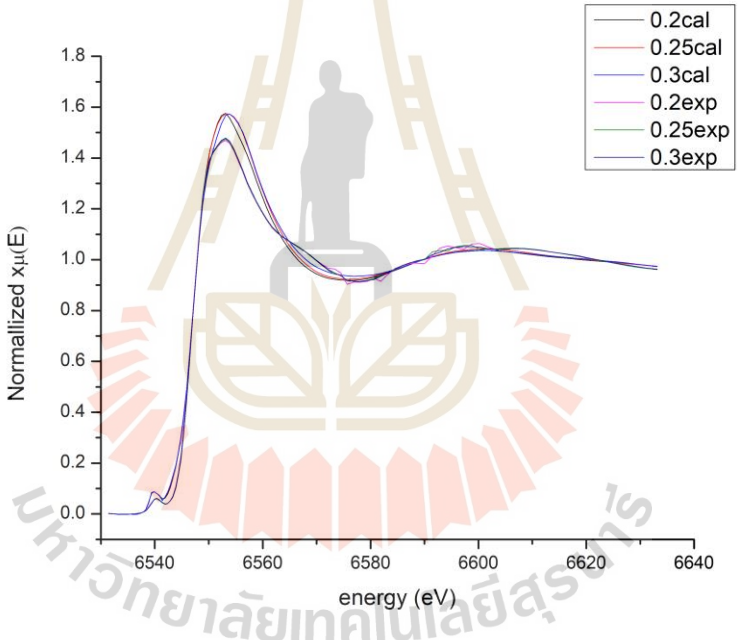

Figure 5.22 XANES calculation spectra of Mn K-edge of 0.2M-0.8LB, 0.25M-0.75LB and 0.3M-0.7LB glass samples and experiment result.

Figure 5.23-5.25 display the comparison of the $k^3\chi(k)$ function and the corresponding $|\chi(R)|$ function between the final calculation and the experiment, showing good agreement. The $k^3\chi(k)$ was converted to R-space by Fourier Transform (FT) within the wavenumber range of 3 - 9 $Å^{-1}$ in the ATHENA program. Despite slight changes in the intensity of R due to a large amount of noisy experimental data beyond

k = 8 $Å^{-1}$, the initial shell distance remained in good agreement at 1.5±0.2 Å. This corresponds to 1.9-2.1 Å when considering the radial size of the core atom. The radial distance of the first shell atom, which points to oxygen atoms, is the only one observed.

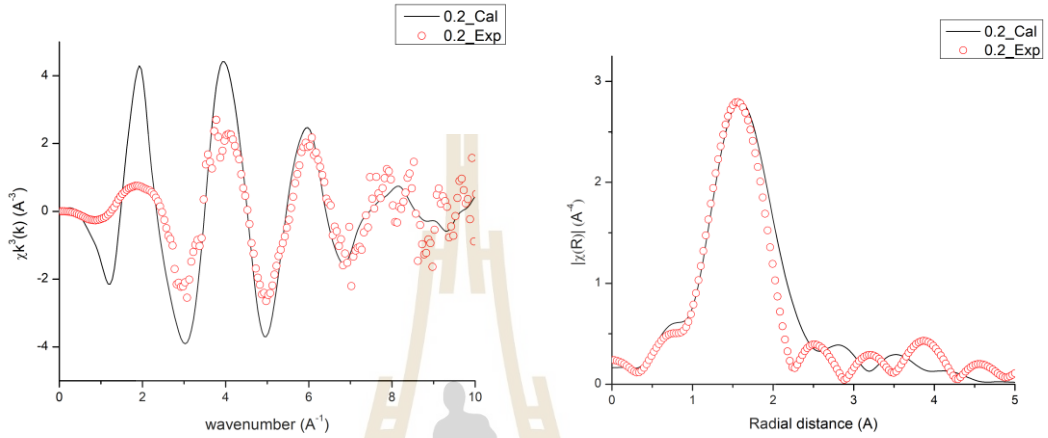

Figure 5.23 The comparison of $\boldsymbol{k^3\chi(k)}$ function (left) and corresponding $\boldsymbol{|\chi(R)|}$ function (right) between final calculation (black line) and experiment (red circle) of 0.2M-0.8LB glass.

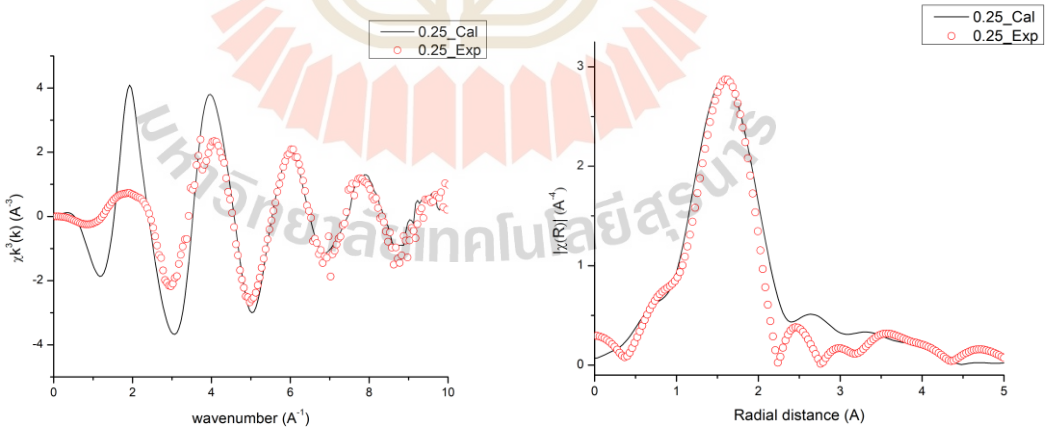

Figure 5.24 The comparison of $\boldsymbol{k^3\chi(k)}$ function (left) and corresponding $\boldsymbol{|\chi(R)|}$ function (right) between final calculation (black line) and experiment (red circle) of 0.25M-0.75LB glass.

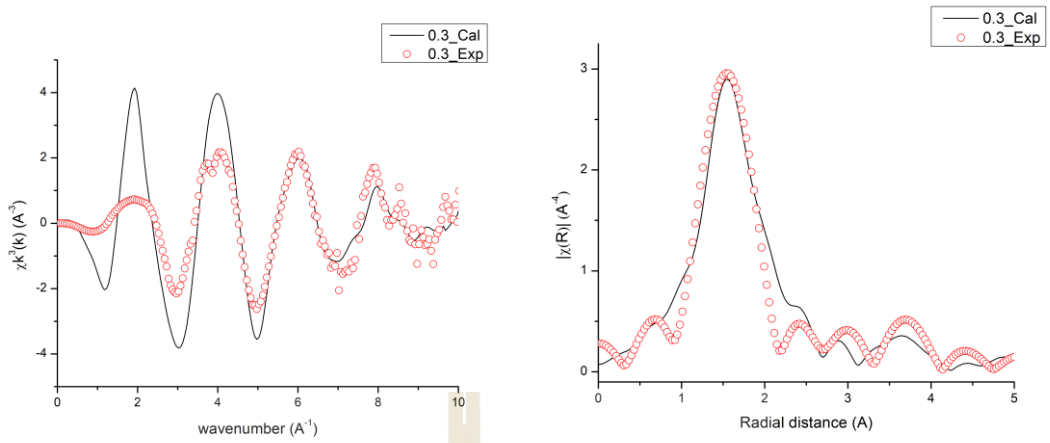

Figure 5.25 The comparison of $k^3\chi(k)$ function (left) and corresponding $|\chi(R)|$ function (right) between final calculation (black line) and experiment (red circle) of 0.3M-0.7LB glass.

5.4 Discussion

The final configuration obtained from the MD simulation served as the initial configuration for the MD-RMC-EXAFS, conducted using the RMC++ program (Gereben et al., 2007b). Addressing the challenge of comparing experimental data beyond k = 8 $Å^{-1}$, the first shell model from ARTHEMIS was employed as the reference data for the RMC method. In Figure 5.26, the MD-RMC-EXAFS is depicted, illustrating the comparison between the RMC-EXAFS (black line) and the first shell model of the 0.2M-0.8LB glass sample (red circle) through the residue. The strong agreement between these datasets underscores the reliability of the potential utilized in the MD process.

The linear combination fitting of the XANES spectrum is presented in Figure 5.27. The two datasets originated from a pure Mn^{2+} and Mn^{3+} system in the 0.2M-0.8LB glass, which had undergone charge neutralization to form $MnLi_8B_{16}O_{29}$ and $MnLi_{16}B_{32}O_{59}$, respectively. The fitting results suggest that the ratio of Mn^{2+} to Mn^{3+} is approximately 6:4. Consequently, it implies that the remaining MLB sample has a similar absorption

edge, indicating a consistent Mn composition ratio. However, this result does not entirely align with the XPS findings.

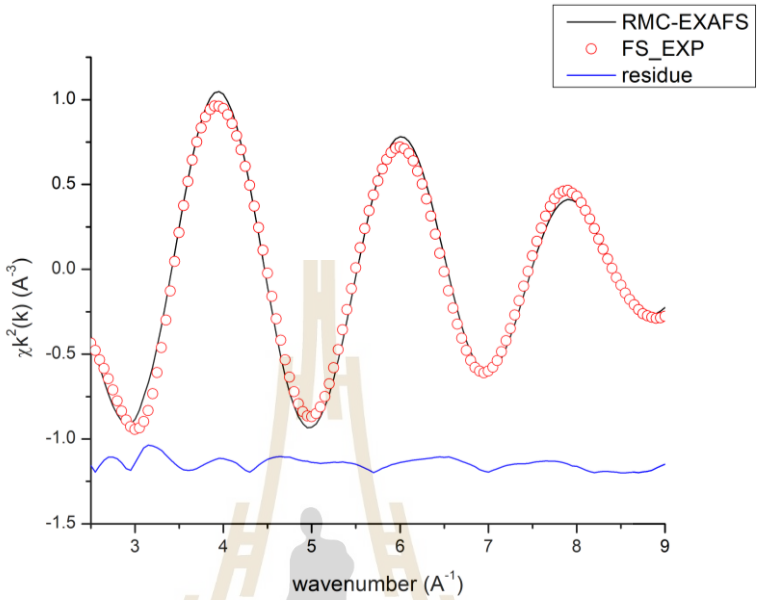

Figure 5.26 The comparison of the EXAFS data between MD-RMC-EXAFS refinement with the first shell model fitting of EXAFS result for 0.2M-0.8LB glass.

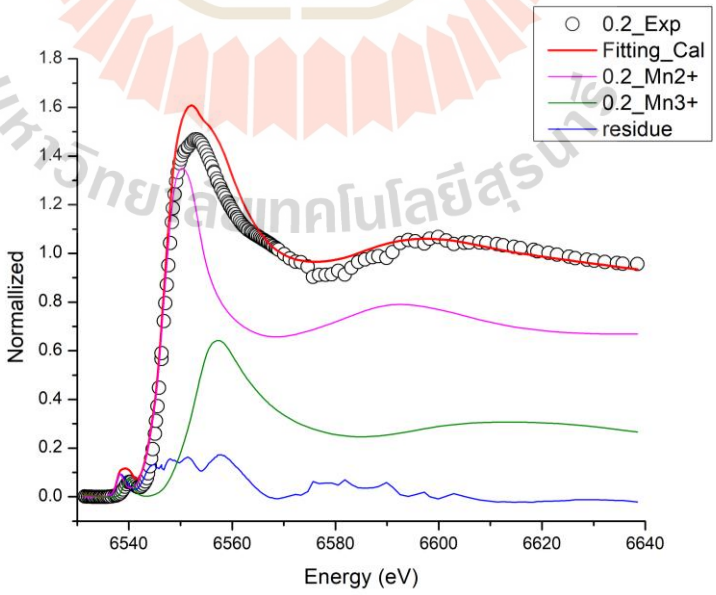

Figure 5.27 Linear combination fitting (red) of 0.2M-0.8LB glass with pure Mn^{2+}(pink) and pure Mn^{3+}(green) system.

Figure 5.28-5.30 illustrate the pairs radial distribution of Mn^{2+}-O and Mn^{3+}-O. The distinct peak positions around 2.0 Å for Mn^{3+} and 2.1 Å for Mn^{2+} are evident in the combined RDF. On the left of each image, the variations in peak position and intensity are displayed, indicating the degree of crystallinity. Despite being less abundant than Mn^{2+}, Mn^{3+} has a notable impact. The signal intensity after the peak for Mn^{3+} approaches zero, suggesting a more crystalline structure, whereas the signal intensity after the peak for Mn^{2+} is slightly higher, indicating that Mn^{2+} has more unbounded O around. In the charge transition process, Mn^{2+} is thus poised to bind with O and initiate the redox reaction as soon as lithium exits the system.

We can further refine the RDF by summarizing the coordination number and bond angle distribution, as demonstrated earlier. Table 5.3 displays the average coordination number of Mn and the average first shell distance. The increase in Mn content in the MLB glass system has resulted in a higher coordination number. Conversely, the first shell distance is slightly reduced due to the increased presence of Mn atoms, indicating a higher proportion of crystallized Mn^{3+}. Figure 5.31 provides an illustration of a Mn cluster with a 6 Å cutoff in the MLB glass system.

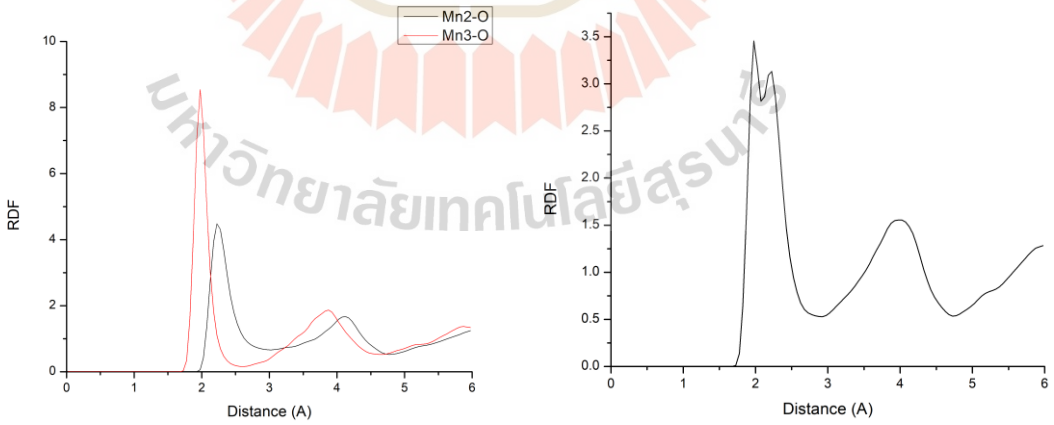

Figure 5.28 Pair radiant distribution function of Mn-O in 0.2M-0.8LB glass for each Mn oxidation state (left) and merged RDF (right).

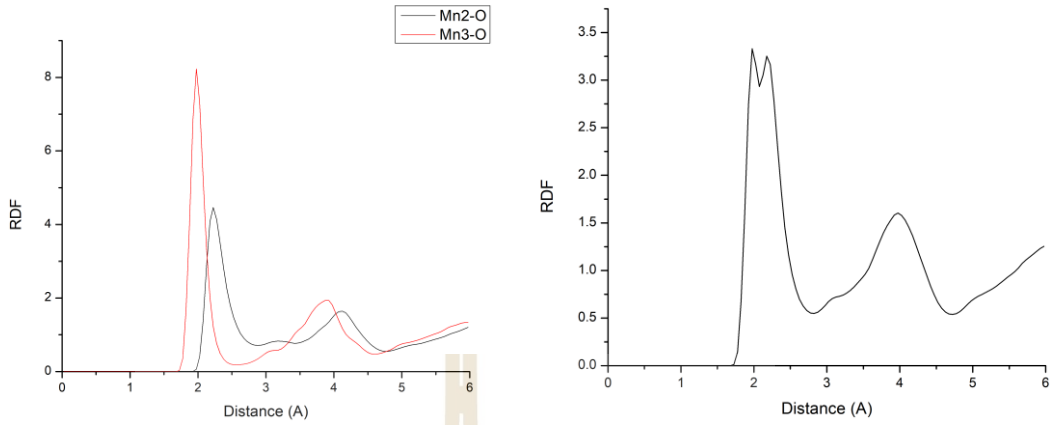

Figure 5.29 Pair radiant distribution function of Mn-O in 0.25M-0.75LB glass for each Mn oxidation state (left) and merged RDF (right).

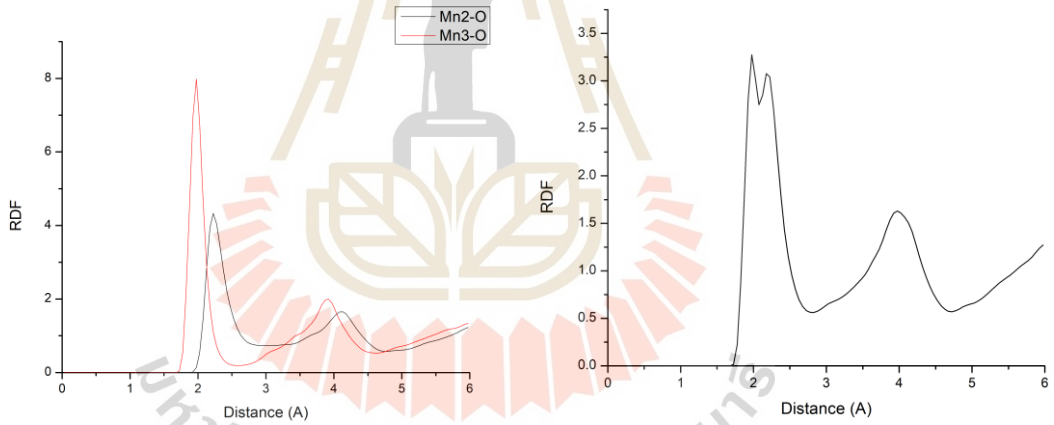

Figure 5.30 Pair radiant distribution function of Mn-O in 0.3M-0.7LB glass for each Mn oxidation state (left) and merged RDF (right).

Table 5.3 Average coordination number and first shell distance of MLB glass from calculation

Sample	Average coordination number (CN), (±0.05)	Average first shell distance (R), (±0.005 Å)
0.2M-0.8LB	4.37	2.081
0.25M-0.75LB	4.42	2.080
0.3M-0.7LB	4.50	2.078

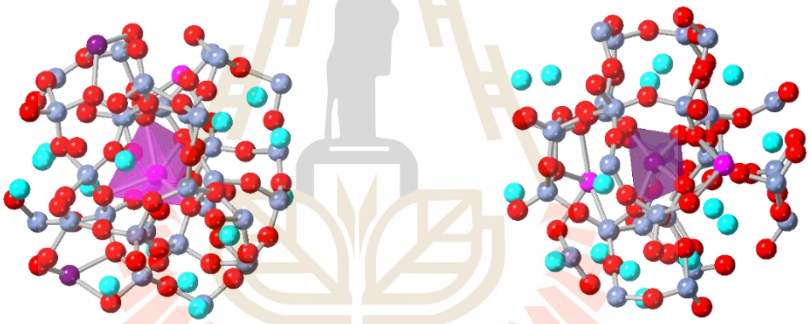

Figure 5.31 The example of Mn cluster with 6 Å cutoff range of Mn^{2+}(left) and Mn^{3+}(right).

มหาวิทยาลัยเทคโนโลยีสุรนารี

CHEPTER VI
CONCLUSION AND SUGGESTION

In this comprehensive investigation, the synergistic application of X-ray Absorption Spectroscopy (XAS), Molecular Dynamics (MD) simulations, and Reverse Monte Carlo (RMC) refinement techniques has been adeptly employed to scrutinize the intricate details of glassy $xMnO_2$-$(1-x)(Li_2O$-$2B_2O_3)$, where x = 0.2, 0.25, and 0.3. The amalgamation of these four methodologies has yielded results that not only demonstrate a robust agreement with prior research but also accentuate the effectiveness of these techniques in tandem. This study stands as a testament to the capability of these sophisticated tools to derive optimal atomistic models for glassy systems, with implications for advancements in Mn-Li-B-O materials technology.

The investigation delves into the local Mn structures within MLB glass, revealing distinctive geometries in two oxidation states. Notably, Mn^{3+} exhibits a proclivity for crystallization compared to Mn^{2+}. The coordination number of Mn ions, elucidated through a harmonious integration of XAS, MD simulation, and MD-RMC refinement, portrays a mixed coordination scenario. For instances where x = 0.2, 0.25, and 0.3, the average coordination numbers are 4.37, 4.42, and 4.50, respectively, corroborating a Mn^{2+}:Mn^{3+} ratio of approximately 6:4. The meticulous choice and verification of potential parameters during the refinement phase emerge as critical considerations. Suggestions for expediting this intricate process include leveraging multiple experimental datasets and custom fitting of potential parameters using a high-performance supercomputer.

Despite the challenges encountered, the amalgamation of XAS, MD simulation, and MD-RMC techniques proves to be a robust and promising approach for obtaining granular structural insights into manganese lithium borate glass. This methodology's

potential extends to future studies investigating other pivotal glass systems, especially those centered around metal borate compositions. Beyond structural elucidation, the atomic structures derived from simulations pave the way for calculating energy band gaps and lithium diffusion coefficients, promising additional avenues for exploration.

Furthermore, this study underscores the potency of Extended X-ray Absorption Fine Structure (EXAFS) spectra as a potent structural constraint for glassy systems. The compelling agreement observed between the MD-RMC configurations and experimental results underscores the importance of meticulous parameter selection for accurate modeling. As this work lays a foundation for advancements in comprehending glass structures and their nuanced properties, it highlights the potential for continued progress in this exciting field.

In addition to the comprehensive findings presented in this study, several key insights and recommendations emerge, contributing to the refinement and enhancement of future investigations in the realm of glassy systems:

- Accelerating Refinement Process: The refinement process, particularly in the choice and verification of potential parameters, poses a time-consuming challenge. Future efforts could explore innovative methodologies or algorithms to expedite this stage, potentially leveraging machine learning approaches to predict suitable parameters based on prior data or employing advanced optimization techniques.
- Diversifying Experimental Datasets: Enhancing the robustness of the MD-RMC refinement process could be achieved by incorporating multiple experimental datasets. A more extensive range of experimental data would provide a broader foundation for refining potential parameters, reducing uncertainties, and ultimately resulting in more accurate structural models.
- Supercomputing Capabilities: Given the computational intensity of MD simulations and RMC refinements, accessing advanced supercomputing resources could significantly enhance the efficiency and scope of these studies. Collaborations with high-performance computing centers or cloud computing

platforms could offer the computational power needed for more intricate simulations and refinements.

- Tailoring Potential Parameters: Instead of relying solely on pre-existing potential parameter libraries, a more customized approach involving the generation of potential parameters specific to the studied glass composition could be explored. This entails fitting potential parameters to experimental data, creating a tailored set of parameters for improved accuracy.
- Multidisciplinary Collaboration: Bridging the expertise from diverse scientific disciplines, including materials science, computational chemistry, and machine learning, can lead to innovative methodologies and a more holistic understanding of glassy systems. Collaborative efforts could unlock novel insights and accelerate progress in this intricate field.
- Exploration of Other Glass Systems: While this study has focused on manganese lithium borate glass, extending these techniques to investigate a broader range of glass systems, including different metal borate compositions or variations in dopants, would contribute to a more comprehensive understanding of the structure-property relationships in glasses.
- Validation and Benchmarking: Continuous efforts to validate the accuracy of MD-RMC simulations against other experimental techniques and benchmarking against well-established glass systems could further establish the reliability of these simulation methods. This iterative validation process ensures the continuous improvement of the simulation models.

In summary, these suggestions aim to propel the field of glass structure studies forward, fostering innovation, efficiency, and accuracy in obtaining detailed insights into the atomic-level structures and properties of glassy materials. The iterative refinement of techniques and methodologies, coupled with interdisciplinary collaborations, promises exciting developments in the broader field of materials science.

REFERENCES

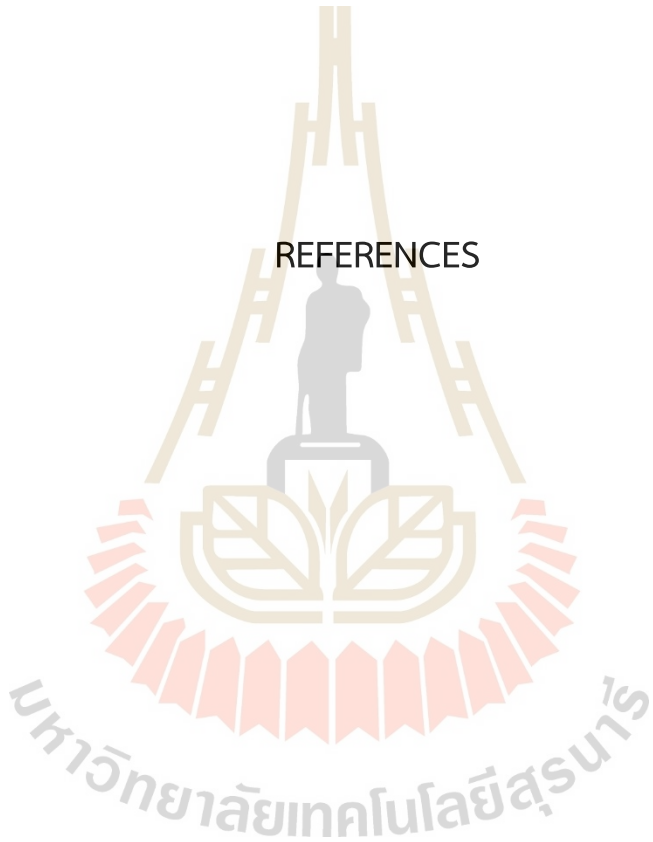

REFERENCES

Afyon, S., Krumeich, F., Mensing, C., Borgschulte, A. and Nesper, R. (2014). New high capacity cathode materials for rechargeable Li-ion batteries: vanadate-borate glasses. Scientific reports*, 4*, 1-7.

Afyon, S., Kundu, D., Krumeich, F. and Nesper, R. (2013). Nano LiMnBO3, a high-capacity cathode material for Li-ion batteries. Journal of power sources*, 224*, 145-151.

Alder, B. J. and Wainwright, T. E. (1959). Studies in molecular dynamics. I. General method. The Journal of Chemical Physics*, 31*, 459-466.

Andersson, A., Abraham, D., Haasch, R., Maclaren, S., Liu, J. and Amine, K. (2002). Surface characterization of electrodes from high power lithium-ion batteries. Journal of The Electrochemical Society*, 149*, A1358.

Berkemeier, F., Shoar Abouzari, M. and Schmitz, G. (2007). Thickness dependent ion conductivity of lithium borate network glasses. Applied physics letters*, 90*, 113110.

Bondareva, O., Simonov, M., Egorov-Tismenko, Y. K. and Belov, N. (1978). Crystal structure of LiZn [BO 3] and LiMn [BO 3]. Kristallografiya*, 23*, 487-490.

Bush, T., Gale, J., Catlow, C. and Battle, P. (1994). Self-consistent interatomic potentials for the simulation of binary and ternary oxides (VOL 4, PG 831, 1994). Journal of Materials Chemistry*, 4*.

Filipponi, A. (2001). EXAFS for liquids. Journal of Physics: Condensed Matter*, 13*, R23.

Filipponi, A., Borowski, M., Bowron, D. T., Ansell, S., Di Cicco, A., De Panfilis, S. and Itie, J.-P. (2000). An experimental station for advanced research on condensed

matter under extreme conditions at the European Synchrotron Radiation Facility-BM29 beamline. Review of Scientific Instruments, *71*, 2422-2432.

Frenkel, D., Smit, B. and Ratner, M. A. 1996. *Understanding molecular simulation: from algorithms to applications*, Academic press San Diego.

Gereben, O., Jóvári, P., Temleitner, L. and Pusztai, L. (2007a). A new version of the RMC++ Reverse Monte Carlo programme, aimed at investigating the structure of covalent glasses. Journal of Optoelectronics and Advanced Materials, *9*, 3021-3027.

Gereben, O., Jóvári, P., Temleitner, L. and Pusztai, L. (2007b). A new version of the RMC++ Reverse Monte Carlo programme, aimed at investigating the structure of covalent glasses. Journal of optoelectronics and advanced materials, *9*, 3021.

Greaves, G. (1985). EXAFS and the structure of glass. Journal of Non-Crystalline Solids, *71*, 203-217.

Henderson, G. S., De Groot, F. M. and Moulton, B. J. (2014). X-ray absorption near-edge structure (XANES) spectroscopy. Reviews in Mineralogy and Geochemistry, *78*, 75-138.

Jóvári, P., Saksl, K., Pryds, N., Lebech, B., Bailey, N. P., Mellergård, A., Delaplane, R. G. and Franz, H. (2007). Atomic structure of glassy Mg 60 Cu 30 Y 10 investigated with EXAFS, x-ray and neutron diffraction, and reverse Monte Carlo simulations. Physical Review B, *76*, 054208.

Karmakar, B. 2017. *Functional glasses and glass-ceramics: processing, properties and applications*, Butterworth-Heinemann.

Khajonrit, J., Montreeuppathum, A., Kidkhunthod, P., Chanlek, N., Poo-Arporn, Y., Pinitsoontorn, S. and Maensiri, S. (2018). New transparent materials for applications as supercapacitors: manganese-lithium-borate glasses. Journal of Alloys and Compounds, *763*, 199-208.

Kim, J. C., Moore, C. J., Kang, B., Hautier, G., Jain, A. and Ceder, G. (2011). Synthesis and electrochemical properties of monoclinic LiMnBO3 as a Li intercalation material. Journal of The Electrochemical Society*, 158*, A309.

Koningsberger, D. C. and Prins, R. (1987). X-ray absorption: principles, applications, techniques of EXAFS, SEXAFS and XANES.

Laorodphan, N., Pooddee, P., Kidkhunthod, P., Kunthadee, P., Tapala, W. and Puntharod, R. (2016). Boron and pentavalent vanadium local environments in binary vanadium borate glasses. Journal of Non-Crystalline Solids*, 453*, 118-124.

Legagneur, V., An, Y., Mosbah, A., Portal, R., La Salle, A. L. G., Verbaere, A., Guyomard, D. and Piffard, Y. (2001). LiMBO3 (M= Mn, Fe, Co):: synthesis, crystal structure and lithium deinsertion/insertion properties. Solid State Ionics*, 139*, 37-46.

Lokhande, C., Dubal, D. and Joo, O.-S. (2011). Metal oxide thin film based supercapacitors. Current Applied Physics*, 11*, 255-270.

Mastelaro, V. R. and Zanotto, E. D. (2018). X-ray absorption fine structure (XAFS) studies of oxide glasses—a 45-year overview. Materials*, 11*, 204.

Montreeuppathum, A., Kidkhunthod, P., Rujirawat, S., Yimnirun, R., Pinitsoontorn, S. and Maensiri, S. (2020). Effect of borate glass network to electrochemical properties: Manganese-doped lithium borate glasses. Radiation Physics and Chemistry*, 170*, 108677.

O'day, P., Rehr, J., Zabinsky, S. and Brown, G. J. (1994). Extended X-ray absorption fine structure (EXAFS) analysis of disorder and multiple-scattering in complex crystalline solids. Journal of the American Chemical Society*, 116*, 2938-2949.

Ozoemena, K. I. and Chen, S. 2016. *Nanomaterials in advanced batteries and supercapacitors*, Springer.

Pye, L. D., Fréchette, V. D. and Kreidl, N. J. 2012. *Borate glasses: structure, properties, applications*, Springer Science & Business Media.

Qi, Z., Younis, A., Chu, D. and Li, S. (2016). A facile and template-free one-pot synthesis of Mn3O4 nanostructures as electrochemical supercapacitors. Nano-micro letters, *8*, 165-173.

Ramteke, D. and Gedam, R. (2014). Study of Li2O–B2O3–Dy2O3 glasses by impedance spectroscopy. Solid State Ionics, *258*, 82-87.

Rao, V., Gopalakrishnan, R., Rao, V. V., Reddy, K. and Buddhudu, S. Physical investigation on lithium borate glasses for solid state battery applications. Materials Science Forum, 1996.

Ravel, B. and Newville, M. (2005). ATHENA, ARTEMIS, HEPHAESTUS: data analysis for X-ray absorption spectroscopy using IFEFFIT. Journal of synchrotron radiation, *12*, 537-541.

Rehr, J. J. and Albers, R. C. (2000). Theoretical approaches to x-ray absorption fine structure. Reviews of modern physics, *72*, 621.

Rehr, J. J., Kas, J. J., Prange, M. P., Sorini, A. P., Takimoto, Y. and Vila, F. (2009). Ab initio theory and calculations of X-ray spectra. Comptes Rendus Physique, *10*, 548-559.

Rehr, J. J., Kas, J. J., Vila, F. D., Prange, M. P. and Jorissen, K. (2010). Parameter-free calculations of X-ray spectra with FEFF9. Physical Chemistry Chemical Physics, *12*, 5503-5513.

Roos, J., Eames, C., Wood, S. M., Whiteside, A. and Islam, M. S. (2015). Unusual Mn coordination and redox chemistry in the high capacity borate cathode Li 7 Mn (BO 3) 3. Physical Chemistry Chemical Physics, *17*, 22259-22265.

Stoch, L. (2001). Flexibility of structure and glass-forming ability: a chemical approach. Glass physics and chemistry, *27*, 167-174.

Takada, A. and Cormack, A. (2008). Computer simulation models of glass structure. Physics and Chemistry of Glasses-European Journal of Glass Science and Technology Part B*, 49*, 127-135.

Todorov, I. T., Smith, W., Trachenko, K. and Dove, M. T. (2006). DL_POLY_3: new dimensions in molecular dynamics simulations via massive parallelism. Journal of Materials Chemistry*, 16*, 1911-1918.

Toupin, M., Brousse, T. and Bélanger, D. (2004). Charge storage mechanism of MnO2 electrode used in aqueous electrochemical capacitor. Chemistry of Materials*, 16*, 3184-3190.

Veena, R., Srimathi, K., Puspamitra, P. and Subramaniam, N. G. (2019). Spherical LiZnBO3: Structural, optical and electrochemical properties. Materials Science for Energy Technologies*, 2*, 267-271.

Woodley, S., Battle, P., Gale, J. and Catlow, C. A. (1999). The prediction of inorganic crystal structures using a genetic algorithm and energy minimisation. Physical Chemistry Chemical Physics*, 1*, 2535-2542.

Yamada, A., Iwane, N. and Harada, Y. (2010). S.-, i. Nishimura, Y. Koyama, I. Tanaka. Adv. Mater*, 22*, 10.1002.

Yu, H. and Zhou, H. (2013). High-energy cathode materials (Li2MnO3–LiMO2) for lithium-ion batteries. The journal of physical chemistry letters*, 4*, 1268-1280.

Zhao, G., Zhang, N. and Sun, K. (2013). Porous MoO3 films with ultra-short relaxation time used for supercapacitors. Materials research bulletin*, 48*, 1328-1332.

APPENDICES

มหาวิทยาลัยเทคโนโลยีสุรนารี

APPENDIX A

THE COORDINATION NUMBER CALCULATOR PROGRAM IN FORTRAN95 COMPILER

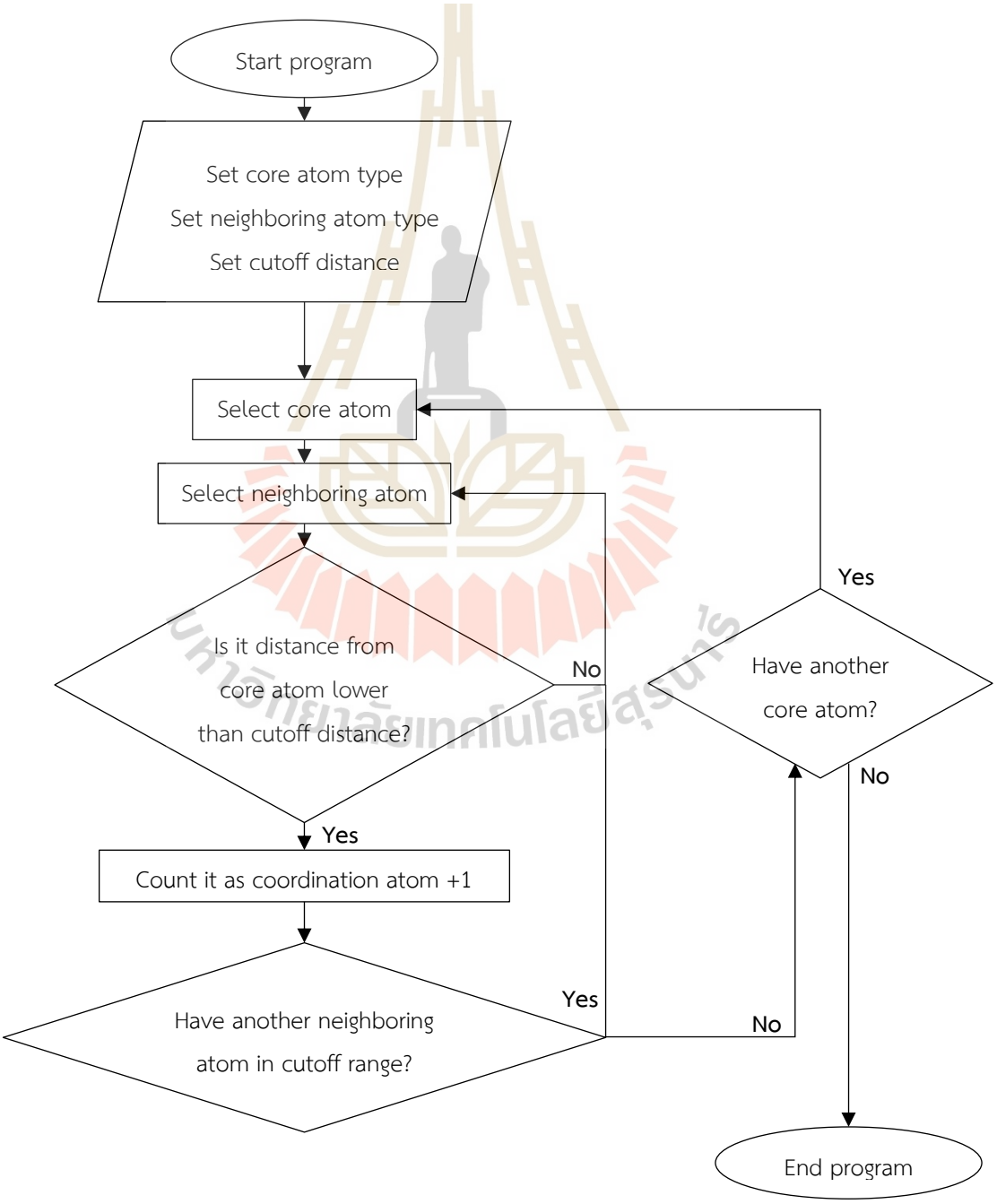

```
program cono
implicit none
integer::
i,j,k,c,v,levcfg,imcon,atomno,a,b,ema,emb,cc,conomax,conotemp,cnt
integer, dimension(10000) :: atmnoe,fsqatm,conoe,conosep,conoa,cnt1
real :: megatm1,megatm2,rx,ry,rz,rtemp,rmin,rmax,at,bt
double precision :: conot
real, dimension(10000,10000) :: rr
real, dimension(10000,10000,3) :: rfeff
real, dimension(3,3) :: box
real, dimension(20000,3) :: atmpos,atmvel,atmfor
character(100) :: fname1, line1
character(5) :: tyatm, core, shell
character(5),dimension(30000) :: tempc1,tempc2

!=====================================================================

   write(*,*) "name of input file >> (REVCON)"
   read(*,'(a)') fname1 !enter file name include file type

   OPEN ( unit=10, FILE=fname1 ) ! opena file and begin read
        READ (10,'(a)') line1
        READ (10,*) levcfg,imcon,atomno,megatm1,megatm2

        do i=1,3
            read (10,*) box(i,:)
        end do

        do i=1,atomno
            read(10, '(A)') tyatm
            tempc1(i)=tyatm

            if(levcfg.eq.0) then
                read(10,*) atmpos(i,:)
            else if(levcfg.eq.1) then
                read(10,*) atmpos(i,:)
                read(10,*) atmvel(i,:)
            else if(levcfg.eq.2) then
                read(10,*) atmpos(i,:)
                read(10,*) atmvel(i,:)
                read(10,*) atmfor(i,:)
            end if
        end do

   close (unit=10)
tempc2(1)=tempc1(1)
fsqatm(1)=1
c=1
v=1
do i=2,atomno
    if(tempc1(i).eq.tempc1(i-1)) then
        v=v+1
        c=c
```

```
        atmnoe(c)=v
    else
        c=c+1
        tempc2(c)=tempc1(i)
        fsqatm(c)=i
        v=1
    end if
end do

write (*,*) "What coorodination which your interested?"
write (*,*) "core >>"
read (*,*) core
write (*,*) "shell >>"
read (*,*) shell

   write(*,*) "r-min to r-max >>"
   read(*,*) rmin,rmax !enter rmin and rmax from g(r)
cc=0
conoa(1)=0
do i=1,c
    if(core.eq.tempc2(i)) then
        a=fsqatm(i) !first atom no. label
        ema=i
    end if

    if(shell.eq.tempc2(i)) then
        b=fsqatm(i) !second atom no. label
        emb=i
    end if
end do

do i=1,atmnoe(ema) !bigest loop
    do j=1,atmnoe(emb)
        rx = atmpos(a+i-1,1) - atmpos(b+j-1,1)
        ry = atmpos(a+i-1,2) - atmpos(b+j-1,2)
        rz = atmpos(a+i-1,3) - atmpos(b+j-1,3)
        rtemp = (rx**2) + (ry**2) + (rz**2)
        rr(i,j)=sqrt(rtemp)
        if(rr(i,j).ge.rmin.and.rr(i,j).le.rmax) then
            cc=cc+1
            rfeff(i,cc,1)=atmpos(b+j-1,1)
            rfeff(i,cc,2)=atmpos(b+j-1,2)
            rfeff(i,cc,3)=atmpos(b+j-1,3)
        end if
    end do
    conoe(i)=cc

    if(i.eq.1) then
        conoa(i) = cc
    else
        conoa(i)=conoa(i-1)+cc
    end if
    cc=0
```

```
end do
    conomax = maxval(conoe)

cnt =0
do j=1,conomax+1
    do i=1,atmnoe(ema)
        if(conoe(i).eq.j-1) then
            cnt = cnt + 1
        end if
    end do
    cnt1(j) = cnt
    cnt = 0
end do

open (unit =20 , file = 'cono.txt' )
write(20,*) "Coordination number of ",trim(core) , " and ", trim(shell)
do j = 1 ,conomax+1
    write (20,*) j-1,cnt1(j)
end do
at = conoa(atmnoe(ema))
bt = atmnoe(ema)
conot = at / bt

write(20,*) "Co No av =" , conot
close (unit=20)

end program cono
```

มหาวิทยาลัยเทคโนโลยีสุรนารี

APPENDIX B

THE BOND ANGLE DISTRIBUTION CALCULATOR IN FORTRAN95 COMPILER

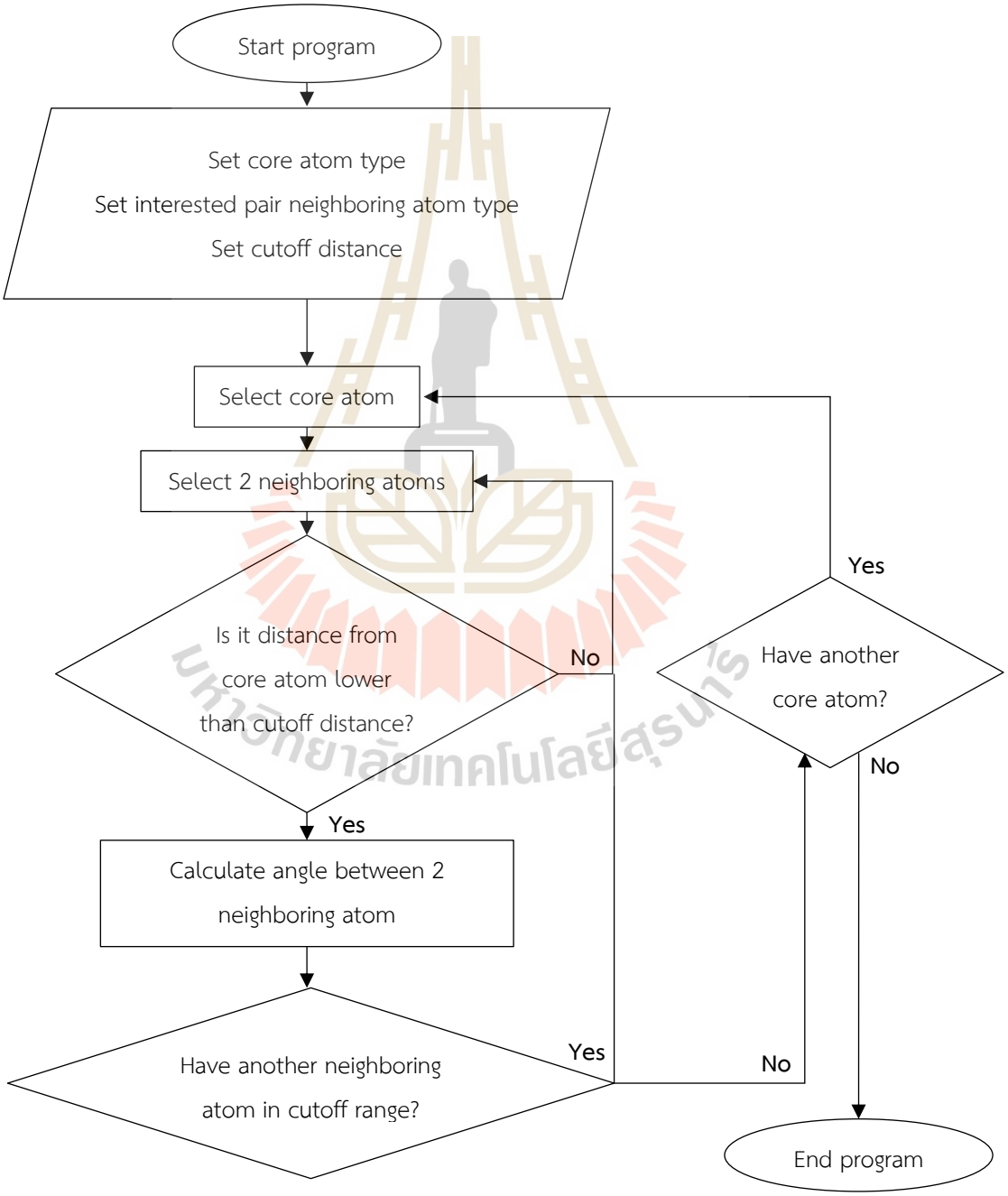

มหาวิทยาลัยเทคโนโลยีสุรนารี

```
program angle
implicit none
integer :: i,j,k,l,c,v,levcfg,imcon,atomno,a,b,ema,emb,cc,nn
integer, dimension(10000) :: atmnoe,fsqatm,cct
integer, dimension(10000) :: degree10,mm
real ::
megatm1,megatm2,rx,ry,rz,rtemp,rmin,rmax,at,bt,xi1,yi1,zi1,xi2,yi2,zi2,
si1,si2,cost,pi,ci
double precision :: xx
real, dimension(100000) :: degree
real, dimension(10000,10000) :: rr
real, dimension(10000,10000,3) :: rfeff
real, dimension(3,3) :: box
real, dimension(20000,3) :: atmpos,atmvel,atmfor
character(100) :: fname1, line1
character(5) :: tyatm, core, shell
character(5),dimension(30000) :: tempc1,tempc2

!=====================================================================

   write(*,*) "name of input file >> (REVCON)"
   read(*,'(a)') fname1 !enter file name include file type

   OPEN ( unit=10, FILE=fname1 ) ! opena file and begin read
        READ (10,'(a)') line1
        READ (10,*) levcfg,imcon,atomno,megatm1,megatm2

        do i=1,3
            read (10,*) box(i,:)
        end do

        do i=1,atomno
            read(10, '(A)') tyatm
            tempc1(i)=tyatm

            if(levcfg.eq.0) then
                read(10,*) atmpos(i,:)
            else if(levcfg.eq.1) then
                read(10,*) atmpos(i,:)
                read(10,*) atmvel(i,:)
            else if(levcfg.eq.2) then
                read(10,*) atmpos(i,:)
                read(10,*) atmvel(i,:)
                read(10,*) atmfor(i,:)
            end if
        end do
```

มหาวิทยาลัยเทคโนโลยีสุรนารี

```
   close (unit=10)
tempc2(1)=tempc1(1)
pi=22/7
fsqatm(1)=1
c=1
v=1
nn=0
do i=2,atomno
    if(tempc1(i).eq.tempc1(i-1)) then
        v=v+1
        c=c
        atmnoe(c)=v
    else
        c=c+1
        tempc2(c)=tempc1(i)
        fsqatm(c)=i
        v=1
    end if
end do

write (*,*) "What coorodination which your interested?"
write (*,*) "core >>"
read (*,*) core
write (*,*) "shell >>"
read (*,*) shell

   write(*,*) "r-min to r-max >>"
   read(*,*) rmin,rmax !enter rmin and rmax from g(r)
cc=0
do i=1,c
    if(core.eq.tempc2(i)) then
        a=fsqatm(i) !first atom no. label
        ema=i
    end if

    if(shell.eq.tempc2(i)) then
        b=fsqatm(i) !second atom no. label
        emb=i
    end if
end do

do i=1,atmnoe(ema) !bigest loop
    do j=1,atmnoe(emb)
        rx = atmpos(a+i-1,1) - atmpos(b+j-1,1)
        ry = atmpos(a+i-1,2) - atmpos(b+j-1,2)
```

```
            rz = atmpos(a+i-1,3) - atmpos(b+j-1,3)
            rtemp = (rx**2) + (ry**2) + (rz**2)
            rr(i,j)=sqrt(rtemp)
            if(rr(i,j).ge.rmin.and.rr(i,j).le.rmax) then
                cc=cc+1
                rfeff(i,cc,1)=atmpos(b+j-1,1)
                rfeff(i,cc,2)=atmpos(b+j-1,2)
                rfeff(i,cc,3)=atmpos(b+j-1,3)
            end if
        end do
        cct(i) = cc

        do k=1,cct(i)-1
            do l=k+1,cct(i)
                xi1 = (rfeff(i,l,1)-atmpos(a+i-1,1))
                xi2 = (rfeff(i,k,1)-atmpos(a+i-1,1))
                yi1 = (rfeff(i,l,2)-atmpos(a+i-1,2))
                yi2 = (rfeff(i,k,2)-atmpos(a+i-1,2))
                zi1 = (rfeff(i,l,3)-atmpos(a+i-1,3))
                zi2 = (rfeff(i,k,3)-atmpos(a+i-1,3))

                si1 = sqrt((xi1**2)+(yi1**2)+(zi1**2))
                si2 = sqrt((xi2**2)+(yi2**2)+(zi2**2))

                cost = ( (xi1*xi2)+(yi1*yi2)+(zi1*zi2) ) / (si1*si2)

                degree(nn) = acos(cost)*180/pi
                degree10(nn) = degree(nn)*10
                nn = nn+1
            end do
        end do
        cc = 0
    end do

    mm(:)=0
    do i = 1,1800
        do j=1,nn-1
            if (degree10(j).eq.i) then
                mm(i)=mm(i)+1
            end if
        end do
    end do

    open (unit = 100, file = "angle.txt")
    write (100,*) "Angle distribution of " ,trim(shell),"-",trim(core),"-
    ",trim(shell) , "betwwen" ,rmin, "to" , rmax
```

มหาวิทยาลัยเทคโนโลยีสุรนารี

```
write (100,*) "Angle   intensity"
    do i=1,1800
        ci=i
        xx=ci/10
        write (100,('(1F5.1,I5)')) xx,mm(i)
    end do
close (unit=100)


end program angle
```

APPENDIX C

THE FEFF8.2 INPUT CONVERTER IN FORTRAN95 COMPILER

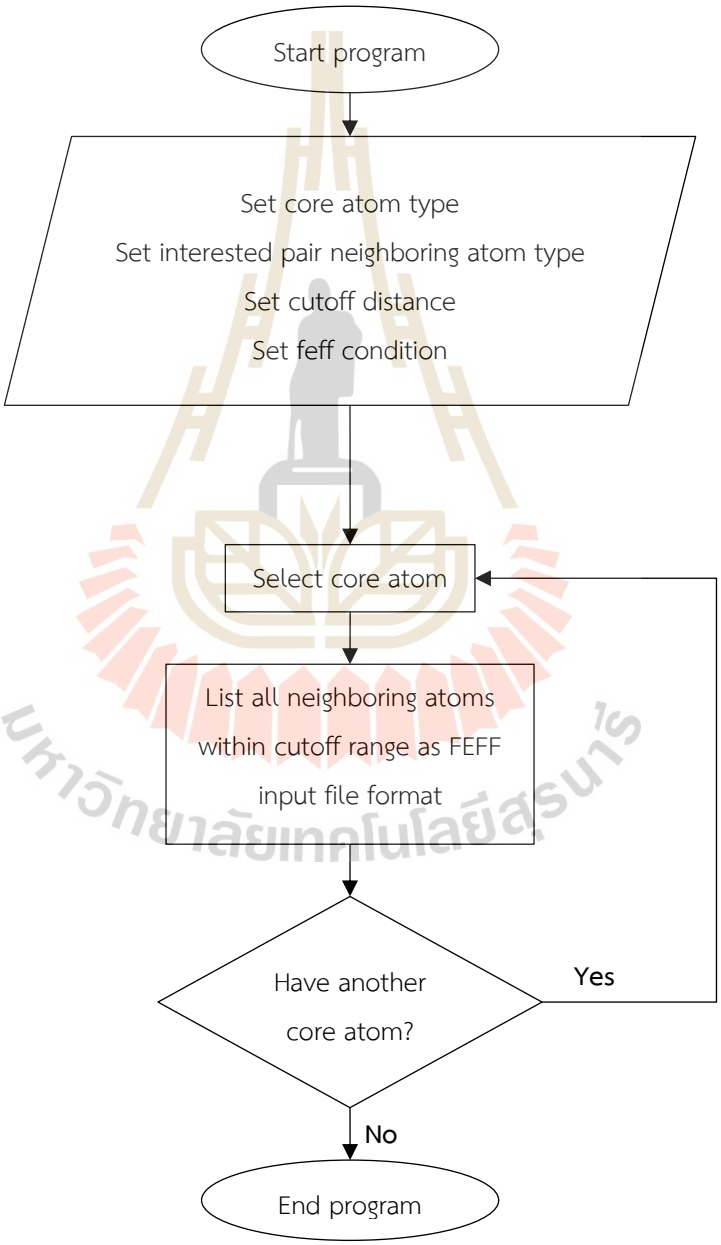

```
PROGRAM convertfeff
IMPLICIT NONE
    integer ::
i,j,a,bb,c,v,k,tk,ema,nn,nn1,nn2,nopair,xasty,edge,sfcheck,cont,statm
    integer :: loopscf,loopfms,scfv,fmsv
    integer,dimension(500) :: emb,cc,atmz,b
    character(100) :: fname1, foname1,itratm1
    character(100),dimension(10) :: itratm2
    character :: fname2*40 ,foname2*40 ,title*40 ,ftemp*10
    character(1000) :: line1
    character(5) :: tyatm,xasty1,edge1
    character(5),dimension(30000) :: tempc1,tempc2
    integer :: levcfg,imcon,atomno,atmtyno
    integer, dimension(10000) :: atmnoe,fsqatm
    integer, dimension(10,10) :: sqatm
    real ::
megatm1,megatm2,rmin,rmax,rx,ry,rz,rtemp,chitemp,mutemp,kkc,k2chi
    real :: scfmin,scfmax,fmsmin,fmsmax,rpath,scf,fms,stepscf,stepfms
    real, dimension(10000,10000) :: rr
    real, dimension(10000,10000,3) :: rfeff
    real, dimension(3,3) :: box
    real, dimension(20000,3) :: atmpos,atmvel,atmfor
    integer :: result1
    integer :: z,m,ccc
    character(1) :: skip,check
    real,dimension(1000,1000) :: omega,e,mu,mu0,etc,kk,chi,mag,phase
    real,dimension(1000000) :: chii,ktmp,muu
    character(len=1024) :: filename1,filename2,filename3
    character(len=1024) :: format_string
    integer :: sk,inpc,atmposi,atmposc,atmposck,linei,pttfline
    character(len=1024),dimension(1000) :: inpline,itratmi,itratmic
    integer,dimension(100) :: nolist,atmzi,atmzic,del
    character(len=17), dimension(10000,3) :: rfeffi
    character(len=4) :: checki
!=====================================================================
   write(*,*) "name of input file >> (REVCON)"
   read(*,'(a)') fname1 !enter file name include file type
   fname2=fname1

   OPEN ( unit=10, FILE=fname2 ) ! opena file and begin read
        READ (10,'(a)') line1
        READ (10,*) levcfg,imcon,atomno,megatm1,megatm2

        do i=1,3
            read (10,*) box(i,:)
        end do
```

```
        do i=1,atomno
            read(10, '(A)') tyatm
            tempc1(i)=tyatm
            if (levcfg.eq.0) then
                read(10,*) atmpos(i,:)
            else if (levcfg.eq.1) then
                read(10,*) atmpos(i,:)
                read(10,*) atmvel(i,:)
            else if (levcfg.eq.2) then
                read(10,*) atmpos(i,:)
                read(10,*) atmvel(i,:)
                read(10,*) atmfor(i,:)
            end if
        end do

   close (unit=10)
tempc2(1)=tempc1(1)
fsqatm(1)=1
c=1
v=1
do i=2,atomno
    if(tempc1(i).eq.tempc1(i-1)) then
        v=v+1
        c=c
        atmnoe(c)=v
    else
        c=c+1
        tempc2(c)=tempc1(i)
        fsqatm(c)=i
        v=1
    end if
end do
atmtyno=c
   write (*,*) "Welcome to FEFF8 converter"
   write (*,*) "What data typr do you want to consider? (type 1=EXAFS ,
2=XANES)"
   read(*,*) xasty
   if (xasty.eq.1) then
        xasty1='EXAFS'
   else if (xasty.eq.2) then
        xasty1='XANES'
   end if

   write (*,*) "What is considered EDGE? (1=K , 2=M , 3=L3)"
   read(*,*) edge
      if (edge.eq.1) then
```

มหาวิทยาลัยเทคโนโลยีสุรนารี

```
        edge1='K'
    else if (edge.eq.2) then
        edge1='M'
    else if (edge.eq.3) then
        edge1='L3'
    end if

    write (*,*) "type of atom is " ,atmtyno
    write (*,*) "for each emblem as " , (tempc2(j),j=1,c)
    write (*,*) "no. of atom for each are" , (atmnoe(j),j=1,c)

    do nn=1,10
        write(*,*) "How many interaction of atoms that we intersted?
(between 1 to", c ,")"
        read(*,*) nopair
            if(nopair.ge.1 .and. nopair.le.c) exit
    end do
    continue

    write(*,*) "What is core atom?"
    read(*,'(a)') itratm1

    do nn=1,10
        call element(itratm1,tk)
        atmz(1)=tk
        if(tk.ne.0) exit
    end do
    continue

    do nn=1,nopair

        write(*,*) "interested", nn ," pair atoms emblem >>"
        read(*,'(a)') itratm2(nn) !enter interested pair atoms
        call element(itratm2(nn),tk)
        atmz(nn+1)=tk
        do i=1,c
            if(itratm1.eq.tempc2(i)) then
                a=fsqatm(i) !first atom no. label
                ema=i
            end if

            if(itratm2(nn).eq.tempc2(i)) then
                b(nn)=fsqatm(i) !second atom no. label
                emb(nn)=i
            end if
        end do
```

```
     cc(nn)=0
    end do

write(*,*) "core atom is     ",itratm1
do nn=1,nopair
     write(*,*) nn, "pair   ",itratm2(nn),"No. ",emb(nn)
end do

    write(*,*) "r-min to r-max >>"
    read(*,*) rmin,rmax !enter rmin and rmax from g(r)

    write(*,*) "scf value >>"
    read(*,*) scf
    if(xasty.eq.2) then
         write(*,*) "fms value >>"
         read(*,*) fms
    end if
ccc=1
check = '#'
title = ' TITLE  '//line1


do i=1,atmnoe(ema) !bigest loop
ccc=1
  do nn=1,nopair
     do j=1,atmnoe(emb(nn))
         rx = atmpos(a+i-1,1) - atmpos(b(nn)+j-1,1)
         ry = atmpos(a+i-1,2) - atmpos(b(nn)+j-1,2)
         rz = atmpos(a+i-1,3) - atmpos(b(nn)+j-1,3)
         rtemp = (rx**2) + (ry**2) + (rz**2)
         rr(i,j)=sqrt(rtemp)
             if(rr(i,j).ge.rmin.and.rr(i,j).le.rmax) then
                 cc(nn)=cc(nn)+1
                 rfeff(i,cc(nn),1)=atmpos(b(nn)+j-1,1)
                 rfeff(i,cc(nn),2)=atmpos(b(nn)+j-1,2)
                 rfeff(i,cc(nn),3)=atmpos(b(nn)+j-1,3)
                 !write(*,*) rfeff(i,cc(nn),:)
                 !write(*,*) itratm2(nn),cc(nn)
             end if
     end do

          if (i < 10) then
             format_string = "(A4,I1)"
          else if (i < 100) then
             format_string = "(A4,I2)"
          else
```

```
            format_string = "(A4,I3)"
         endif
        write (filename1,format_string) "feff",i
        write (filename2,format_string) "chi",i
        write (filename3,format_string) "xmu",i

    open (unit=20000,file=trim(filename1))

    open (unit=100,file='feff.inp')
    if (nn.eq.1) then
        write(100,'(a)') title
        write(100,*) "EDGE      ",edge1 !for consider edge
        write(100,*) "S02       1.0"
        write(100,*) "CONTROL   1     1     1     1     1      1"
        write(100,*) "PRINT     1     0     0     0     0      0"
        write(100,*) "SCF       ",scf ,"   0      30     0.2   1"
!r_scf @@
        write(100,*) "EXCHANGE  0      0   0   2"
        if (xasty.eq.1) then
            write(100,*) "EXAFS" !to exafs calculation
            write(100,*) "RPATH     12" !considered
        else if (xasty.eq.2) then
            write(100,*) "XANES     6.0     0.05     0.5" !to xanes
calculation, kmax delta_k delta_e
            write(100,*) "FMS       " ,fms,"     0"  !considered
            write(100,*) "LDOS -20  20   0.1"
            write(100,*) "RPATH     -1"       !considered
        end if
        write(100,*) "POTENTIALS"
        write(100,*) "          0",atmz(1),itratm1

        do nn2=1,nopair

            write(100,*) nn2,atmz(nn2+1),itratm2(nn2)
        end do

        write(100,*) "ATOMS"
            write(100,*) atmpos(a+i-1,:),"          0 ",itratm1
    end if
      do nn2=1,nopair
        do k=1,cc(nn2)
            if (itratm2(nn2).eq.itratm1.and.k.eq.1) go to 2
                write(100,*) rfeff(i,k,:),nn2,itratm2(nn2)
            2 continue
        end do
      end do
```

```
    if (nn.eq.nopair) then
        write(100,*) "END"
    end if
    cc(nn)=0
  end do
  close (unit=100)

linei=1
atmposc=1
del(:)=0
inpline(:)= ''
    OPEN ( unit=1234, FILE='feff.inp' )

        do sk =1,1000
            read(1234, '(A)') inpline(linei)
            linei=linei+1
            if (inpline(sk).eq.' POTENTIALS') go to 134

        end do
134 continue
inpline(linei)=' POTENTIALS'
pttfline=linei-1
    do inpc=1,1000
        read(1234,'(I12,I12,A4)')
nolist(inpc),atmzi(inpc),itratmi(inpc)
        write(inpline(linei),'(I12,I12,A4)')
nolist(inpc),atmzi(inpc),itratmi(inpc)
        linei=linei+1

        if (nolist(inpc).eq.nopair) go to 135
    end do
135 continue

inpline(linei)=' ATOMS'
linei=linei+1
read(1234,'(A)') checki
    do atmposi=1,1000
        read(1234,'(A4)') checki
            if (checki.eq.' END') go to 136
        backspace(unit=1234)
        read(1234,'(3A17,I12,A5)')
rfeffi(atmposi,1),rfeffi(atmposi,2),rfeffi(atmposi,3),atmzic(atmposi),i
tratmic(atmposi)
        itratmic(atmposi)=' '//itratmic(atmposi)
```

มหาวิทยาลัยเทคโนโลยีสุรนารี

```
        write(inpline(linei),'(3A17,I12,A5)')
rfeffi(atmposi,1),rfeffi(atmposi,2),rfeffi(atmposi,3),atmzic(atmposi),i
tratmic(atmposi)
        linei=linei+1
        atmposc=atmposc+1

    end do
136 continue
inpline(linei)=' END'
    CLOSE ( unit=1234 )

    do bb=1,2
    do inpc=1,nopair+1
        do atmposi=1,atmposc
            if (nolist(inpc).eq.atmzic(atmposi)) then
                del(inpc)=1
                go to 137
            else if (nolist(inpc).ne.atmzic(atmposi)) then
                del(inpc)=0
            end if
        end do
    137  continue
            if (del(inpc).eq.0) then
                inpline(pttfline+inpc)= ''
            end if
    end do
    end do

    OPEN ( unit=1235, FILE='feff.inp' )
    do inpc=1,linei
        write(1235,'(A)') trim(inpline(inpc))
    end do
    CLOSE ( unit=1235 )

        call SYSTEM ('mkdir inp')
end do
END PROGRAM convertfeff

subroutine element(b,c) !list of the atom to call symbol
integer:: c
character(5):: b
if (b.EQ."H") then
    c=1
elseif (b.EQ."He") then
    c=2
elseif (b.EQ."Li") then
```

มหาวิทยาลัยเทคโนโลยีสุรนารี

```
    c=3
elseif (b.EQ."Be") then
    c=4
elseif (b.EQ."B") then
    c=5
elseif (b.EQ."C") then
    c=6
elseif (b.EQ."N") then
    c=7
elseif (b.EQ."O") then
    c=8
elseif (b.EQ."F") then
    c=9
elseif (b.EQ."Ne") then
    c=10
elseif (b.EQ."Na") then
    c=11
elseif (b.EQ."Mg") then
    c=12
elseif (b.EQ."Al") then
    c=13
elseif (b.EQ."Si") then
    c=14
elseif (b.EQ."P") then
    c=15
elseif (b.EQ."S") then
    c=16
elseif (b.EQ."Cl") then
    c=17
elseif (b.EQ."Ar") then
    c=18
elseif (b.EQ."K") then
    c=19
elseif (b.EQ."Ca") then
    c=20
elseif (b.EQ."Sc") then
    c=21
elseif (b.EQ."Ti") then
    c=22
elseif (b.EQ."V") then
    c=23
elseif (b.EQ."Cr") then
    c=24
elseif (b.EQ."Mn") then
    c=25
elseif (b.EQ."Fe") then
```

มหาวิทยาลัยเทคโนโลยีสุรนารี

```
    c=26
elseif (b.EQ."Co") then
    c=27
elseif (b.EQ."Ni") then
    c=28
elseif (b.EQ."Cu") then
    c=29
elseif (b.EQ."Zn") then
    c=30
elseif (b.EQ."Ga") then
    c=31
elseif (b.EQ."Ge") then
    c=32
elseif (b.EQ."As") then
    c=33
elseif (b.EQ."Se") then
    c=34
elseif (b.EQ."Br") then
    c=35
elseif (b.EQ."Kr") then
    c=36
elseif (b.EQ."Rb") then
    c=37
elseif (b.EQ."Sr") then
    c=38
elseif (b.EQ."Y") then
    c=39
elseif (b.EQ."Zr") then
    c=40
elseif (b.EQ."Nb") then
    c=41
elseif (b.EQ."Mo") then
    c=42
elseif (b.EQ."Tc") then
    c=43
elseif (b.EQ."Ru") then
    c=44
elseif (b.EQ."Rh") then
    c=45
elseif (b.EQ."Pd") then
    c=46
elseif (b.EQ."Ag") then
    c=47
elseif (b.EQ."Cd") then
    c=48
elseif (b.EQ."In") then
```

มหาวิทยาลัยเทคโนโลยีสุรนารี

```
    c=49
elseif (b.EQ."Sn") then
    c=50
elseif (b.EQ."Sb") then
    c=51
elseif (b.EQ."Te") then
    c=52
elseif (b.EQ."I") then
    c=53
elseif (b.EQ."Xe") then
    c=54
elseif (b.EQ."Cs") then
    c=55
elseif (b.EQ."Ba") then
    c=56
elseif (b.EQ."La") then
    c=57
elseif (b.EQ."Ce") then
    c=58
elseif (b.EQ."Pr") then
    c=59
elseif (b.EQ."Nd") then
    c=60
elseif (b.EQ."Pm") then
    c=61
elseif (b.EQ."Sm") then
    c=62
elseif (b.EQ."Eu") then
    c=63
elseif (b.EQ."Gd") then
    c=64
elseif (b.EQ."Tb") then
    c=65
elseif (b.EQ."Dy") then
    c=66
elseif (b.EQ."Ho") then
    c=67
elseif (b.EQ."Er") then
    c=68
elseif (b.EQ."Tm") then
    c=69
elseif (b.EQ."Yb") then
    c=70
elseif (b.EQ."Lu") then
    c=71
elseif (b.EQ."Hf") then
```

มหาวิทยาลัยเทคโนโลยีสุรนารี

```
    c=72
elseif (b.EQ."Ta") then
    c=73
elseif (b.EQ."W") then
    c=74
elseif (b.EQ."Re") then
    c=75
elseif (b.EQ."Os") then
    c=76
elseif (b.EQ."Ir") then
    c=77
elseif (b.EQ."Pt") then
    c=78
elseif (b.EQ."Au") then
    c=79
elseif (b.EQ."Hg") then
    c=80
elseif (b.EQ."Tl") then
    c=81
elseif (b.EQ."Pb") then
    c=82
elseif (b.EQ."Bi") then
    c=83
elseif (b.EQ."Po") then
    c=84
elseif (b.EQ."At") then
    c=85
elseif (b.EQ."Rn") then
    c=86
elseif (b.EQ."Fr") then
    c=87
elseif (b.EQ."Ra") then
    c=88
elseif (b.EQ."Ac") then
    c=89
elseif (b.EQ."Th") then
    c=90
elseif (b.EQ."Pa") then
    c=91
elseif (b.EQ."U") then
    c=92
elseif (b.EQ."Np") then
    c=93
elseif (b.EQ."Pu") then
    c=94
elseif (b.EQ."Am") then
```

มหาวิทยาลัยเทคโนโลยีสุรนารี

```
    c=95
elseif (b.EQ."Cm") then
    c=96
elseif (b.EQ."Bk") then
    c=97
elseif (b.EQ."Cf") then
    c=98
elseif (b.EQ."Es") then
    c=99
elseif (b.EQ."Fm") then
    c=100
elseif (b.EQ."Md") then
    c=101
elseif (b.EQ."No") then
    c=102
elseif (b.EQ."Lr") then
    c=103
elseif (b.EQ."Rf") then
    c=104
elseif (b.EQ."Db") then
    c=105
elseif (b.EQ."Sq") then
    c=106
elseif (b.EQ."Bh") then
    c=107
elseif (b.EQ."Hs") then
    c=108
elseif (b.EQ."Mt") then
    c=109
elseif (b.EQ."Ds") then
    c=110
elseif (b.EQ."Rg") then
    c=111
elseif (b.EQ."Cn") then
    c=112
elseif (b.EQ."Uut") then
    c=113
elseif (b.EQ."Fl") then
    c=114
elseif (b.EQ."Uup") then
    c=115
elseif (b.EQ."Lv") then
    c=116
elseif (b.EQ."Uus") then
    c=117
elseif (b.EQ."Uuo") then
```

มหาวิทยาลัยเทคโนโลยีสุรนารี

```
    c=118
else
    write(*,*) "Wrong format please try again"
    c=0
end if

return
end
```

CURRICULUM VITAE

Name: Pattarapong Nijapai

Date of birth: 23 Febuarry 1994

Place of birth: Chaiyaphum, Thailand

Education:

2006-2012: Chaiyabhum Bhakdeechumphon School, Chaiyaphum, Thailand

(High school)

2012-2016: Department of Physics, Science, KhonKaen University, KhonKaen, Thailand

(Bachelor of Science)

2016-2023: School of Physics, Science, Suranaree University of technology,

Nakhonratchasima, Thailand

(Doctor of philosophy in Physics)

Academic experience:

1. Ph.D. Research of NY State College of Ceramics at Alfred University, New York, USA.
2. Physics Lab Teaching Assistant in Suranaree University of Technology.
3. Beamline 5.2 assistance scientist in Synchrotron Light Research Institute (Public Organization).
4. Staff and team organizer in 5th International Conference on Smart Materials and Nanotechnology (SmartMat@2020), Pattaya, Thailand.

มหาวิทยาลัยเทคโนโลยีสุรนารี